Government of **Western Australia**
Department of **Mines and Petroleum**

RECORD 2014/10

GEOLOGICAL SETTING OF MINERAL DEPOSITS IN THE EASTERN YILGARN CRATON — A FIELD GUIDE

compiled by
S Wyche



Geological Survey of Western Australia

Government of **Western Australia**
Department of **Mines and Petroleum**

Record 2014/10

GEOLOGICAL SETTING OF MINERAL DEPOSITS IN THE EASTERN YILGARN CRATON — A FIELD GUIDE

compiled by
S Wyche

Perth 2014

Geological Survey of Western Australia

MINISTER FOR MINES AND PETROLEUM
Hon. Bill Marmion MLA

DIRECTOR GENERAL, DEPARTMENT OF MINES AND PETROLEUM
Richard Sellers

EXECUTIVE DIRECTOR, GEOLOGICAL SURVEY OF WESTERN AUSTRALIA
Rick Rogerson

REFERENCE
The recommended reference for this publication is:
Wyche, S (compiler) 2014, Geological setting of mineral deposits in the eastern Yilgarn Craton — a field guide: Geological Survey of Western Australia, Record 2014/10, 56p.

National Library of Australia Card Number and ISBN 978-1-74168-577-0

Grid references in this publication refer to the Geocentric Datum of Australia 1994 (GDA94). Locations mentioned in the text are referenced using Map Grid Australia (MGA) coordinates, Zone 51. All locations are quoted to at least the nearest 100 m.

Published 2014 by Geological Survey of Western Australia
This Record is published in digital format (PDF) and is available online at <www.dmp.wa.gov.au/GSWApublications>.

Further details of geological products and maps produced by the Geological Survey of Western Australia are available from:
Information Centre
Department of Mines and Petroleum
100 Plain Street
EAST PERTH WESTERN AUSTRALIA 6004
Telephone: +61 8 9222 3459 Facsimile: +61 8 9222 3444
www.dmp.wa.gov.au/GSWApublications

Contents

Figures

Geological setting of mineral deposits in the eastern Yilgarn Craton — a field guide

compiled by

S Wyche

with contributions from

S Wyche, NL Patison, MJ Pawley[1], SP Hollis[2], ML Fiorentini[3], JL Miller[2], and TC McCuaig[2]

Preface

The Yilgarn Craton preserves evidence of the oldest crust on Earth back to c. 4400 Ma. The earliest recognizable volcano-sedimentary greenstones were deposited after c. 3100 Ma. Isotopic data show that there have been several periods of crust generation and recycling, the earliest of which are not recognized in the Eastern Goldfields Superterrane. Two major episodes of plume-related magmatism, at c. 2800 and 2700 Ma, had major consequences for the development and evolution of the craton. The c. 2800 Ma event, the scale of which has only recently been recognized, produced huge mafic–ultramafic igneous complexes in the central part of the craton and was associated with rifting and breakup of the preserved eastern part. The c. 2700 Ma plume, which is responsible for the creation of the world-class nickel deposits of the Eastern Goldfields Superterrane, generated greenstone successions between the older cratonic blocks created at the time of the c. 2800 Ma breakup. The arc-like volcano-sedimentary successions in the Kalgoorlie and Kurnalpi Terranes of the Eastern Goldfields Superterrane may have formed as result of the re-assembly of the older crustal blocks. Structures developed at this time, particularly deeply penetrating, extensional structures that allowed large-scale fluid fluxes, provided loci for the deposition of gold deposits.

The Gold14@Kalgoorlie excursions will visit the central part of the Kalgoorlie Terrane and adjacent Kurnalpi Terrane (Figs 1 and 2) in the Eastern Goldfield Superterrane of the Yilgarn Craton. The excursions will visit localities that illustrate the structural and stratigraphic setting of gold, base metal and nickel deposits in the region.

Introduction

by S Wyche, ML Fiorentini, JL Miller, and TC McCuaig

The Paleo- to Neoarchean Yilgarn Craton in Western Australia (Fig. 3) is a highly mineralized granite–greenstone terrain with world-class deposits of gold and nickel, and significant iron and volcanic-hosted massive sulfide (VHMS) base-metal deposits. Economic iron deposits are confined to the western part of the craton.

Over the past 15 years, the acquisition of large datasets and major advances in the understanding of the geological evolution of the Yilgarn Craton at all scales, have encouraged the application of the holistic mineral systems approach to mineral exploration as a tool for developing targeting criteria, particularly for nickel and gold (McCuaig et al., 2010). In this review, examples from the Kambalda district in the Eastern Goldfields region illustrate how the size, distribution and concentration of gold and nickel deposits are controlled by factors from the craton to the regional scale, down to the deposit cluster and individual deposit scale. While there has been little recent, regional-scale work on Yilgarn VHMS deposits, comparison with similar terrains in Canada suggests that the fundamental controls on nickel mineralization also influence the distribution and endowment of VHMS mineralization (Huston et al., 2005).

1 Geological Survey of South Australia, PO Box 320, Adelaide SA 5001

2 CSIRO Earth Science and Resource Engineering, Locked Bag 10, Clayton South VIC 3169

3 Centre for Exploration Targeting, School of Earth and Environment, The University of Western Australia, M006, 35 Stirling Highway, Crawley WA 6009

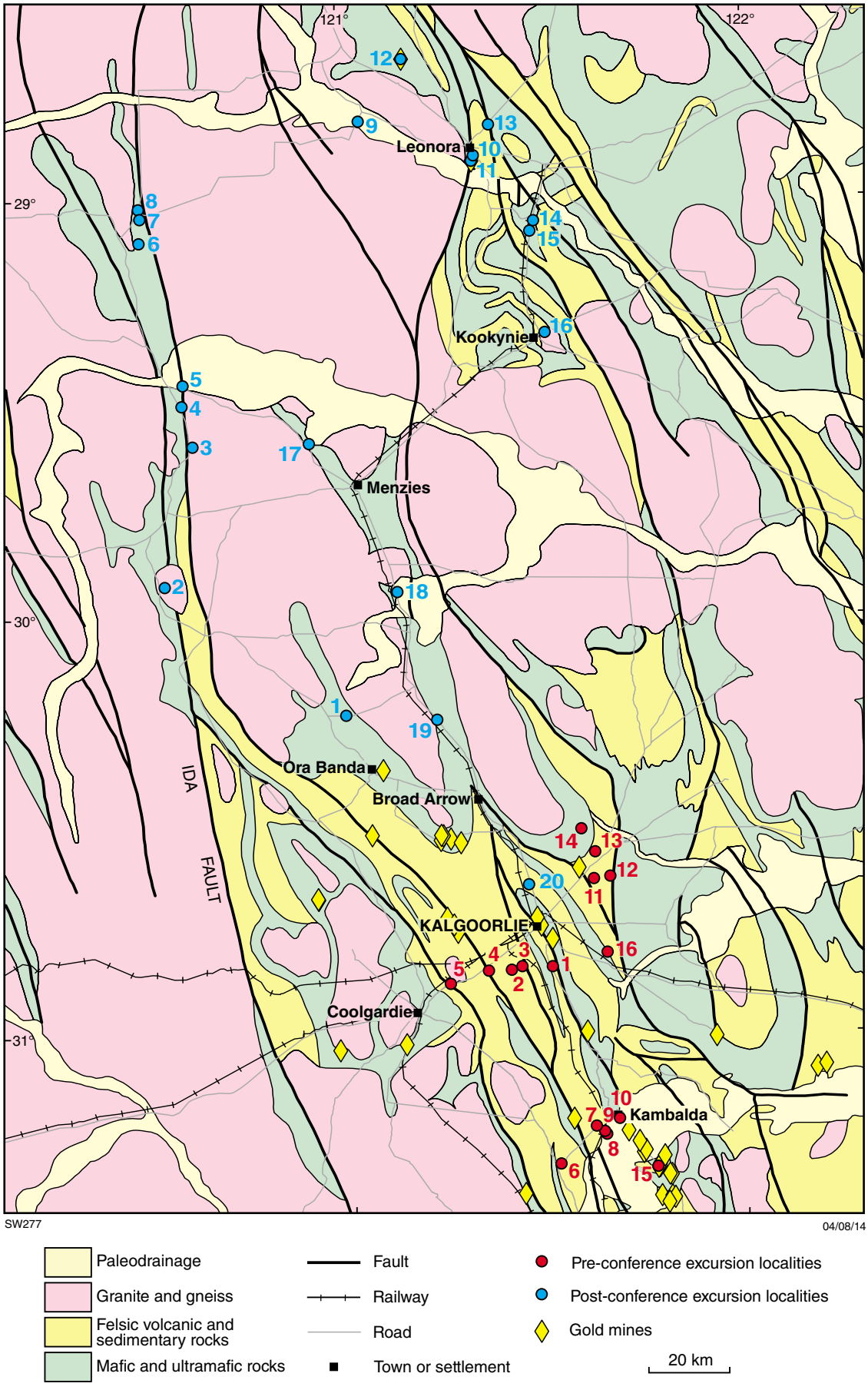

Figure 1. Itineraries for the Gold14@Kalgoorlie pre- and post-conference excursions showing major gold deposits

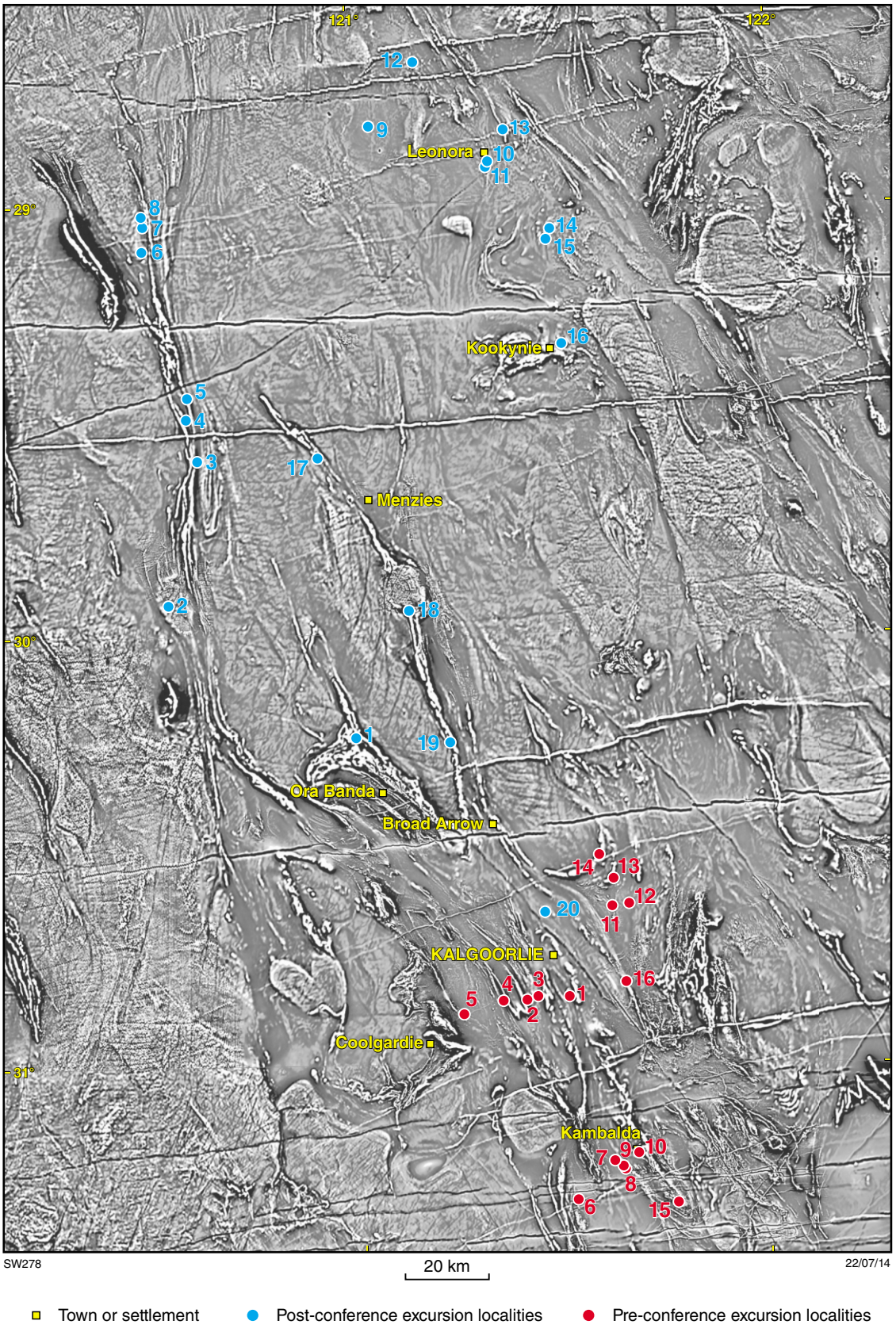

Figure 2. Pre- and post-conference excursion localities shown on a TMI 1VD aeromagnetic image

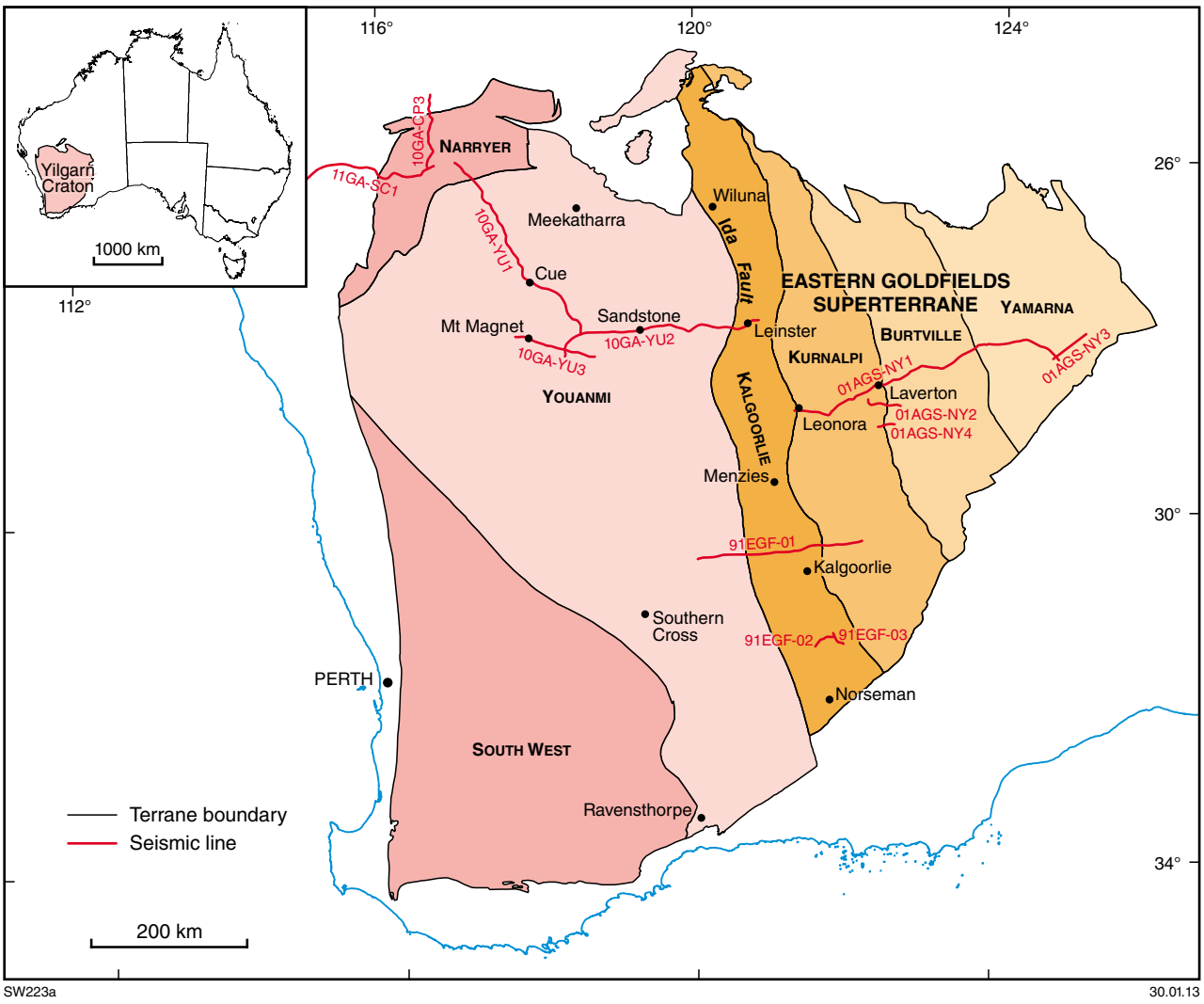

Figure 3. Subdivision of the Yilgarn Craton into tectonostratigraphic terranes; names in bold capitals (modified from Pawley et al., 2012)

Yilgarn Craton

Cassidy et al. (2006) divided the Yilgarn Craton into terranes defined on the basis of distinct sedimentary and magmatic associations, geochemistry, and ages of volcanism. The Narryer and South West Terranes in the west are dominated by granite and granitic gneiss with minor supracrustal greenstone inliers, whereas the Youanmi Terrane and the Eastern Goldfields Superterrane contain substantial greenstone belts separated by granite and granitic gneiss. Subsequent revision has further subdivided the Eastern Goldfields Superterrane into the Kalgoorlie, Kurnalpi, Burtville and Yamarna Terranes (Fig. 3; Pawley et al., 2012).

The Ida Fault (Fig. 3), which marks the boundary between the western Yilgarn Craton and the Eastern Goldfields Superterrane, is a major structure that extends to the base of the crust (Drummond et al., 2000). Various geophysical techniques, including deep-crustal seismic seismic surveys (Drummond et al., 2000; Goleby et al., 2004), seismic receiver-function analysis (Reading et al., 2007), and magnetotelluric surveys (Dentith et al., 2012), show the Yilgarn crust to be 32–46 km thick, with the shallowest Moho beneath the Youanmi Terrane. The crust is thicker in the southwest, and thickest in the eastern part of the Eastern Goldfields Superterrane. Seismic and gravity data suggest that the greenstones are 2–7 km thick (Swager et al., 1997).

Isotopic data, including Sm–Nd (Fig. 4; Champion and Cassidy, 2007) and Lu–Hf (Mole et al., 2010; Wyche et al., 2012) data, show that the terrane subdivisions of the Yilgarn Craton reflect regions with distinctive crustal histories. The Narryer Terrane, which contains both the oldest detrital zircons found on Earth (back to c. 4400 Ma; Wilde et al., 2001) and the oldest rocks in Australia (back to c. 3730 Ma; Kinny et al., 1988), shows abundant evidence of very old model ages. The Youanmi Terrane has a more mixed history, whereas the Eastern Goldfields Superterrane is distinctly more juvenile than the terranes to the west.

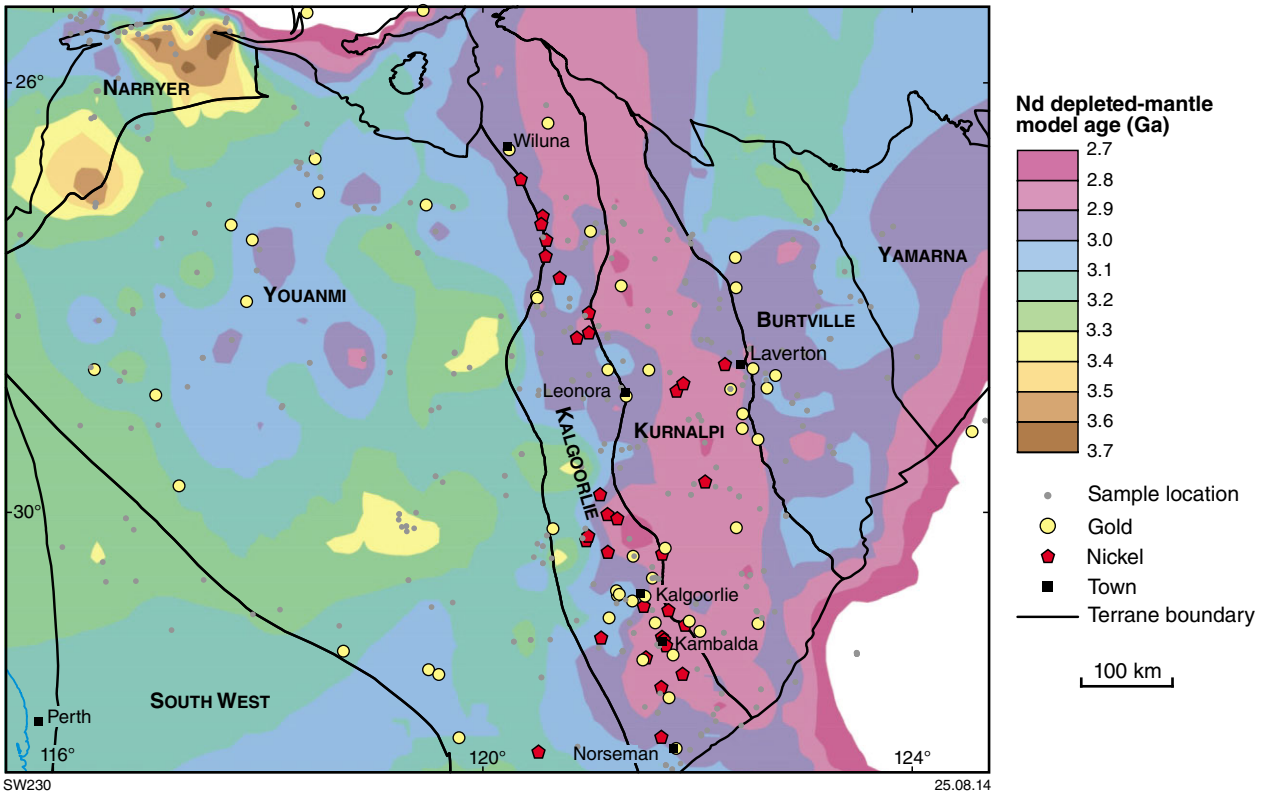

Figure 4. Nd depleted-mantle model age map for the Yilgarn Craton showing terrane subdivisions and locations of major nickel and gold deposits (modified from Champion and Cassidy, 2007)

Yilgarn granite–greenstones

The supracrustal rock record in the Yilgarn Craton dates back to at least c. 3080 Ma in the Youanmi Terrane in the west (Yeats et al., 1996; Rasmussen et al., 2010; Van Kranendonk et al., 2013; Wang et al., 1998) and c. 2960 Ma in the Burtville Terrane in the northeast (Pawley et al., 2012). However, greenstone successions across the Yilgarn Craton are dominated by rocks that formed after c. 2820 Ma.

In the central Youanmi Terrane, a cycle of mafic–ultramafic–felsic volcanism between c. 2820 and 2735 Ma is likely due to a major plume that produced large mafic–ultramafic layered intrusions between c. 2820 and 2800 Ma (Ivanic et al., 2010), coincident with similar, but less voluminous, magmatism in the eastern part of the craton (Wyche et al., 2012). This event may have resulted in partial breakup of the early Yilgarn Craton with rifting in the east (Czarnota et al., 2010) and incipient rifting marked by younger Nd model ages and the layered intrusions in the Youanmi Terrane (Ivanic et al., 2010). A protracted period of mafic–felsic volcanism and associated sedimentation continued from c. 2800 to 2735 Ma. Calc-alkaline volcanism was dominant after c. 2760 Ma, and broadly coincided with a period of mafic tonalite–trondhjemite–granodiorite (TTG) and enriched high field strength element (HFSE) granite magmatism (Cassidy et al., 2002; Van Kranendonk et al., 2013).

The last recognized regional greenstone-forming event in the Youanmi Terrane was a mafic–felsic volcanic cycle between c. 2740 and 2725 Ma (Van Kranendonk et al., 2013), which was contemporaneous with high-Ca TTG granite magmatism (Cassidy et al., 2002).

Except for rare greenstones in the South West Terrane (Allibone et al., 1998), after c. 2715 Ma volcanic activity and greenstone development in the Yilgarn Craton was restricted to the Eastern Goldfields Superterrane. Andesite-dominated calc-alkaline volcanism in the eastern Kurnalpi Terrane (Figs 3 and 5; Barley et al., 2008) and dacitic volcanism in the northern Kalgoorlie Terrane (Rosengren et al., 2005) was prevalent between c. 2715 and 2705 Ma (Fiorentini et al., 2005; Kositcin et al., 2008). Barley et al. (2008) interpreted the andesite-dominated successions as oceanic intra-arc volcanic centres.

In the Eastern Goldfields Superterrane, a second major plume event (Campbell and Hill, 1988) produced voluminous komatiites which occur as both high-level intrusions and flows (Trofimovs et al., 2004b; Fiorentini et al., 2005; Fiorentini, 2010). They are preserved in a distinct north to northwesterly trending belt, 600 x 100 km, between Norseman and Wiluna (Fig. 3). The mafic–ultramafic succession also contains tholeiitic and komatiitic basalts (Lesher, 1983; Said and Kerrich, 2009; Squire et al., 1998). It is well constrained between c. 2710 and 2692 Ma (Kositcin et al., 2008) and partly

overlaps in age with the andesite-dominated calc-alkaline volcanism. The Norseman–Wiluna komatiites, which host major nickel deposits, are not only younger than ultramafic rocks in the Youanmi Terrane, but also differ in chemical character. Komatiites of the Youanmi Terrane include Al-depleted, and Al-undepleted and Ti-enriched varieties, whereas those in the Norseman–Wiluna belt are Al-undepleted (Barnes et al., 2007). Abundant sensitive high-resolution ion microprobe (SHRIMP) geochronological data on greenstones from throughout the Eastern Goldfields Superterrane (Kositcin et al., 2008; GSWA, 2014) suggest that thinner and more sparsely distributed komatiite units east of the Norseman–Wiluna belt (e.g. east and southeast of Leonora; Fig. 5) are mainly the same age as the more voluminous material within the main belt and may represent thin flows or channel deposits, which have travelled farther as result of paleotopography.

Between c. 2692 and 2680 Ma, volcanic centres in the western part of the Kurnalpi Terrane produced bimodal (basalt–rhyolite) volcanic and associated intrusive and sedimentary rocks (Fig. 5), coinciding with the main period of high HFSE granite magmatism (Cassidy et al., 2002). Barley et al. (2008) interpreted these successions, the Gindalbie association, as representing an arc-rift environment. Gindalbie-style volcanism, which locally hosts VHMS mineralization, overlapped in age with, and was succeeded by, TTG volcanism and associated sedimentary rocks and mafic intrusions represented by the Black Flag Group in the Kalgoorlie Terrane (Fig. 5). The deposition of the Black Flag Group between c. 2690 and 2660 Ma coincided with voluminous high-Ca TTG granite magmatism in the Eastern Goldfields Superterrane (Champion and Cassidy, 2007). Krapež and Hand (2008) interpreted the Black Flag Group (their 'Kalgoorlie Sequence') as representing a strike-slip intra-arc basin, whereas Squire et al. (2010) argued that they are the result of volcanism and sedimentation associated with extensional deformation due to the emplacement of large granite batholiths. Felsic volcanic and associated plutonic rocks of this age have also been recorded in a poorly exposed bimodal greenstone succession in the Yamarna Terrane in the far east of the Eastern Goldfields Superterrane (Fig. 3; Pawley et al., 2012). Barnes and Van Kranendonk (2014) argued that all of these associations can be explained entirely within a plume-driven tectonic setting.

The youngest supracrustal successions in the Yilgarn Craton are the so-called 'late basins', which rest unconformably on all earlier greenstones in the Eastern Goldfields Superterrane. Likely deposited in a very short time (about 10 m.y.) after c. 2665 Ma (Squire et al., 2010), they preserve fluvial and deep-marine facies, which Krapež and Barley (2008) interpreted as having formed in a tectonic escape corridor after arc closure. The late-basin sediments, which range from turbidites through to coarse, braided-stream sediments (Krapež et al., 2008), contain a range of detrital zircon ages and postdate the cessation of TTG granite magmatism. They contain material derived from both proximal and distal sources during ongoing extension and uplift (Squire et al., 2010).

Finally, the cessation of greenstone deposition was accompanied by cratonwide, low-Ca granite magmatism (Cassidy et al., 2002). A distinctive belt of alkaline granites, emplaced at this time, appears to coincide with deeply penetrating crustal structures and is mainly restricted to the Kurnalpi Terrane (Smithies and Champion, 1999).

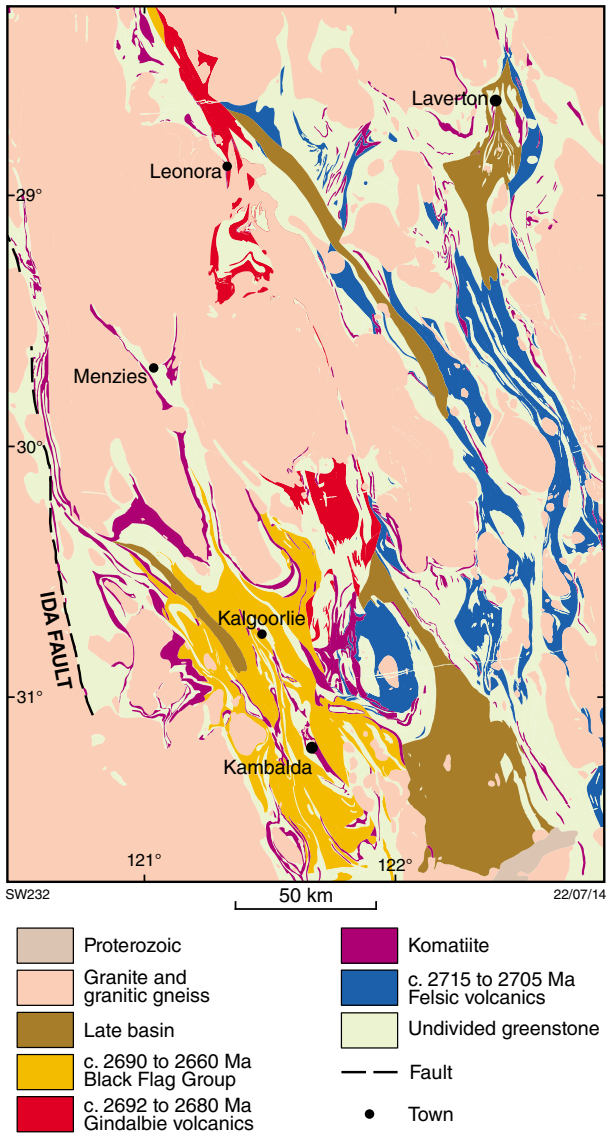

Figure 5. Distribution of main volcanic facies in the central part of the Eastern Goldfields Superterrane

Eastern Goldfields — stratigraphy and structure

Stratigraphy

Poor exposure, deep weathering, lack of detailed geochronology, and structural and metamorphic overprints preclude description of detailed stratigraphy in many of the Yilgarn greenstones. West of the Ida Fault (Fig. 3), only the northwestern part of the Youanmi Terrane has an established stratigraphy (Van Kranendonk et al., 2013). East of the Ida Fault, local stratigraphy has been established in some greenstone belts (Kositcin et al., 2008) but detailed regional stratigraphy has been described only for the southern part of the Kalgoorlie Terrane.

The southern Kalgoorlie Terrane (Fig. 6; Woodall, 1965; Gresham and Loftus-Hills, 1981; Swager et al., 1995) comprises a lower mafic–ultramafic succession consisting of the Lunnon Basalt, Kambalda Komatiite (including the Silver Lake and Tripod Hill Members), Devon Consols Basalt, Kapai Slate and Paringa Basalt. The mafic–ultramafic succession is unconformably overlain by the Black Flag Group, which comprises extensive volcaniclastic rocks, rhyolitic to dacitic volcanic rocks, intrusive mafic complexes and minor mafic volcanic rocks (Squire et al., 2010). The late-basin sediments are represented in this area by polymictic conglomerate of the Kurrawang Formation, which contains a variety of clasts, including banded iron-formation and granite that indicate a distal provenance, probably in the Youanmi Terrane (Krapež et al., 2008). In less deformed areas, many primary igneous features and textures are still visible despite locally complete replacement by alteration assemblages.

The abundant pillow lavas and hyaloclastites in basalts, the presence of marine sediments, and quench textures in komatiites and basalts, indicate a submarine eruption of the mafic–ultramafic succession (Hill et al., 1995; Squire et al., 1998; Said and Kerrich, 2009). Squire et al. (1998) proposed that the Lunnon Basalt is either distal to a shield volcano, or represents a ponded lava field in an extensional basin distant from the eruptive centre. Similarly, Hill et al. (1995) suggested that the komatiite flows at Kambalda are distal deposits in contrast with the thick, cumulate dunite bodies to the north and northwest of Kalgoorlie (Fig. 5), which are proximal to the eruptive centre.

The nature of basement to the mafic–ultramafic succession in the Kalgoorlie region is unknown. Xenocrystic zircon age data (Compston et al., 1986), and trace element and isotopic data suggest the mafic–ultramafic succession may have been generated through varying degrees of crustal contamination (Arndt and Jenner, 1986) and mixing of a depleted mantle source with an enriched subcontinental lithospheric mantle (Said and Kerrich, 2009). Model age data based on Lu–Hf analyses on zircons have peaks after 3.5 Ga, and mainly after 3.1 Ga. This is significantly younger than the earliest model age recognized in the Youanmi Terrane (Wyche et al., 2012).

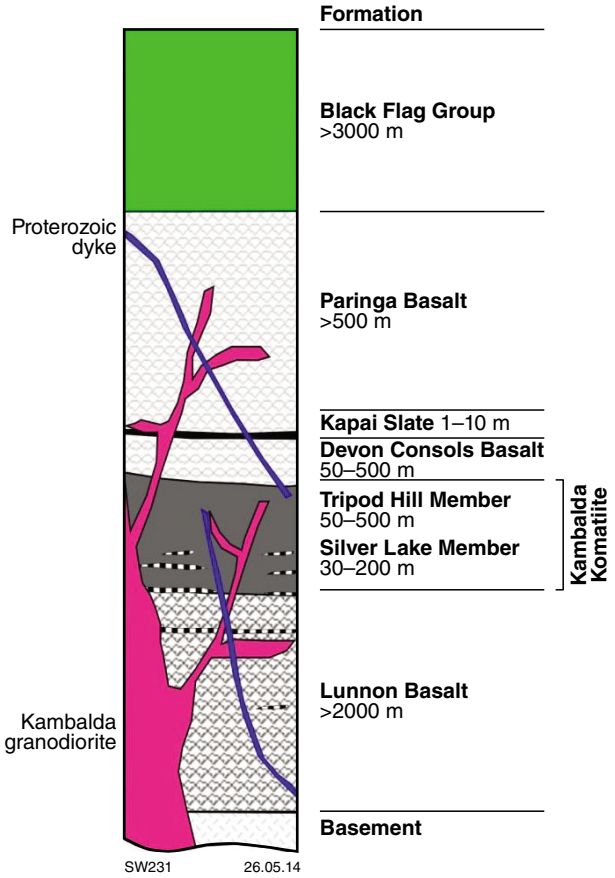

Figure 6. Kambalda stratigraphy (modified from Beresford et al., 2005)

Structure and metamorphism

Building on the regional framework established by Swager (1997), Blewett et al. (2010a) produced a six-stage, integrated structural-event framework (Fig. 7) for the Eastern Goldfields Superterrane to account for the documented magmatic, depositional, structural and metamorphic history (Czarnota et al., 2010). In this scheme, the period of greenstone deposition between c. 2715 and 2705 Ma, characterized by calc-alkaline and komatiite magmatism, was a time of dominantly extensional tectonics that marked the initiation of regional-scale granite doming.

The deposition of the Black Flag Group, between c. 2690 and 2660 Ma, was accompanied by the widespread emplacement of a high-Ca TTG granite suite. Granite doming was probably coeval with local contraction indicated by upright folding and dextral shearing at this time. The peak period of granite doming began during the last depositional phase of the Black Flag Group (Squire et al., 2010). Ongoing doming and extension produced the clastic late-basin sediments. After the cessation of high-Ca magmatism, low-Ca granite magmatism, which appears to be the result of melting of a mid–lower crustal

source of TTG/high-Ca composition (Champion and Cassidy, 2007), was accompanied by a major contractional deformation, which produced both upright folds and regional-scale sinistral shearing that may have reactivated earlier structures. Subsequent, relatively minor, brittle contractional and extensional events affected the now rigid Yilgarn Craton (Czarnota et al., 2010).

Local evidence of early, low-pressure granulite-facies metamorphism, consistent with a high geothermal gradient (Fig. 7; Goscombe et al., 2009), was contemporaneous with the eruption of the Norseman–Wiluna komatiites. Later medium-pressure metamorphism was most likely due to exhumation of deep-seated early structures around granite domes (Goscombe et al., 2009). Subsequent periods of low-pressure metamorphism, accompanied by moderate- to high-geothermal gradients, reflect exhumation during granite doming prior to and during late-basin development. Very low pressures and geothermal gradients mark the end of the period of granite doming and the initiation of widespread exhumation (Goscombe et al., 2009).

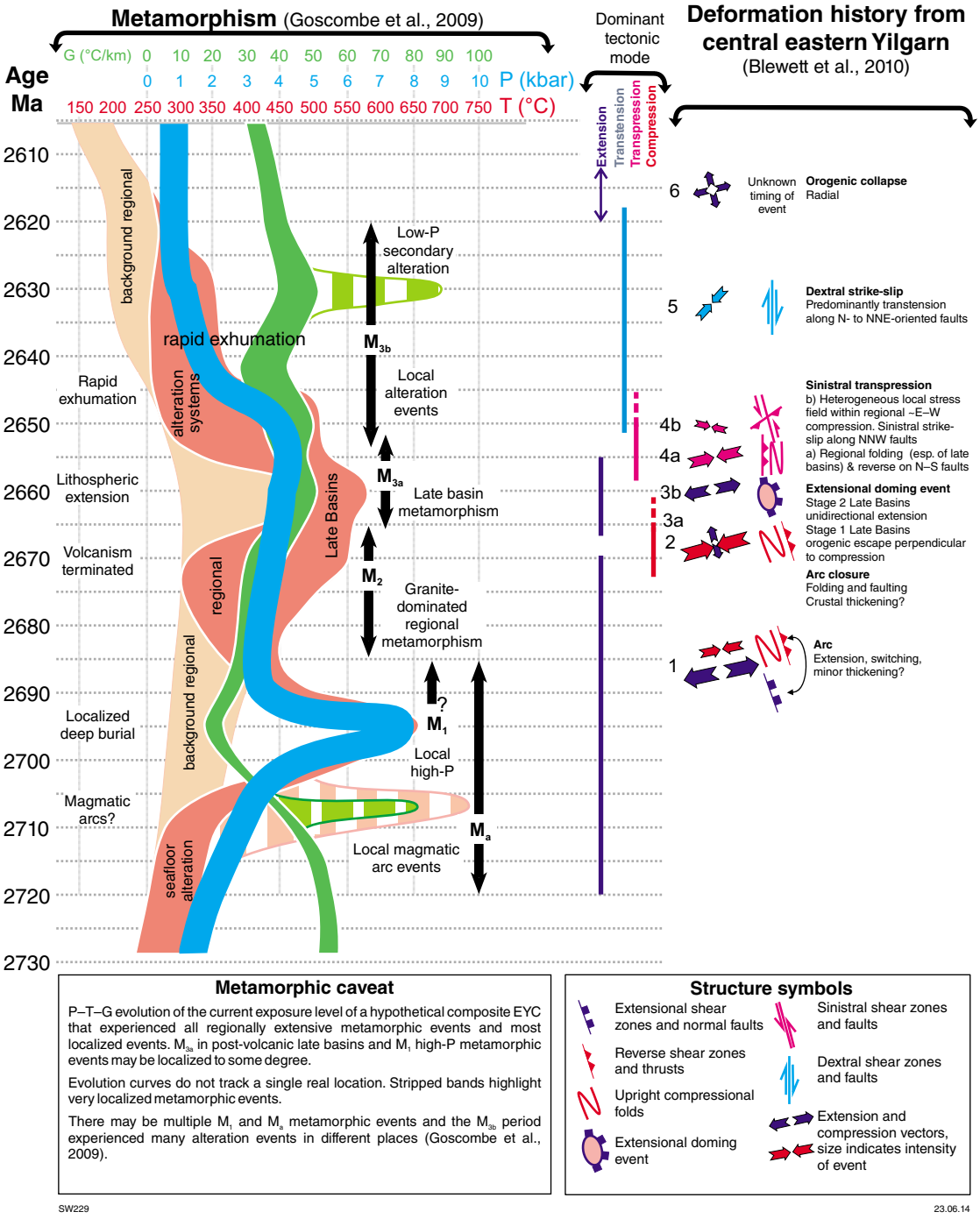

Figure 7. Metamorphic and structural history of the Eastern Goldfields Superterrane (modified from Czarnota et al., 2010)

Eastern Goldfields — nickel and gold

The stratigraphy, structure and metamorphic history of the southern Kalgoorlie Terrane remain the most comprehensively studied and documented part of the Yilgarn Craton. Consequently, this region provides the best insight into the multi-scale factors that control the distribution of the world-class nickel and gold deposits of the eastern Yilgarn Craton.

Nickel

The most significant recent advances in understanding komatiite-hosted nickel-sulfide deposits in the Yilgarn Craton (Barnes, 2006) have been the recognition of: 1) different modes of emplacement, sulfur assimilation, and the difference in resultant mineralization styles; and 2) large-scale architectural control on the location of nickel-sulfide deposit clusters. This new understanding has come from work on a number of major nickel deposits in the Eastern Goldfields such as Mount Keith (Fiorentini et al., 2007), Black Swan (Barnes, 2004) and Kambalda (Gresham and Loftus-Hills, 1981; Lesher, 1983). The Kambalda deposits were the first discovered and have the longest history of both exploitation and research. They provide a useful illustration of how factors at all scales affect the accumulation of major nickel deposits in this geological province.

Nickel-sulfide mineralization was first discovered at Kambalda (Fig. 5) in 1966, about 70 years after the discovery of gold in the region. Mineralization is hosted in the Kambalda dome, a doubly plunging anticline cored by granitic intrusions, which post-date the nickel-sulfide mineralization. Mineralization is primarily within the volcanic stratigraphy exposed along the flanks of the intrusions and occurs as discontinuous to semi-continuous lenticular bodies termed 'ore shoots' (Gresham and Loftus-Hills, 1981). The local stratigraphic, metamorphic and structural history at Kambalda closely reflects the regional history in the Kalgoorlie Terrane.

Geodynamic setting of the Kambalda nickel deposits

Begg et al. (2010) argued that fundamental lithosphere-scale architecture has a major influence on the distribution of magmatic-hosted nickel deposits and showed that most nickel deposits in the Eastern Goldfields are found along the boundaries of very early developed lithospheric blocks. The Nd model-age map of the Yilgarn Craton (Fig. 4) shows the distribution of major nickel and gold deposits in the Eastern Goldfields in relation to the model ages.

The isotopic map can be interpreted as providing a snapshot of the lithospheric architecture at 2.65 Ga. This map can be considered as a proxy to image major lithospheric discontinuities, which may have acted as active pathways for large volumes of hot, mantle-derived melt to reach upper crustal levels without undergoing any significant differentiation. In other words, steep colour gradients (interpreted as lithosphere-scale boundaries) in Figure 4 show areas where hot magmas were most likely focused.

Highly mineralized komatiites are most abundant on the western side of the Eastern Goldfields Superterrane, along the boundary between the isotopically juvenile part of the Kalgoorlie Terrane and the older Youanmi Terrane (Fig. 4). This boundary may represent a significant lithospheric discontinuity at 2.7 Ga, along which high volumes of hot komatiites were emplaced and interacted with crustally derived sulfur (cf. Bekker et al., 2009) to generate giant nickel-sulfide ore systems.

Nickel-sulfide mineralization at Kambalda

The complete mafic–ultramafic stratigraphy of the Kalgoorlie Terrane is exposed at Kambalda, including the tholeiitic Lunnon Basalt (Fig. 6). Nickel mineralization is hosted in the Silver Lake Member of the Kambalda Komatiite. Thin, sulfidic sedimentary units, comprising dominant pale siliceous sediments, dark, carbonaceous slaty sediments, and minor mafic sediments occur throughout the mafic–ultramafic succession, but are most abundant within the Silver Lake Member of the Kambalda Komatiite (Bavinton, 1981; Gresham and Loftus-Hills, 1981). These sediments may have been a source of sulfur for the mineralization (Lesher and Campbell, 1993).

Basal contact mineralization between the ultramafic flows of the Kambalda Komatiite and the underlying Lunnon Basalt occurs within troughs or channels in the top of the footwall basalts (Lesher, 1983). These troughs or channels have been interpreted as primary features formed through thermal-mechanical erosion by flowing ultramafic lavas that cut down into the sediments overlying the pillowed basalts of the Lunnon Basalt (Lesher, 1983; Beresford et al., 2005). Alternatively, troughs could have formed along pre-existing faults with syneruptive graben development (Connors et al., 2002), or during subsequent deformation of the greenstone belt (Stone and Archibald, 2004; Stone et al., 2005). A combination of mechanisms is most likely responsible for the current ore surface configuration.

Troughs in the Kambalda dome area vary in size, but are commonly narrow and elongate with lengths up to 2300 m and widths to 300 m (Gresham and Loftus-Hills, 1981). Mineralization in major troughs is mainly continuous and occurs as small (20–130 m), elliptical orebodies in minor troughs. Stratiform, hangingwall ore is spatially associated with the basal ore but stratigraphically higher, typically at the contact between first and second flow units and within 100 m of the komatiite–basalt contact (Gresham and Loftus-Hills, 1981). Some secondary orebodies have been produced by the remobilization of sulfides into areas of dilation and lower tectonic pressure (e.g. fold hinges, fault dilation zones and shear zones) away from the primary accumulation site (Lesher and Keays, 2002).

The Kambalda nickel deposits illustrate how a series of scale-dependent processes, which are reflected in different datasets, have aligned to focus komatiitic magmas and nickel-sulfide deposits from the craton to deposit scale.

Gold

The Eastern Goldfields has produced more than 130 Moz of gold. While there are more than 20 deposits with >1 Moz of contained gold in the region, the Golden Mile at Kalgoorlie is unique in terms of its size and historical production of more than 50 Moz (DMP, 2012).

The three recent key advances in the understanding of the distribution of gold mineralization in the Eastern Goldfields are: 1) the recognition of the influence of large-scale lithospheric architecture on the localization of mineralization; 2) the recognition of multiple sources of fluid involved in the deposit genesis, sparking a resurgence of intrusion-related mineralization models; and 3) the recognition of multiple timings of mineralization within single gold deposits or deposit clusters.

Other important advances include the recognition that at least some high-temperature deposits have been metamorphosed and the characterization of large-scale footprints of gold-related hydrothermal alteration that can be potentially be mapped by combinations of spectral and lithogeochemical means.

Large-scale lithospheric architecture

Blewett et al. (2010b) showed that the distribution of large gold deposits in the Eastern Goldfields is controlled by a favourable convergence of factors from the lithospheric to the deposit scale. A variety of approaches to examining deep-crustal structures, including potential field, magnetotelluric, seismic tomography and reflection seismic data, in combination with regional isotopic data, have allowed interpretation of deep, crust-penetrating shear zones which link to structures identified in the upper crust (Blewett et al., 2010b). These fundamental structures, which may act as conduits for fluids, reflect the deep structures identified by Begg et al. (2010) as playing a major role in the distribution of nickel deposits.

Metal sources

Recent paragenetic and analytical studies have indicated the involvement of three fluids in gold deposits of the Eastern Goldfields (Walshe et al., 2009): 1) a reduced and acid fluid, interpreted to be derived from the upper crust; 2) an oxidized fluid, interpreted as sourced from oxidized magmas; and 3) a reduced fluid, interpreted as sourced from the lower crust or mantle. Despite debate concerning the timing and genesis of the fluids, there is a mounting body of evidence that differing alteration signatures can be detected in regional datasets, including spectral and lithogeochemical data, when normalized to rock type. Recent work indicates that gold is deposited at gradients in mineralogy and chemistry visible in these datasets. Thus they provide the potential to map alteration systems and possible sites of deposition (Neumayr et al., 2008).

Timing and structural controls on gold mineralization

The distribution of gold mineralization is structurally controlled, and the timing, style and reactivation of structures are major factors in determining the size of deposits. Blewett et al. (2010a) suggested that gold was deposited through most of the deformation history but that the major mineralization took place after the D_3 deformation (Fig. 7), with Vielreicher et al. (2010) demonstrating, via a variety of techniques, that the main Golden Mile mineralization at Kalgoorlie took place about 2642 Ma.

Although the mineralization event at Kalgoorlie was quite late with respect to the overall structural history of the region, various stages of the structural evolution were responsible for the creation of favourable sites for gold deposition. Weinberg et al. (2004) recognized that deviations on the Boulder–Lefroy shear zone — a major structure common to a number of large deposits in the Kalgoorlie district — provided a first-order focus for the concentration of mineralizing fluids in the Kalgoorlie region. These deviations or jogs, which are spaced about 30 km apart, were developed during the sinistral transpression stage (D_{4b}; Fig. 7) of Blewett et al. (2010a), probably at about the same time as the main mineralizing event. Going back in time, the extensional event that is associated with granite doming and the development of the late basins (D_3; Fig. 7), played a major role in the creation of sites favourable for gold deposition (Hall, 2007) through the development of suitable fluid pathways (Blewett et al., 2010a).

Going further back in time, a significant recent advance in understanding gold mineral systems has been the recognition of the role that the very early structural architecture of greenstone belts plays on the clustering of gold deposits. Studies at St Ives near Kambalda (Figs 4 and 5) have shown that a structural architecture, established at the time of mafic–ultramafic volcanism at c. 2700 Ma, has been continually reactivated over about 70 million years, controlling the subsequent greenstone depositional events, all subsequent responses of the crust to deformation and the location of gold deposits (Miller et al., 2010).

Summary

Taken together, the advances in understanding craton-scale control on deposit clusters, and emplacement controls on deposit style and mineralization potential, can be used as scale-dependent proxies for exploration (McCuaig et al., 2010). The isotopic datasets can be used as proxies for identifying regions with high potential magma and fluid flux, whereas stratigraphic components such as felsic volcanic and associated sediments, mappable komatiite thickness and presence of assimilated volcanogenic sulfur, may mark the position of rifts within these belts, and therefore, regions with the highest potential for nickel sulfide- and VHMS-ore concentrations. Furthermore, these fundamental flaws in the crust appear to control the subsequent response of the crust to deformation and have again focused fluids during late-cratonic gold mineralization. An understanding of the local structural architecture and chemically receptive host rocks for hydrothermal mineralization becomes important at the scale of clusters of deposits, and individual deposits.

Pre-conference excursion — structural and stratigraphic setting of mineral deposits in the Kalgoorlie district

This excursion (Figs 8, 9) examines the structural and stratigraphic setting of mineral deposits in the Kalgoorlie–Kambalda region. The itinerary includes outcrops that show the range of lithotypes and highlight the difficulties in determining stratigraphic correlations in this region. The excursion visits two distinctly different auriferous deposits.

All locality descriptions by S Wyche, NL Patison, and MJ Pawley unless otherwise indicated.

Locality 1: Mount Hunt

Modified from Swager (1990) and Wyche (2007)

Hannan Lake and Mount Hunt

Most of the described stratigraphy of the southern Kalgoorlie Terrane, except for the lower basalt unit that is not exposed in the Kalgoorlie district, can be seen in the Mount Hunt area. The komatiite unit is represented by the Kambalda Komatiite (formerly called the 'Hannan Lake Serpentinite'; Travis et al., 1971), and the Devon Consols Basalt. The Kapai Slate marks the top of the Devon Consols Basalt. The Paringa Basalt, which represents the upper basalt unit, occupies the highest part of Mount Hunt. The Black Flag Group, which outcrops on the western side of the Goldfields Highway, represents the upper felsic volcanic and volcaniclastic association. The late-basin succession is not exposed at Mount Hunt, but lies about 10 km to the west, where it is represented by the Kurrawang Formation.

The Hannan Lake – Mount Hunt traverse examines the stratigraphy of the Kambalda Domain, which is interpreted as a D_1 thrust sheet, repeating and overlying the sequence at Kambalda. The traverse crosses the axial plane of the regional F_2 anticline, the northern continuation of the Kambalda Anticline. The F_2 hinge is sheared out by the D_3 Boulder–Lefroy Fault. At Hannan Lake, the succession youngs eastwards and is the continuation of the mineralized sequence south from Kalgoorlie. At Mount Hunt, the overall younging is to the west, but the succession is complexly folded and sheared.

The Hannan Lake – Mount Hunt traverse*

Serpentine Bay

Extensive outcrops of serpentinite of the lowest exposed unit of the Kambalda Komatiite are found on the western shore of Hannan Lake (Locality 1 on Fig. 10 — MGA 358690E 6587100N). The rocks at Serpentine Bay are atypical in that they have been strongly affected by talc–carbonate alteration. However, this alteration has preserved spinifex textures indicating the extrusive nature of the ultramafic flows, which vary in thickness 1–10 m. Some flows show classic asymmetries in the spinifex textures (Fig. 11), indicating that the sequence youngs to the east. A typical cumulate base (B-zone) now consists of talc–carbonate–serpentine(–magnetite), which has replaced an original dunite or peridotite with 2–3 mm olivine grains. The spinifex zones, with coarse sheaf-spinifex blades up to 30 cm long followed by fine-grained, random spinifex and a thin aphanitic flow top, are now talc–carbonate–albite–chlorite(–magnetite). Albite content may be up to 15%.

To the west, the bulk of the Kambalda Komatiite is a strongly serpentinized orthocumulate peridotite comprising medium-grained, granular olivine pseudomorphs with interstitial amphibole and chlorite. East of the headland (Fig. 10), islands in Hannan Lake contain east-facing pillow basalt (Devon Consols Basalt), cherty sedimentary rock (Kapai Slate), and komatiitic basalt (Paringa Basalt). Deep drilling below the lake has helped establish the regional stratigraphy (Travis et al., 1971).

Mount Hunt

The outcrop of Devon Consols Basalt at the start of the Mount Hunt traverse is best exposed in the creek immediately south of the track (Location 2 on Fig. 10 — MGA 357824E 6586567N). Here it consists of variolitic basalt with well-preserved pillow structures. The pillows have a pale, feldspar-rich core and a greenish marginal phase with a groundmass of chlorite, clinozoisite, and tremolite (Hallberg, 1972). A transitional zone between core and margin consists of varioles made up of locally coalescing, spherical masses of radiating albite and amphibole plus chlorite, i.e. uralitized acicular pyroxene, whereas the marginal phase consists of plagioclase ($An_{5–25}$) in a felted groundmass of chlorite, clinozoisite, and tremolite (Hallberg, 1972). The origin of the varioles remains unresolved, but they are common in basalts at the lower end of the MgO range within high-Mg series (10–18 wt% MgO). Because they locally overprint primary volcanic structures, but have themselves been deformed during regional deformation events, the varioles may represent early alteration or devitrification textures.

A few metres west of the creek, the Kapai Slate, which overlies the Devon Consols Basalt, outcrops as a well-exposed chert marker (MGA 357785E 6586530N). At depth, the chert becomes carbonaceous and pyritic slate. Several episodes of deformation are indicated by the presence of small-scale, low-angle faults and two phases of steep-dipping, tight folds.

* Locality descriptions are mainly modified from Griffin et al. (1983), and (Keats, 1987), with contributions from Hallberg (1972), Williams and Hallberg (1973), and Groves and Gee (1980)

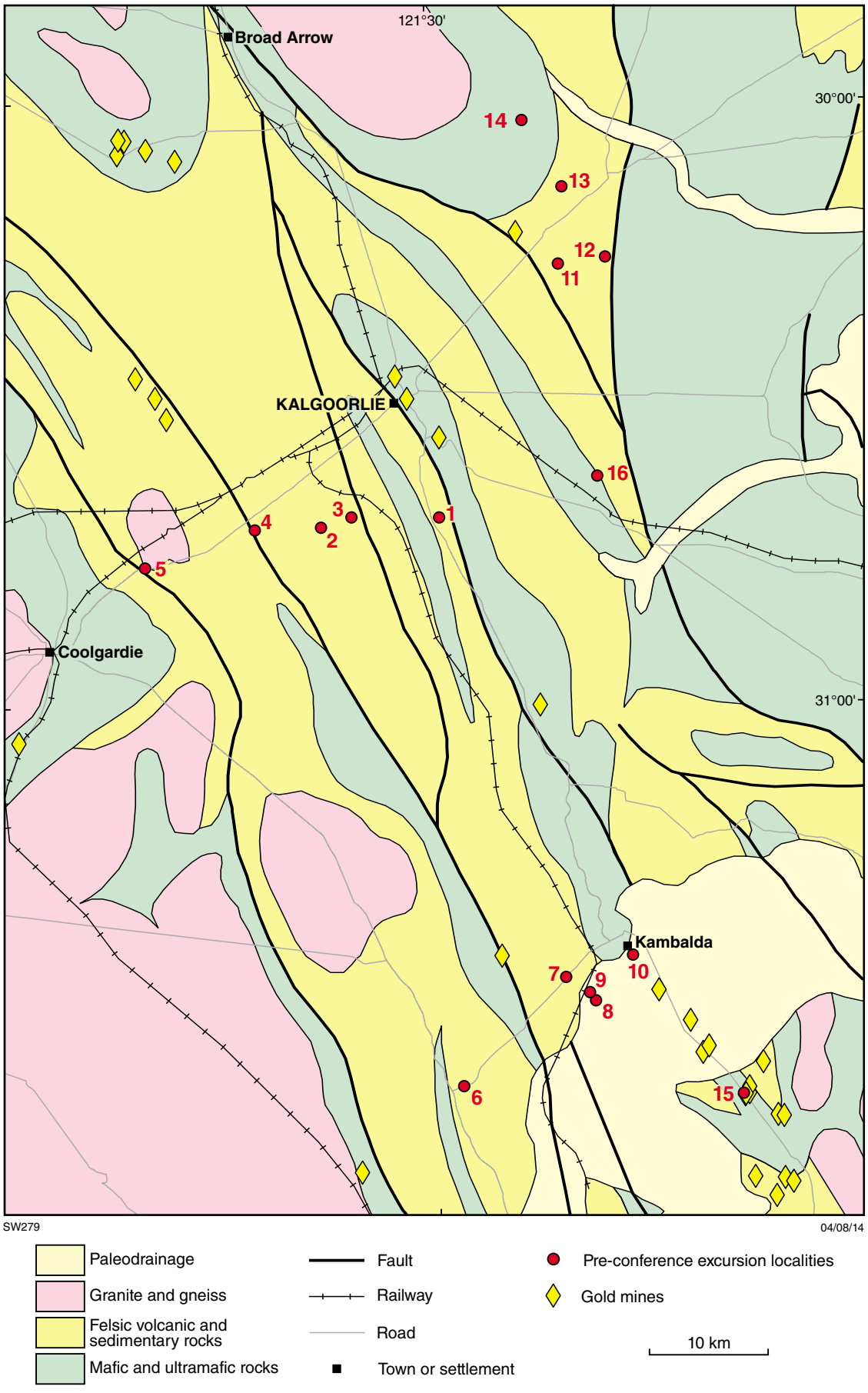

Figure 8. Pre-conference excursion localities showing major gold deposits

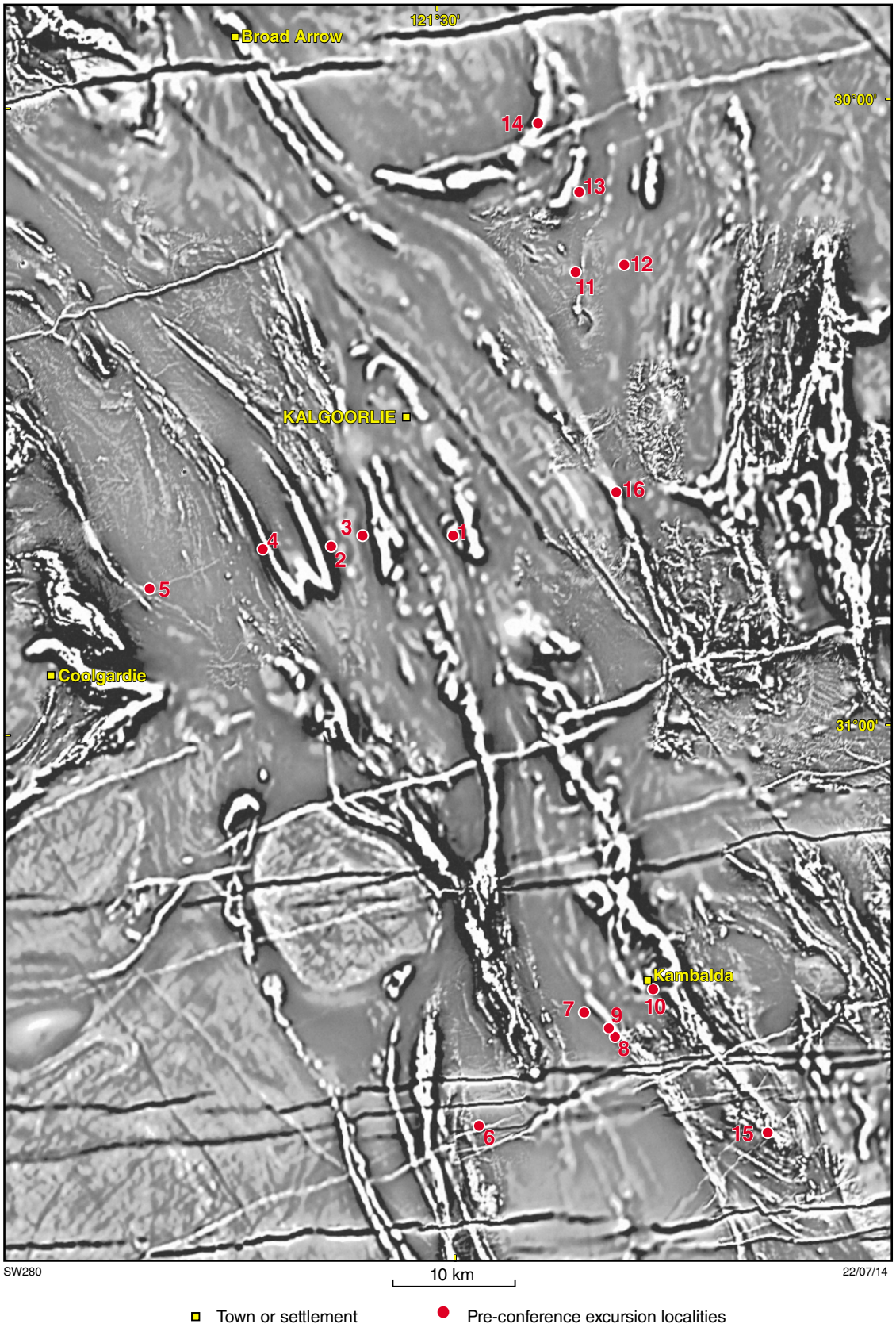

Figure 9. Pre-conference excursion localities shown on a TMI 1VD aeromagnetic image

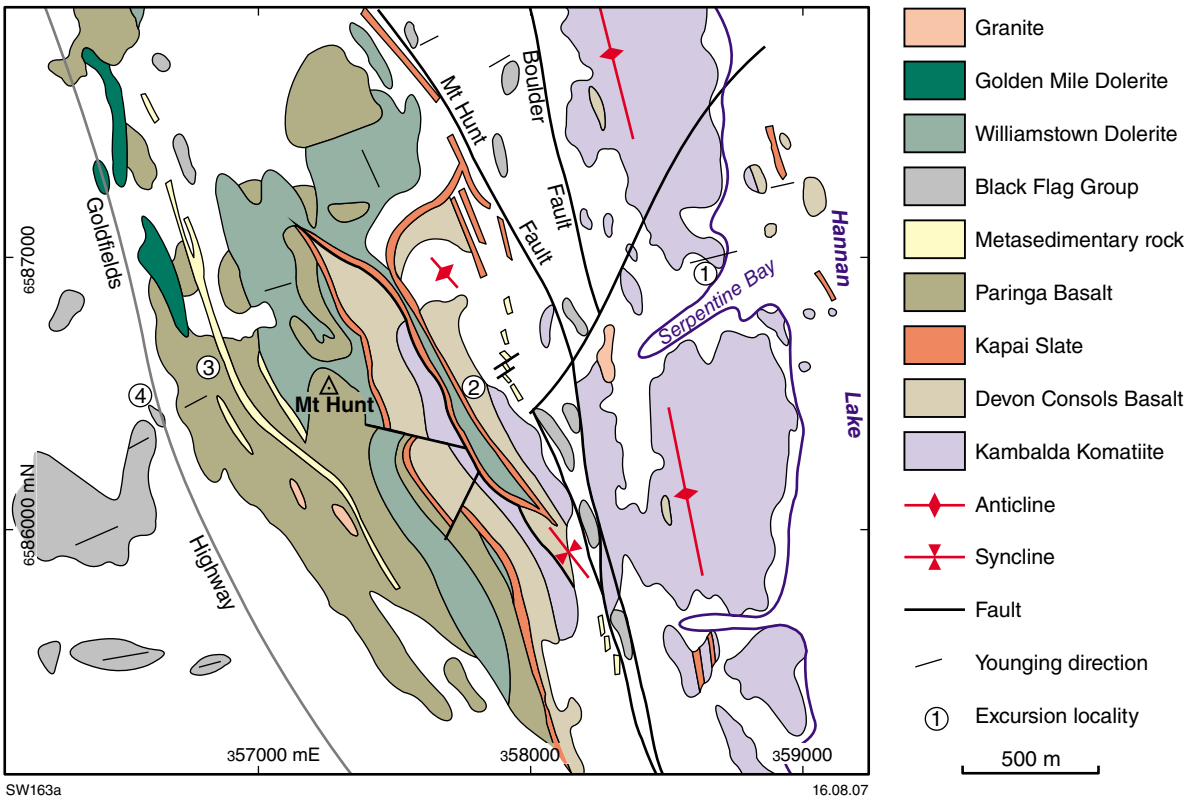

Figure 10. Outcrop sketch of the Mount Hunt – Hannan Lake area (adapted from Griffin et al., 1983; Keats, 1987)

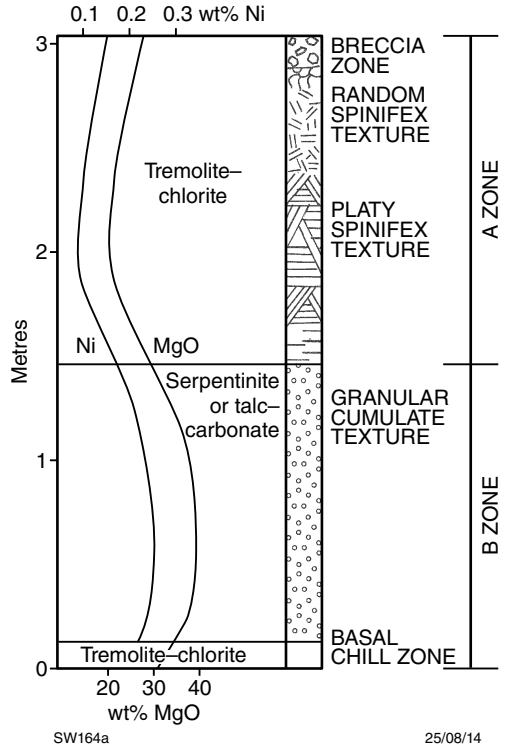

Figure 11. Diagrammatic section and geochemical profile through a thin, unmineralized, metamorphosed komatiite flow unit differentiated from peridotite to picrite (after Marston, 1984)

Immediately west of the Kapai Slate and south of the track, the base of the Williamstown Dolerite can be seen in small rubbly outcrops of peridotite, now a talc–tremolite–serpentine(–magnetite–apatite) rock. Euhedral olivine has been pseudomorphed by serpentine; euhedral prismatic orthopyroxene has been replaced by talc–tremolite; and intergranular clinopyroxene has been replaced by chlorite, serpentine, or both. Farther south, a more differentiated portion of the Williamstown Dolerite consists of gabbro in which pyroxene has been altered to fine, fibrous tremolite and chlorite, and to plagioclase that is partially altered to chlorite.

Williams and Hallberg (1973) studied the Williamstown Dolerite sill in some detail in the hinge of the major fold, about 1 km to the north. They showed that the sill outcrops continuously over at least 2 km, is bifurcated, has a thickness of about 400 m, and displays marked differentiation. All primary minerals are altered, but texture preservation allows recognition of the original mineralogy. A lower ultramafic zone consisted of a peridotite unit (olivine and orthopyroxene) overlain by a thin orthopyroxenite unit, followed by a mafic zone with a lower norite–gabbro unit (orthopyroxene, plagioclase, and clinopyroxene) and an upper gabbro (plagioclase and clinopyroxene).

Continuing the traverse westwards, the Kapai Slate is crossed again (MGA 357725E 6586490N) in what is interpreted as the west limb of a very tight D_1 syncline.

Next are some small rubbly outcrops of Devon Consols Basalt. A major fault is crossed next and the whole sequence is repeated. A possible interpretation of the geometry is shown in Figure 12. According to this interpretation, an early, isoclinal fold pair (F_1), in which the short limb is thinned and sheared out (Figs 12a,b), was tilted into a steep west-dipping orientation on the west limb of the regional anticline (F_2), and refolded by a discontinuous, asymmetric F_3 fold (Swager, 1989). In the side of the hill, extensive outcrop of variolitic Devon Consols Basalt contains large, weathered-out varioles (MGA 357525E 6586500N). The overlying Kapai Slate is marked by a line of shallow gold workings that have now been infilled (MGA 357495E 6586475N). The Williamstown Dolerite is poorly exposed, being largely covered by talus from Mount Hunt. The final ascent to the summit of Mount Hunt crosses Paringa Basalt, which consists of metamorphosed pyroxene-spinifex-textured basalt characterized by skeletal and acicular amphibole that pseudomorphs primary clinopyroxene, and minor biotite in a matrix of fine-grained amphibole, chlorite, clinozoisite, albite, and quartz. The acicular textures range in scale from a few millimetres up to 30 mm.

Just west of the summit (MGA 357293E 6586523), the Paringa Basalt contains a thin unit (<1 m) of olivine spinifex-textured komatiite. Scattered blocks of the komatiite can be traced along strike, suggesting the unit is in situ. The Paringa Basalt belongs to the high-Th siliceous suite of Barnes et al. (2012). This suite is interpreted to have been derived by the contamination of fractionated komatiitic magmas, thus allowing the possibility of local occurrences of uncontaminated parent magma.

Paringa Basalt

Deeply weathered, pillowed Paringa Basalt outcrops on the eastern side of the highway (Location 3 on Fig. 10; MGA 356815E 6586475N). Younging to the northwest is indicated by the pillows, whose weathered margins are marked by variolitic textures. Breccias, probably representing hyaloclastite, are also preserved (MGA 356785E 6586300N). Fresher material from the breakaway edge consists of metamorphosed komatiitic basalt like that in the rest of the Mount Hunt area.

Some pillows have well-preserved hyaloclastite textures. In particular, one pillow has an irregular, lobate margin with common angular fragments of fine-grained material that have jigsaw fit, and likely represents the remnants of the autobrecciated chilled margin.

The Paringa Basalt is more massive and homogeneous towards the southern end of the outcrop, with little evidence of the pillows that dominate the outcrop to the north. At one locality (MGA 356785E 6586300N), there are several thin (less than 1 m thick) breccia units, one of which has a very irregular lower contact with relief of about 0.5 m. Here, the substrate appears to be breaking up in situ. There is a transition from cracking of the substrate and in-filling of fractures, through angular blocks with jigsaw fit that match the substrate, to a clast-rich breccia over a distance of less than 30 cm. The breccia unit has a relatively planar top. The irregular base, the common in situ jigsaw fit, and the very local deposition of the clasts, may indicate that fragmentation was due to local uplift by inflation of a flow unit. Based on the erosional lower contact of the fragmenting unit, the facing direction is towards the southwest, consistent with the pillow structures to the north.

Black Flag Group

Metasedimentary rocks of the Black Flag Group (Krapež and Hand, 2008; Squire et al., 2010) outcrop on the western side of the Goldfields Highway (Location 4 on Fig. 10 — MGA 356695E 6586300N). Graded bedding, current bedding and scours indicate a consistent westward younging, except where there are local reverses due to minor folding. The basal beds contain zones of oligomictic conglomerate. Farther west, conglomerates are rarer and the sequence contains an appreciable felsic volcaniclastic component.

Minor folds in the sedimentary rocks (MGA 356695E 6586300N) have axial planes that are sub-parallel to the main bedding trend, with the folds forming a narrow zone bounded by a pair of metre-scale layer-parallel shears. The shears have well developed C-S planes and C' extensional shear bands that indicate a dextral sense of shear. The shears also contain abundant blocks of the sedimentary rocks, ranging from millimetre-scale up to 30 cm within a groundmass of very dark, fine-grained material. The blocks are typically elongate, commonly with shapes similar to mica fish and σ-porphyroclasts in mylonites.

Locality 2: Gibson Honman Rock (MGA 350005E 6586552N)

Modified from Morris (1998)

Gibson Honman Rock is an approximately 1 km^2 outcrop of volcanic rocks within the Black Flag Group about 12 km southwest of Kalgoorlie (Fig. 13). It is similar in character to the volcanic rocks exposed at Spargoville east of Kambalda (Locality 6). The outcrop at Gibson Honman Rock consists of poorly sorted, weakly polymictic breccia, rare slate beds, and cohesive felsic lava. Breccia clasts are of fine-grained porphyritic volcanic rock (dacite or possibly rhyolite) and less common slate. Clasts of volcanic rocks reach a maximum diameter of 2 m, but most are less than 10 cm long. Shale clasts are elongate and up to 1 m long. Breccias are largely of open framework with a felsic volcaniclastic matrix. Dacite clasts from Gibson Honman Rock have a SHRIMP U–Pb zircon age of 2676 ± 5 Ma (Krapež et al., 2000).

Cohesive lava outcrops as 3–4 m wide units that have lava-lobe form. They show weakly developed flow banding and have a few scattered phenocrysts of feldspar up to 3 mm long, set in a cryptocrystalline groundmass. Parts of the unit are brecciated, and northeast of the outcrop the lava contains hornblende, is weakly amygdaloidal, and bordered by schistose sedimentary rock. The central part of the lobe association is coarser grained, and bordered to the east by a 15 m-thick breccia unit.

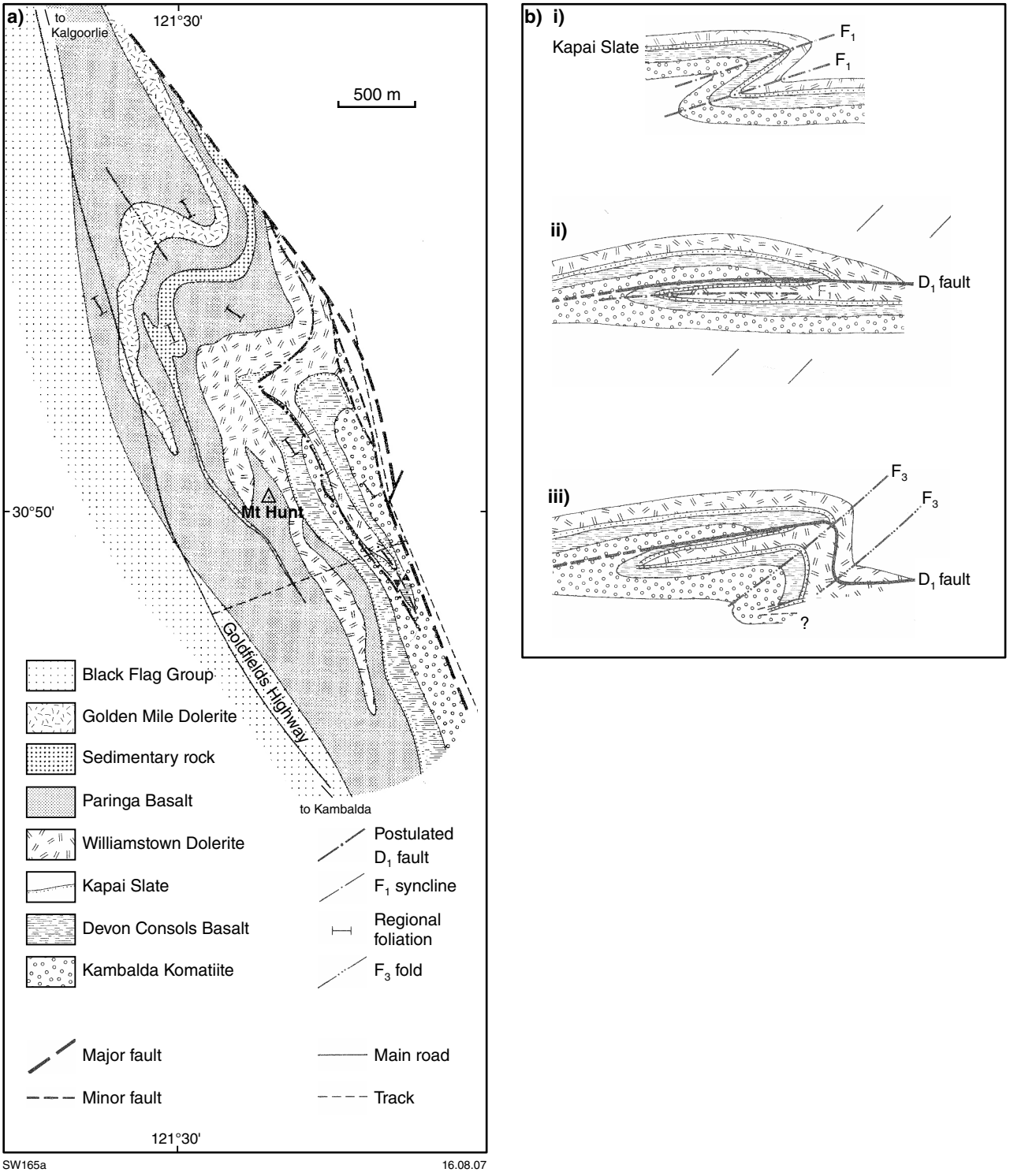

Figure 12. a) Interpretive geological map of Mount Hunt (modified from Swager, 1989, 1990); b) schematic development of fold structures at Mount Hunt: i) initial, asymmetric F_1 fold; ii) development of small-scale F_1 nappe structure, with largely sheared-out short limb; iii) F_3 refolding of the F_1 structure, after it was tilted into a steep orientation during the F_2 upright folding (after Swager, 1989)

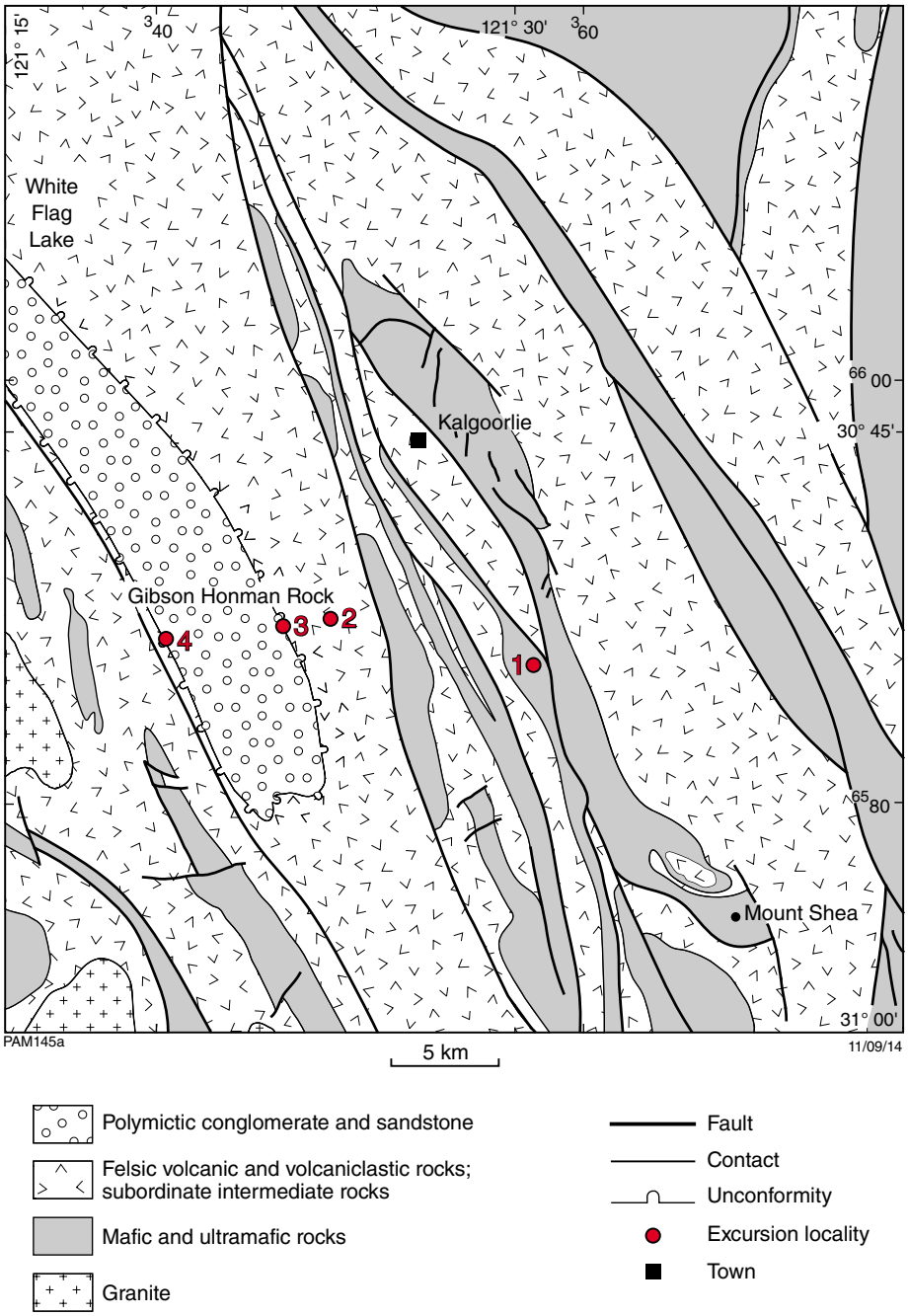

Figure 13. Excursion localities in the Kalgoorlie area (modified from Morris, 1998)

All breccia clasts appear to be of local derivation. Rare lensoidal shale units are lithologically similar to shale clasts (although some shale 'units' may themselves be 3–4 m long and 50 cm-wide shale rafts), and clasts of volcanic rocks are lithologically similar to lava lobes.

In thin sections of the lava unit, euhedral alkali feldspar crystals range from microphenocrysts to 6 mm in length and show well-developed cross-hatched twinning. They are slightly cloudy, and speckled with carbonate and sericite. Grain margins show weak oscillatory zoning. Grains are locally aggregated and intergrown. Euhedral phenocrysts of less common albitic plagioclase are up to 3 mm long. The groundmass is inhomogeneous, comprising weakly granoblastic quartz and feldspar (the former locally developed as microphenocrysts) and patches of coarse granoblastic quartz. One millimetre-diameter aggregates of a brown, tabular, pleochroic mineral (?oxybiotite) are scattered throughout. A typical sample from the lava unit has about 25 vol% crystals.

Volcanic clasts from the breccia are petrographically similar to the lava. They are dominated by single (locally intergrown) crystals of alkali feldspar up to 6 mm long. Also present are a few fine-grained felsic rock fragments up to 6 mm long and less common rock fragments composed of granoblastic quartz. The matrix is granoblastic quartz and sericite, and a brown alteration mineral possibly after amphibole or biotite.

The spatial relationships of lava and breccia, and the lithological similarity of volcanic clasts in the breccia to lava lobes, suggest that breccia is derived from the lava by wastage and mass-flow deposition. Shale clasts represent rip-ups of the local substrate. With lava movement the breccia was spalled off the lobe margin and accumulated as a gravity-deposited massflow unit at the lobe foot. Shale clasts may represent fragments dislodged during lobe extrusion involving substrate inflation. The coarse-grained nature of the lava and the intergrowth of alkali feldspar prior to emplacement are consistent with either extrusion of the lava as a crystal mush or intrusion and cooling at a high level. The suggestion that the lava margin was once partly glassy favours the former interpretation.

Locality 3: Navajo Sandstone (MGA 347420E 6585604N)

The Navajo Sandstone is a coarse-grained, quartz-rich, typically well-sorted sandstone with minor conglomerate containing felsic clasts (Krapež et al., 2008; Squire et al., 2010), which has been correlated with the Merougil Formation near Kambalda (Localities 7 and 9). It rests unconformably between the Black Flag Group below and the Kurrawang Formation above (Krapež et al., 2008), and was deposited c. 2670 to 2660 Ma (Krapež et al., 2000; Squire et al., 2010). Krapež et al. (2008) interpreted it as a fluvial deposit based on various sedimentary features including planar-bedded sandstones and conglomerates, trough cross-beds and channels. However, Squire et al. (2010) argued that the sediment contains very abundant volcanic quartz grains and proposed that the textural immaturity of the deposits and their limited range of detrital zircon ages suggest that they were produced by a large-volume, quartz-rich pyroclastic flow deposit.

Locality 4: Kurrawang Formation (MGA 341885E 6585335N)

The Kurrawang Formation lies within an open, northwesterly trending syncline, which is up to 5 km wide with a strike length of about 75 km. Coarse, poorly sorted conglomerates of the Kurrawang Formation are the youngest exposed component of the succession in the Kalgoorlie region (Fig. 13). The lower part of the formation consists of polymictic conglomerate, which grades up into medium- to coarse-grained, cross-bedded sandstone, which in turn grades up into fine-grained sandstone and siltstone (Hunter, 1990a). Clasts in the conglomerate are rounded to well-rounded, elongate to equidimensional and composed of granite, gneiss, felsic volcanic rocks, mafic and ultramafic rocks and sedimentary rocks including sandstone and banded iron-formation (Krapež et al., 2008). Detrital zircon studies indicate that the Kurrawang Formation was deposited after c. 2655 Ma (Kositcin et al., 2008). The clast compositions and wide range of detrital zircon ages back to greater than c. 3000 Ma (Krapež et al., 2000; Kositcin et al., 2008) indicate a diverse provenance. Krapež et al. (2008) interpret the Kurrawang Formation as a submarine fan deposit.

Locality 5: Mungari Monzogranite (MGA 332681E 6581816N)

Modified from Hunter (1990b)

At Mungari, a small, late-stage monzogranite pluton intrudes the core of a syncline containing felsic volcanic and volcaniclastic rocks with minor dolerite. To the west, a regionally extensive shear zone (Kunanalling Shear Zone) comprises mafic–ultramafic schists. To the south of the intrusion, andalusite is found in a well-developed thermal aureole which is itself affected by shearing and faulting.

The road cutting on the Great Eastern Highway, 12 km northeast of Coolgardie (Fig. 14), exposes the western contact of the Mungari Monzogranite with felsic volcaniclastic rocks. The contact clearly shows the post-tectonic intrusive nature of the granite. Finer grained volcaniclastic rocks can also be seen. The outcrop is in the saprolite zone of a pervasive and deep lateritic weathering profile, and both lithotypes have been reduced to assemblages of clays and resistant minerals. However, there has been excellent preservation of fine textural detail.

The contact is sharp, discordant and slightly undulose, with a moderate westerly dip and no apparent veining or interleaving. The granite shows slight reduction in grain size near the contact and its margin is weakly foliated. The felsic volcaniclastic rocks are fine grained, white to grey, and thinly bedded to laminated. Bedding and pervasive foliation are subvertical and parallel. There is a zone of dark, massive hornfelsed felsic material within a few centimetres of the contact.

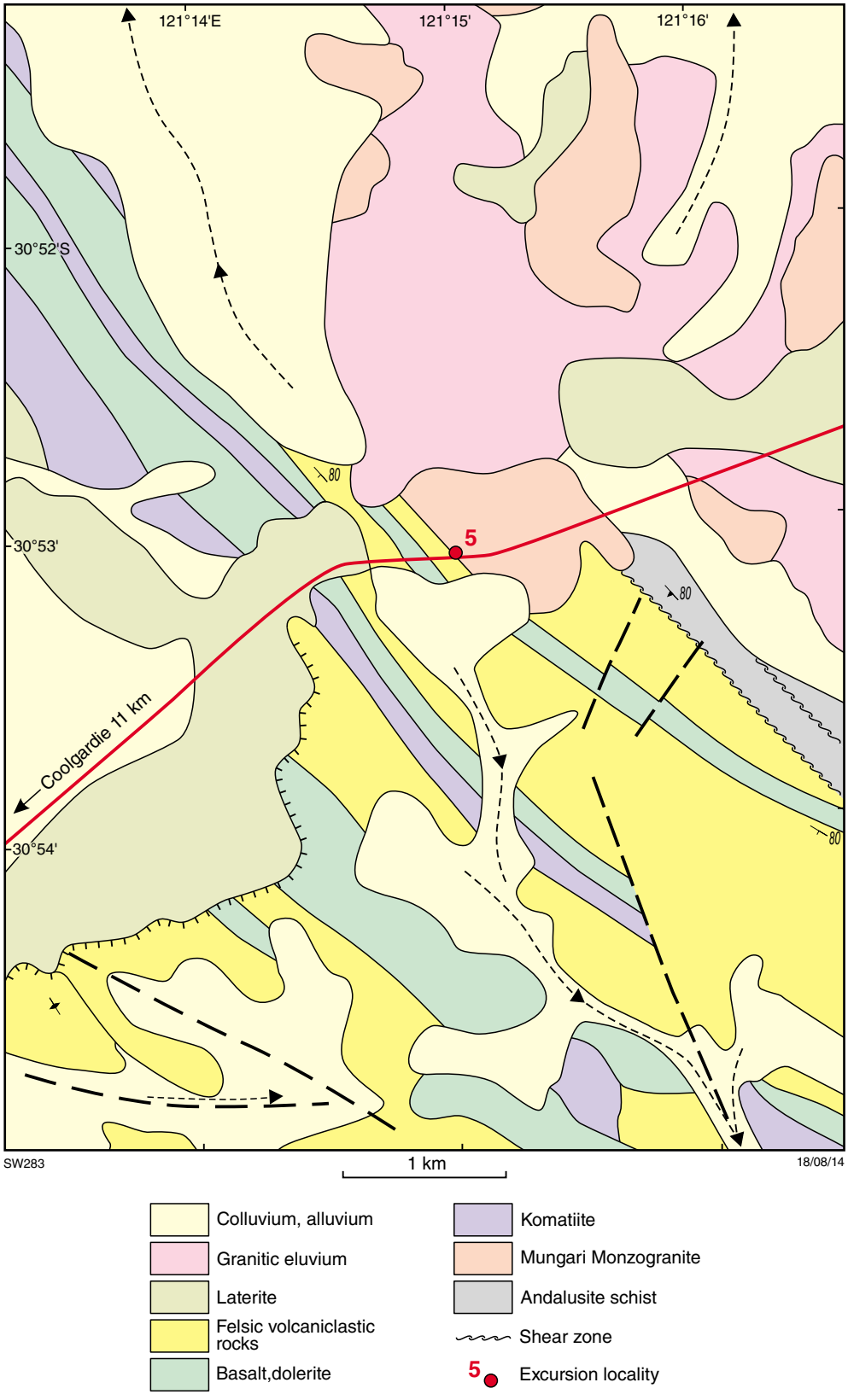

Figure 14. Geological setting of the Mungari Monzogranite (modified from Hunter, 1990b)

The Mungari Monzogranite is a well-exposed, ovoid body, 4 km wide and 8 km long, which is homogeneous and isotropic except for a moderate to strong foliation within a few metres of its western margin. The foliation is parallel to the prevailing greenstone trend. The intrusion is medium grained and mainly equigranular, with scattered subhedral to anhedral zoned feldspars which appear to be slightly coarser than the groundmass. The monzogranite belongs to the low-Ca group of Cassidy et al. (2002). There is a sharp magmatic contact with enclosing felsic volcaniclastic rocks of the Black Flag Group and a broad thermal-metamorphic aureole to the south.

In thin sections, the monzogranite is a medium, fairly even-grained rock with a relic allotriomorphic-granular to hypidiomorphic-granular texture. Quartz, zoned K-feldspar, Ca-albite, and 3–4% red-brown biotite are the main constituents, with accessory zircon, opaques and fluorite. Slight alteration has produced turbid feldspars, variable chloritization of biotite and the secondary growth of muscovite. Quartz and some plagioclase shows trained extinction and incipient recrystallization into domains. There are scattered myrmekitic intergrowths and annealed microshears.

Attempts to date the Mungari Monzogranite using the SHRIMP U–Pb zircon technique have been unsuccessful but its composition and associations suggest that it is younger than c. 2660 Ma (Cassidy et al., 2002).

Locality 6: Spargoville volcanic rocks (MGA 359428E 6534230N)

Felsic igneous rocks form low, lithologically homogeneous outcrops west and south of Kambalda. Morris (1998) describes the rocks as dacitic in composition. Bouldery outcrops of grey, plagioclase-porphyritic felsic igneous rock contain numerous inclusions of pink feldspar-phyric material. In thin section, the rock is recrystallized and heterogeneous. Aggregates of granoblastic feldspar, quartz, and biotite up to 7 mm in diameter are set in a groundmass of quartz, feldspar, biotite, and subordinate chlorite and muscovite. Less common single crystals of subhedral plagioclase (up to 5 mm long) are cloudy and variably sericitized, and some are replaced by feldspar and biotite. Some thin sections contain partly resorbed and sericitized alkali feldspar crystals, up to 5 mm long, showing cross-hatched twinning. Subordinate quartz grains (less than 2 mm long) are weakly embayed. The rocks are similar in character to those at Gibson Honman Rock (Locality 2) and Morgans Island (Locality 9).

Locality 7: Merougil Formation (MGA 368013E 6544262N)

Outcrops of coarse-grained, quartz-rich sandstone and conglomerate of the Merougil Formation (Locality 7), which has been correlated with the Navajo Sandstone (Krapež et al., 2008; Squire et al., 2010) to the north (Locality 3), crop out beside the Goldfields Highway just west of the Kambalda turnoff.

Locality 8: Merougil Formation base (MGA 370518E 6542136N)

On the northern side of Lake Lefroy near Kambalda, there is an excellent exposure of the contact between sandy turbidites of the Black Flag Group and conglomerate and quartz-rich sandstone of the Merougil Formation (Krapež and Hand, 2008; Squire et al., 2010). The Black Flag Group sediments at this locality include conglomerate and sandstone turbidites. The contact with the overlying Merougil Formation is sharp.

The Merougil Formation is similar in character to the Navajo Sandstone (Locality 3) with which it has been correlated (Krapež et al., 2008; Squire et al., 2010). The felsic clasts in conglomerate near the base of the formation become less abundant away from the contact. Krapež et al. (2008) have interpreted the Merougil Formation as a high-discharge deposit in an area of high relief, which is likely to have formed a braid-plain in a fault-bounded basin. Squire et al. (2010) interpret it, like the Navajo Sandstone, as a rapidly reworked pyroclastic deposit associated with contemporaneous high-Ca granite magmatism (Cassidy et al., 2002).

Locality 9: Top of Black Flag Group (MGA 369978E 6542861N)

Modified from Morris (1998)

Morgans Island

Cohesive felsic lava, breccia, and volcaniclastic sandstone and siltstone of the Black Flag Group outcrop on the northwestern side of Lake Lefroy at Morgans Island. Sedimentary structures in the upper part of the succession at Morgans Island indicate that the succession youngs to the west. At the bottom of the succession, rhyolite lava forms an elongate northerly trending outcrop at Lake Lefroy at point 1 on Figure 15. The rock is structureless and buff-coloured, with scattered phenocrysts of feldspar and subordinate quartz in an originally glassy groundmass. The minimum thickness is 200 m and the rock lacks any internal subdivision. Rhyodacite from Morgans Island has a SHRIMP U–Pb zircon age of 2678 ± 8 Ma (Krapež et al., 2000).

On the small headland at points 5 and 6 on Figure 15, oligomictic breccia has subangular dacite clasts lithologically identical to cohesive lava. The breccia is clast supported, with individual clasts up to 40 cm in diameter. At point 6 on Figure 15, the dacite is more cohesive. Lithologically similar breccias at point 4 on Figure 15 show pseudo jigsaw-fit texture. Weakly foliated breccias outcrop at points 2 and 3 on Figure 15.

Cohesive lava in thin section is porphyritic with euhedral phenocrysts of plagioclase (optically oligoclase; up to 2.5 mm long) that are weakly resorbed and sericitized. Quartz phenocrysts (up to 4.5 mm long) are locally embayed and rounded, and show weak undulose extinction. These phenocrysts and scattered disseminated

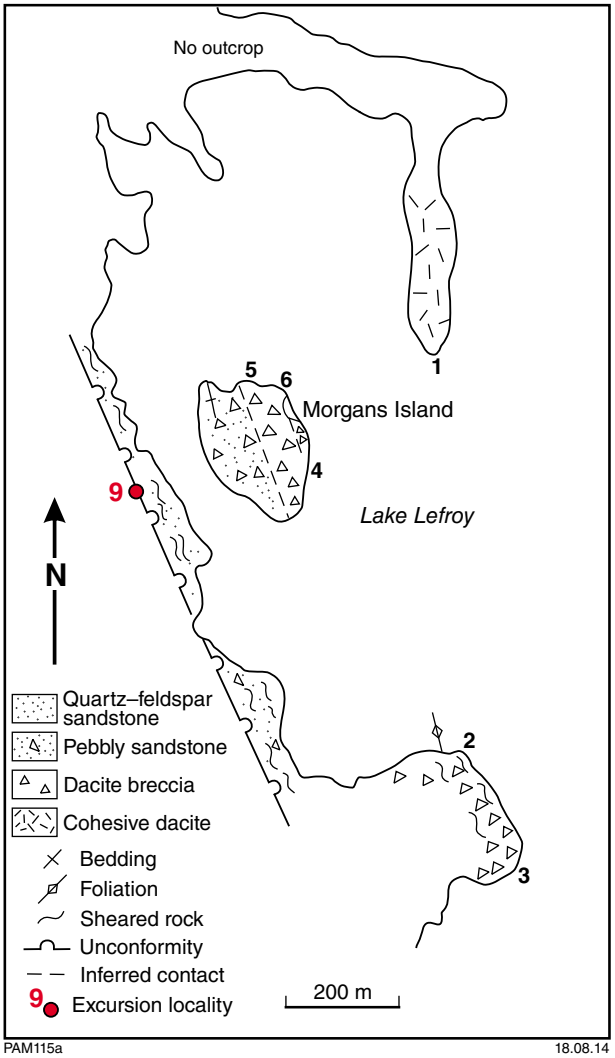

Figure 15. Geological sketch map of Morgans Island (modified from Brauns, 1991; Morris, 1998). For regional setting, see Figure 8

aggregates of biotite flakes (some ghosts after ?amphibole) are set in a groundmass of weakly granoblastic quartz and feldspar with wispy muscovite.

In thin sections, a porphyritic rhyolite clast from a breccia on the northwestern shore of Lake Lefroy is weakly foliated with euhedral to subhedral unzoned plagioclase phenocrysts (up to 1 mm long) that are optically albite–oligoclase. The groundmass has cryptocrystalline quartz and feldspar, and scattered biotite, chlorite, and opaque oxide. Unlike the lava, the rock lacks quartz phenocrysts and the groundmass shows relict perlitic texture.

Between breccia clasts, the matrix is strongly foliated and iron stained. Scattered elongate subhedral to euhedral albitic plagioclase (up to 2 mm long) are set in a granoblastic matrix of quartz and feldspar with scattered muscovite. Crude bedding is preserved as grain size changes.

At Morgans Island, cohesive lava could represent a subaqueous lava lobe bordered by in situ breccia, the latter resulting from the quenching of lava by contact with water. Following extrusion and brecciation, spalled-off lava fragments accumulated as mass-flow breccias adjacent to lobes. Finer grained spalled-off components represent sand- to silt-grade quench fragmentation of the lobe. Breccias are interbedded with volcaniclastic sandstones dominated by felsic volcanic debris with a minor mafic component. These represent turbidity current deposits of reworked lobe-derived detritus.

Locality 10: Red Hill (MGA 373579E 6546323N)

The Red Hill lookout overlooks Lake Lefroy. Salt lakes such as these are abundant across the Yilgarn Craton where they occupy paleodrainage systems, in this case the Lefroy paleodrainage (Anand and Paine, 2002). These lakes may be filled during intense rainfall episodes which include rare cyclones. Significant gold deposits have been discovered and mined from beneath the lake deposits at Lake Lefroy. The Agamemnon and Revenge deposits can be seen across the lake to the southeast.

The following description comes from Anand and Paine (2002), which provides a comprehensive overview of the evolution of regolith in the Yilgarn Craton:

> ‘Numerous buried palaeochannels occupy the lower parts of the landscape and are up to several hundreds of metres wide and many kilometres long. Drainage incision along palaeovalleys on the weathered landsurface resulted in development of channels that were subsequently filled with sand, lignite and kaolinite- and smectite-rich sediments with lenses of ferruginous gravel. Palaeochannels are younger than the palaeodrainage system of broad, shallow valleys in which they occur and were probably incised during the final stages of rifting between Australia and Antarctica during the Early–Middle Tertiary*. Sediments were deposited under fluvial, lacustrine, estuarine and marine environments during the Middle–Late Eocene. Further deep weathering occurred in both sediments and bedrock. Mixing occurred between the accumulating sediments and the underlying saprolite, possibly as a result of the formation of palaeosols. The collapse features and associated nodular and pisolitic materials in the underlying saprolite were probably formed during this period. Hematitic megamottles have developed in sediments and the upper part of some palaeochannel sediments contain ferruginous nodules and pisoliths. All this indicates post-depositional weathering within the sedimentary sequence. The similarities in the nature and characteristics of palaeochannel sediments in

* Obsolete: Paleogene in current usage

the southern and northern regions suggest that similar conditions prevailed not only during the deposition of sediments, but also during their subsequent weathering. Parts of the palaeochannel sediments were eroded prior to deposition of Quaternary colluvium and alluvium. Colluvial, alluvial and aeolian sediments unconformably overlie palaeochannel sediments, ferruginous duricrust or saprolite. These sediments have been derived from increased erosion following the change to a more arid climate during the Late Miocene – Pliocene, in part a result of instability caused by a reduction in the vegetative cover.'

Locality 11: Kanowna Town Dam (MGA 367310E 6609870N)

The Kanowna Town Dam locality preserves spectacular examples of volcaniclastic turbidites of the Black Flag Group. They were described by Trofimovs et al. (2006) as:

> 'texturally well-preserved sedimentary rock deposits comprising laminated siltstone and mudstone, centimetre- to metre-scale graded beds of coarse sand to granule-sized particles and pebble-sized conglomerate lenses. The deposit dips moderately, 40–55º, towards the east. Sedimentary structures, such as graded beds, flame structures, load casts, and scour and fill structures, indicate an east-younging direction.
>
> The succession coarsens up-sequence. The basal sedimentary layers comprise graded sandstone and mudstone in 2–100 cm-thick beds. Intraformational slumping is commonly preserved in the basal units, together with abundant flame structures and load casts, pseudonodules and dewatering conduits. The middle of the sequence is dominated by coarse-grained quartzofeldspathic (with a minor fuchsitic component) sandstone beds, observed on a metre scale, together with lensoidal felsic porphyry clast-dominated conglomerate channels that have scoured into the underlying sandstone sequence. Amalgamated beds of sandstone and conglomerate form the top of the sequence.
>
> The dominant clast population in the conglomerates comprises ~90% quartz-phyric felsic porphyry clasts with subordinate ultramafic- and mafic-derived fuchsitic clasts (~8%) and siliceous metapelite clasts (~2%). Clasts are rounded and poorly sorted. Intense weathering has altered the primary mineralogy in the matrix to a predominantly phyllosilicate-rich assemblage. Individual volcanic quartz crystals in the matrix are observed. These quartz grains are commonly fragmented, although rare embayment structures are preserved, indicating a volcanic or high-level intrusive provenance.'

An open, macroscopic, southeasterly plunging fold (about 100 m across) can be seen in the western and southern sides of the exposure.

East of the Kanowna Town Dam, a thin sequence of komatiite flows overlies the turbidites. Trofimovs et al. (2004b) recognized five distinct komatiite flow units in this area. The komatiites range from medium-grained, equigranular cumulate rocks to very coarse grained, olivine spinifex-textured komatiite. The contact between the turbidites and the komatiites is poorly exposed (MGA 367750E 6610110N) but can be constrained to within 10 m. Immediately above the contact, ultramafic rocks are pale brown, equigranular altered rocks that are likely after olivine cumulates. These rocks are relatively massive, with little deformation, although there is a variably developed spaced foliation near the contact.

Towards the breakaway, the outcrop alternates between equigranular cumulate textures and olivine spinifex-textured rocks, representing the sequence of stacked komatiite flow units which were recognized by Trofimovs et al. (2004b). Primary textures are well preserved, despite the intense alteration, in the breakaway (MGA 367778E 6609989N) where medium-grained cumulate ultramafic rock grades up into a coarse-grained, randomly oriented, olivine spinifex-textured rock, which then grades into a very coarse olivine spinifex-textured rock with blades up to 30 cm long. The textural zonation in the komatiite flow suggests the top is to the east.

Locality 12: Perkolilli volcanic breccia (MGA 371250E 6610520N)

Poorly sorted felsic volcanic breccias crop out at Perkolilli, 21 km northeast of Kalgoorlie. The breccias contain mainly rhyolite and dacite clasts, and show both open and closed framework. A nearby cross-bedded unit consists of crystal fragments in a devitrified glassy groundmass (Morris et al, 1993). Morris (1998) has noted that the glassy nature of these rocks — the limited clast content, the presence of welding and the small volume — are consistent with deposition as a hot, small-volume pyroclastic flow.

A SHRIMP U–Pb zircon age of 2676 ± 3 Ma (Nelson, 1995) for rhyolite from Perkolilli is within error of ages determined for various volcanic and volcaniclastic rocks of the Black Flag Group (Krapež et al., 2000; Kositcin et al., 2008). Morris (1998) relates the volcanic rocks at Perkolilli to those of the Gindalbie association (Barley et al., 2008) at Melita to the north (see Post-conference excursion, Locality 14) based on geochemical criteria. However, the age and affinities of the felsic volcanic rocks at Perkolilli suggest a possible relationship with the Black Flag Group.

Locality 13: Breakaway locality, Kanowna (MGA 367575E 6616985N)

A detailed description and interpretation of the Breakaway locality is given by Trofimovs et al. (2004a). As described by Trofimovs et al. (2004b), the locality:

'preserves continuous, texturally well-preserved outcrop exhibiting both coherent and fragmental komatiite–dacite associations. These rocks outcrop over a 600 m × 600 m area and the sequence dips steeply (75º) to the southwest providing a cross-sectional view of the preserved volcanic facies (Fig. 16). The coherent dacite and komatiite associations are preserved within meter- to hectometer-scale megablocks that form the 'block' facies (Glicken, 1991) of a volcanic debris avalanche deposit (Trofimovs et al., 2004a). The megablocks within this primary volcanic breccia preserve original lithological and stratigraphic contact relationships and primary igneous textures and structures. Surrounding these megablocks is a brecciated facies comprising quartz- and subordinate feldspar-phyric dacite and komatiite-derived fuchsite granule- to boulder-sized angular clasts, supported by a predominantly quartzofeldspathic, with subordinate fuchsite (1–2%), coarse-grained matrix. The brecciated matrix exhibits the same composition as the megablocks (quartz- and feldspar-phyric dacite and komatiite). The matrix is interpreted to have formed by abrasion and grain-to-grain collision of the large volcanic megablocks during transport. Previous work at the Breakaway/Alunite Locality describes the breccia as an olistostrome deposit, where large olistoliths have gravitationally collapsed into a pre-existing conglomeratic matrix (Grey, 1981; Taylor, 1984; Ahmat, 1990; Hand, 1998). The genetic relationship established between the megablocks and surrounding matrix disputes this interpretation and features such as jigsaw-fit textures between blocks and the lack of internal stratification in the deposit are indicative of a volcanic debris avalanche origin (Trofimovs et al., 2004a).

The coherent dacite megablocks at this locality are characterized by 15% relict quartz phenocrysts, with subordinate (2–5%) relict plagioclase phenocrysts, preserved in 80% fine-grained, originally quartzofeldspathic groundmass. Phenocrysts are euhedral and on average 2–4 mm in size. However, rare (~2%) quartz phenocrysts up to 0.8 cm are observed. The groundmass shows intense, pervasive clay alteration, which has obliterated the original feldspar content, groundmass grain size and texture. Autobrecciation and flow banding are commonly preserved within the dacite unit.

Komatiite is intercalated with the coherent dacite, the primary contact relationships preserved within the large volcanic debris avalanche blocks. Komatiite at the locality shows much variation in preservation of primary texture and is most commonly represented as fuchsite–talc-carbonate-chlorite schist. However, low-strain pockets preserve small (0.5–2 cm), randomly oriented spinifex-texture along the margins of komatiite units. The random spinifex texture grades towards the center of the komatiite into larger (3–10 cm) oriented pseudomorphed olivine (now chlorite) spinifex blades.

Contacts between the dacite and komatiite in places appear extremely irregular, exhibiting morphologies suggesting both were fluidal at the time they were juxtaposed (Trofimovs et al., 2004b, figure 9a). Komatiite apophyses have injected centimeters to meters into the dacite unit (Trofimovs et al., 2004b, figure 9b). The apophyses are randomly aligned and distributed along the komatiite–dacite boundaries with each apophysy preserving centimetre-scale lobate and flame-like structures along its margins. Spinifex texture is observed along some of the komatiite margins adjacent to contacts with the dacite unit. However, the majority of boundaries have been altered to fine-grained assemblages, largely consisting of fuchsite. A small, 2 m × 2 m, zone of magma mingling, where both lithologies were physically intercalated as liquids, is observed along a komatiite–dacite contact.'

This is the only locality in the Yilgarn Craton from which stromatolites have been positively identified (Grey, 1981).

Locality 14: Harper Lagoon (MGA 364230E 6623120N)

At Harper Lagoon, the succession described by Trofimovs et al. (2006) consists of:

'a minimum thickness of 30 m of ultramafic olivine orthocumulate to mesocumulate, pseudomorphed by serpentine with a chromite oxide component, grades into pyroxene spinifex textured, high-Mg, komatiitic basalt. Tabular serpentine crystals grade into acicular pseudomorphed pyroxene crystals then into ~3 m of centimetre-scale randomly oriented pyroxene spinifex textured high-Mg basalt. The original clinopyroxene phenocrysts are pseudomorphed to an actinolite–chlorite mineral assemblage. Chlorite is observed in the centre of the acicular crystals, while amphibole and subordinate plagioclase rim the pseudomorphed phenocrysts and fill the interstitial voids. A gradational change to an ophitic gabbro unit occurs at the top of the clinopyroxene-dominant basalt. The ~4 m-thick gabbro, contains primary, 5–20 mm, euhedral, acicular, and bladed clinopyroxene crystals that have been pseudomorphed by actinolite, associated with euhedral to subhedral plagioclase crystals. A second clinopyroxene (now amphibole) spinifex textured horizon (Trofomivs et al., 2006, figure 9a) overlies the gabbro. This pyroxene spinifex textured unit is ~2–4 m thick and exhibits randomly oriented 2–3 cm spinifex blades together with larger, 4–6 cm oriented spinifex blades that form radial patterns.

Shearing truncates the top of the spinifex textured zone, and a 7–10 m-thick breccia horizon comprising high-Mg basalt clasts stratigraphically overlies the shear zone and the basalt – komatiitic

basalt sequence. Angular, 5–10 cm, amygdaloidal basalt clasts are bound together by a recrystallized carbonate, with subordinate chlorite and amphibole, cement. The clasts appear to be the fragments of the overlying, coherent, pillowed, amygdale-rich, high-Mg basalt lavas. In these overlying lava flows, well-preserved pillow structures indicate a southeast younging direction (125–130º) and clearly show that the basalt forms the stratigraphic top of the sequence. A high abundance of amygdales (40–50%) is typical in the pillows, particularly around the pillow rims. Concentric layering is defined by amygdale zonation, with variations between amygdale-rich and amygdale-poor zones. Amygdale-rich zones exhibit spherical to coalesced albite-filled vesicles. The amygdale-poor layers and pillow cores exhibit an amphibole-dominant (tremolite) mineralogy with chlorite (Mg-rich) and subordinate carbonate, plagioclase and epidote. The size of the pillow structures decreases upsequence through the pillow basalt pile. Large, 1 – 1.5 m pillows directly overlie the basaltic breccia, whereas the average pillow size decreases to 30–50 cm, 15 m upsequence. Associated amygdale-rich, high-Mg basaltic dykes are also observed within the pillowed basalt pile.'

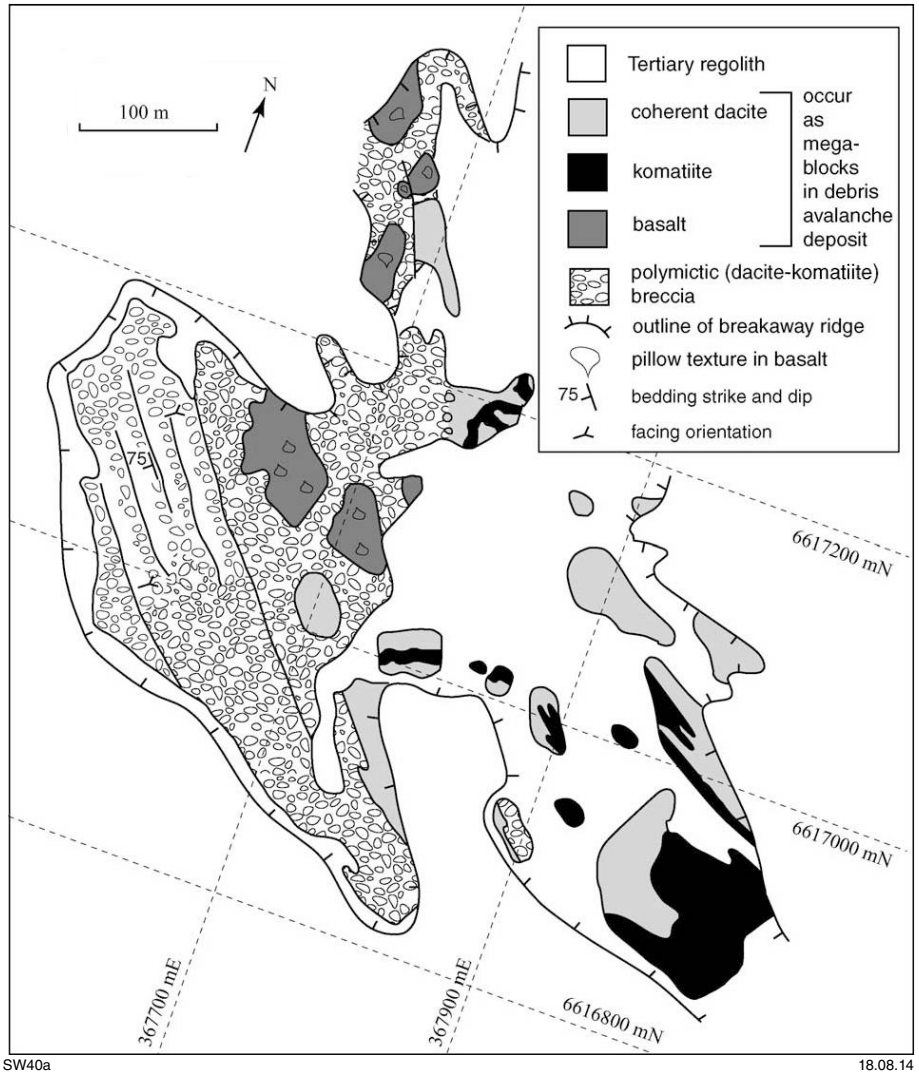

Figure 16. Geological outcrop map of the Breakaway locality showing coherent basalt, dacite and komatiite megablocks within a polymictic breccia deposit. Bedding planes are observed in the western section of the deposit. Normal graded bedding indicates a southwest facing orientation (after Trofimovs et al., 2004b)

Locality 15: St Ives goldfield

The Victory–Defiance deposit forms part of the world-class St Ives goldfield at Kambalda. The camp has produced 12 Moz, with the gold deposits mostly located on a series of major contractional jogs to the west of the Boulder–Lefroy Fault (e.g. the Revenge and Repulse Faults; Nguyen et al., 1998; Cox and Ruming, 2004). This contrasts with the Golden Mile at Kalgoorlie, which is interpreted to lie on dilational jogs (Weinberg et al., 2004).

The St Ives goldfield lies within a north-northwesterly trending corridor that is bounded by the regional Boulder–Lefroy Fault to the east, and the Speedway Fault to the west (Fig. 17). It is in the southern part of the Kalgoorlie Terrane, whose structural and stratigraphic setting is described in the Introduction to this volume.

The Leviathan (Victory–Defiance) gold deposit

Gold was first won from the Victory–Defiance gold deposit, 20 km south of Kambalda, in 1983 from underground workings which exploited a large system of gently dipping quartz-rich lodes (Blewett et al., 2010b). The original 'room and pillar' workings are now exposed in the lower levels of the openpit (Fig. 18). Near-mine exploration resulted in discoveries of extensive mineralization in the Repulse shear zone and felsic intrusions to the east. These discoveries were initially worked as the Victory–Defiance deposits, but have grown into the Leviathan openpit. To date, more than 1 Moz of gold have been extracted from the deposit, with high-grade ore averaging 2 g/t. Further exploration resulted in discovery of the nearby Orion/Britannia, Sirius and Conqueror deposits, which host a variety of styles of gold-bearing lodes over an area of 2 × 2 km (Blewett et al., 2010b). These deposits are considered to be part of a linked architectural system (Nguyen, 1997; Ruming, 2006).

The Leviathan pit contains most units of the Kambalda stratigraphy (Fig. 6). From east to west, these include the Tripod Hill Member of the Kambalda Komatiite, which forms a series of thin komatiite flows, the Devons Consol Basalt, the Kapai Slate, and the Paringa Basalt (Watchorn, 1998). The supracrustal units dip steeply to the east at Leviathan, indicating that the package is overturned and, at the camp-scale, the pit is interpreted to be on the western limb of an overturned anticline (Miller et al. 2010; Fig. 19a,b).

The greenstone succession at Victory–Defiance has been intruded by four main phases:

1. The Defiance Dolerite is a laterally extensive sill, constrained at c. 2690 Ma, which intruded the contact between the Kapai Slate and overlying Paringa Basalt (Miller et al., 2010).

2. A wedge-like body of lamprophyre intruded along the Kapai Slate (Watchorn, 1998).

3. The 2658 ± 4 Ma Flames Porphyry suite (Nguyen, 1997), which form a series of northwesterly trending, subvertical to steeply dipping sheets (Ruming, 2006).

4. Easterly trending, subvertical mafic dykes that may be part of the c. 2400 Ma Widgiemooltha Dyke Suite (Hallberg, 1987; Nemchin and Pidgeon, 1998).

The first three intrusive phases are cut by the Repulse Fault, with sheets of the Flames Porphyry suite also forming a series of boudinaged lenses in the hangingwall of the fault (Miller et al., 2010). The easterly trending dykes crosscut all features in the pit.

A series of structures cut the greenstones in the south wall of the Leviathan pit (Fig. 19b). The northerly trending, easterly dipping listric Repulse Fault forms a 15–20 m wide, high-strain zone, with a complex history of reactivation. These include an early phase of ductile compressional deformation that resulted in boudinaging of Flames Porphyry dykes and two later stages of brittle deformation: an early phase related to northeast-directed extension, which is overprinted by a later phase related to compressional deformation (Ruming, 2006; Blewett et al., 2010b; Miller et al., 2010). It is the later phase of brittle, compressional deformation that is related to gold mineralization (Ruming, 2006). In its final configuration, the Repulse Fault is a thrust with about 400 m of displacement of the contact between the Tripod Hills Member and the Devon Consols Basalt (Miller et al., 2010; Fig. 19b). The Repulse Fault has been interpreted as a second-order structure off the Playa Fault with marked changes in orientation along strike (Fig. 19a). Both these features are considered to play a role in the mineral endowment at Victory–Defiance (Cox and Ruming, 2004; Miller et al., 2010).

A sub-horizontal array of en echelon tension gashes are exposed in the lower western side of the Leviathan pit (Fig. 18). These veins, known as the 'Defiance lodes', indicate a top to the west sense of shear. This is consistent with the stress field acting on the final thrust movement on the Repulse Fault, and suggests they may be products of the same deformation event.

Three main lode systems can be observed in the Leviathan pit. These systems can be related to the same deformation event, i.e. D_{4b} shortening (Fig. 7), which occurred following the switch of stress field at c. 2650 Ma.

1. Mineralization along the Repulse Fault is related to the component of west-directed thrusting.

2. The mineralized, sub-horizontal Defiance lodes are also associated with the east-west shortening.

3. There is also mineralization at the intersection between the dykes of the Flames Porphyry and the Repulse Fault.

The high-grade ore is characterized by an albite assemblage; the low-grade ore has a biotite+disseminated sulfide alteration assemblage; and the waste rock has chlorite alteration.

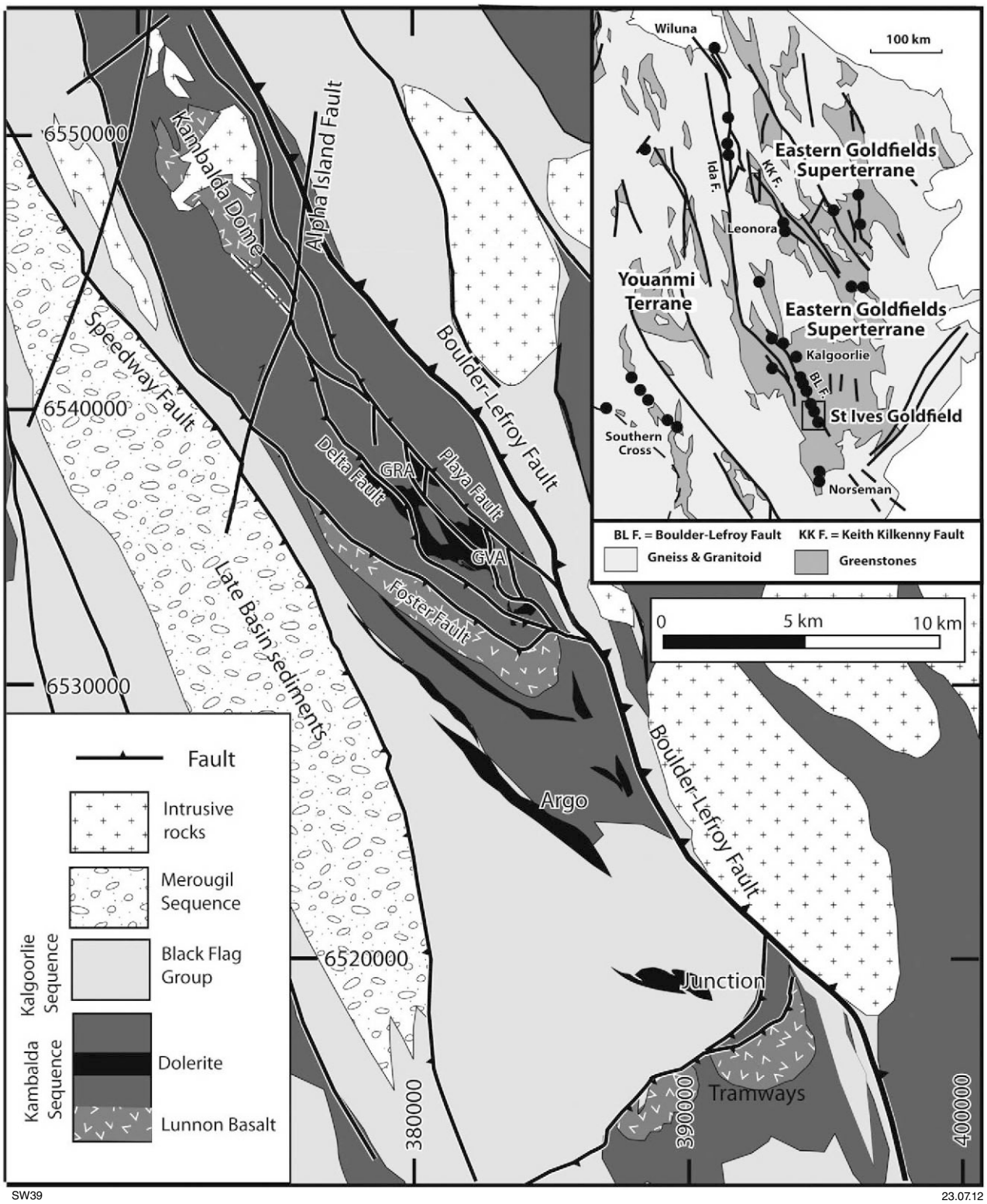

Figure 17. Regional geology map of the St Ives Goldfield. Inset figure at top right highlights the location of the St Ives Goldfield with other major gold deposits marked by black filled circles (after Miller et al., 2010)

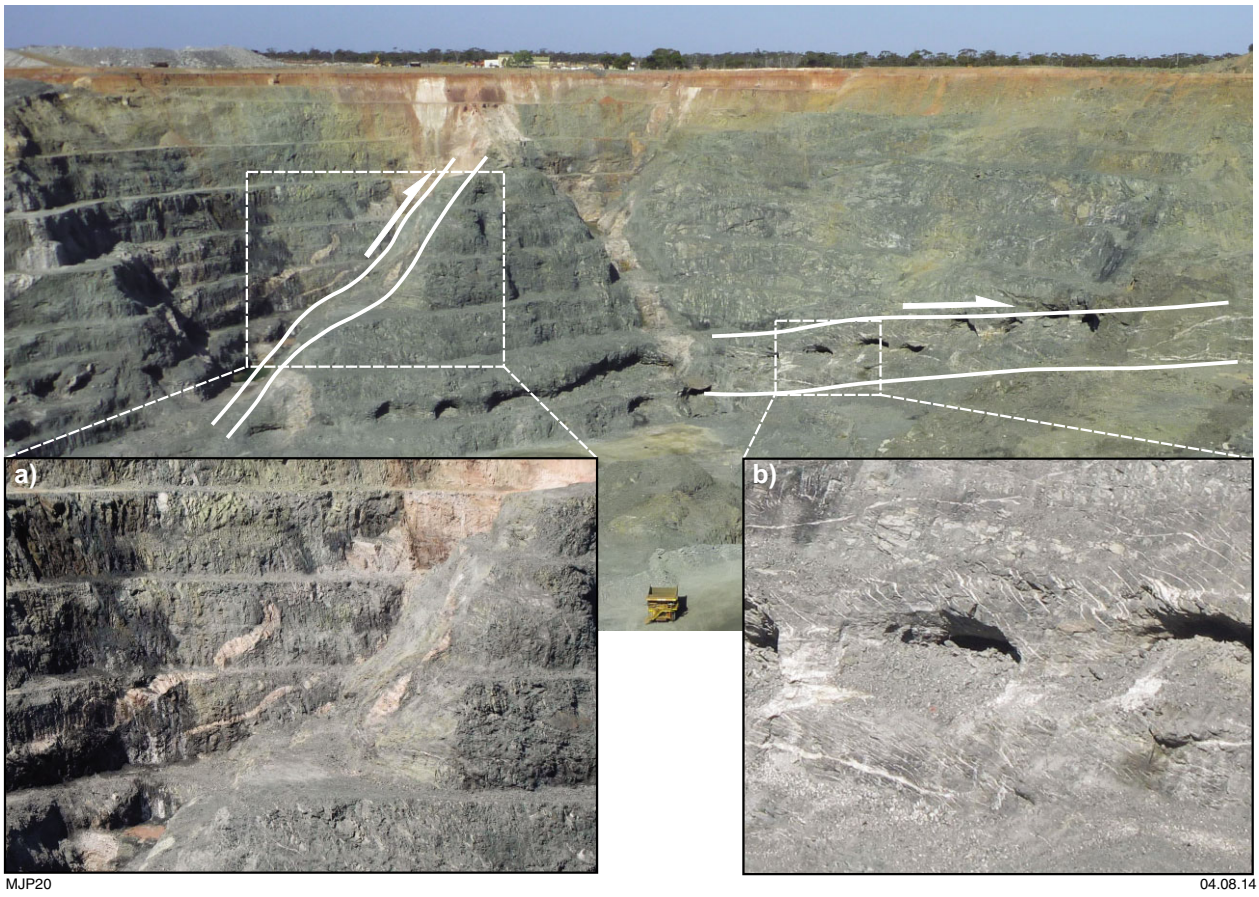

Figure 18. View of the southeast wall of the Leviathan openpit showing the main mineralized features. The historic underground works are visible in the lower levels of the pit: a) the Repulse Fault and the Flames Porphyry, which are the pale, boudinaged units; b) the shallowly dipping Defiance lodes, which have a top to the north sense of shear, and the historical workings.

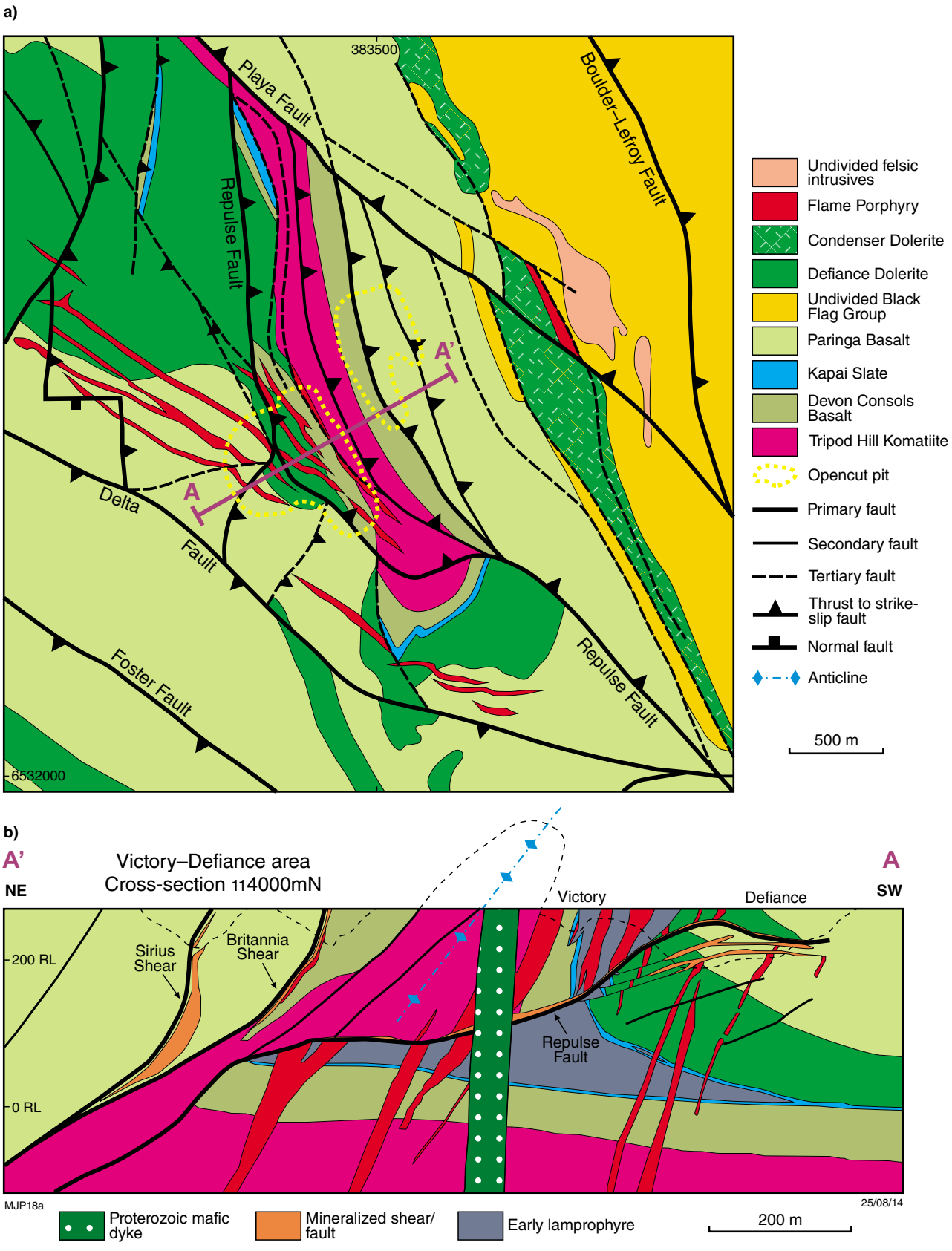

Figure 19. a) Generalized geological map of the St Ives area, focusing on the Victory–Defiance area (now the Leviathan openpit), showing the main units and structures (modified from Miller et al., 2010); b) cross-section through the Victory–Defiance area (see Figure 22a for location). The view is to the southeast (modified from Watchorn, 1998)

Locality 16: The Nimbus Ag–Zn–Au deposit

By SP Hollis

The Nimbus Ag–Zn–Au VHMS deposit is located approximately 17 km east-southeast of Kalgoorlie and 6.5 km north-northwest of the Golden Ridge gold mining centre. Initially discovered in 1995, the deposit lies in the uppermost felsic rocks of the Boorara Domain of the Kalgoorlie Terrane (Cassidy et al., 2006) in a package of rocks bound to the west and east by the Boorara and Kanowna shear zones. The regional stratigraphy comprises a lower succession of mafic to ultramafic volcanic rocks overlain by felsic and sedimentary rocks of the Black Flag Group (Trofimovs et al., 2006). Locally, mineralization occurs in a northwesterly trending and steeply dipping bimodal package of volcanic rocks (quartz–feldspar-phyric dacite and lesser basalt, and their autoclastic equivalents) with subordinate carbonaceous black shale, chert and polymictic conglomerates. The felsic stratigraphy is dominated by rocks of dacitic composition. Mafic rocks are absent beneath the Discovery Pit, but have been found in and below the East Pit, with at least three units observed to date. Peperitic upper contacts between mafic rocks and black shale, and abundant hyaloclastites, suggest the upper two units represent very shallow invasive flows or sills. All rocks have been subjected to lower greenschist facies metamorphism.

Mineralization at Nimbus includes polymetallic sulfide mineralization and overlying zones of supergene and oxide mineralization. Deeply weathered oxide and supergene material was mined by Polymetals WA from the two small open pits (Discovery and East) for a total production of 0.319 Mt at 352 g/t Ag (3.6 Moz Ag and 6.5 t Hg) between 2004 and 2007. The deposit is strongly oxidized to a depth of ~90 m, with mineralization in the oxide zone including silver halides, native silver and mercury in kaolinite–quartz–sericite-altered rocks (Hadlow et al., 2011). Primary sulfide mineralization at Nimbus comprises a series of stacked plunging lenses parallel to a mineral elongation lineation at 28° to the east-southeast (Henderson et al., 2012). An upper unit of early, well-developed ?colloform massive pyrite (which replaced glassy quartz–feldspar-phyric felsic lavas [Crawford, 2012]) may have sealed the hydrothermal system, facilitating economic underlying base- and precious-metal mineralization. Underlying mineralization occurs as 1) semi-massive, stringer and breccia-type Ag–Zn±Pb(–Cu–Au) sulfides associated with the dacites autoclastic top; and 2) as stringer and disseminated pyrite±sphalerite in largely coherent dacite at depth. Early colloform pyrite was initially fragmented by quartz–pyrite associated with hydraulic brecciation, which was subsequently brecciated in turn by yellow, Fe-poor sphalerite and then galena. The latter is closely associated with pyrargyrite (Ag_3SbS_3), marrite ($AgPbAsS_3$) and boulangerite ($Pb_5Sb_4S_{11}$). Chalcopyrite, arsenopyrite, tetrahedrite and bournonite ($PbCuSbS_3$) are also present. The Nimbus reserve currently stands at 1.126 Mt at 297g/t silver equivalent (Ag-Eq), with a resource of 4.9 Mt at 149 g/t Ag-Eq (23.4 Moz Ag-Eq including 65 000 t Zn and 46 000 oz Au). Mineralization is open along strike and to depth (MacPhersons Resources Ltd, 2014). Hydrothermal alteration is dominated by extensive and pervasive quartz–sericite–carbonate alteration, which becomes more intense towards mineralization. Anatomosing networks of fuchsite–sericite veinlets, together with silicification, produce pseudobreccia textures in dacite. Late quartz–carbonate veins contain trace pyrite–sphalerite–galena±chalcopyrite. Minor chlorite is most commonly associated with peperitic contacts of mafic rocks.

A detailed study of the stratigraphy, geochemistry and mineralization at Nimbus is currently in progress. Several samples have been also collected for U–Pb zircon geochronology and isotope analysis (Nd–Hf–O). Compared with other VHMS occurrences in the Yilgarn Craton (e.g. Golden Grove, Teutonic Bore – Jaguar–Bentley, Hollandaire, Austin), the Nimbus deposit is unusual in terms of its tectono-stratigraphic position, mineralogy and alteration. A lack of chlorite, low Cu–Au (throughout most of the deposit), Ag-enrichment, the presence of kaolinite at depth and high Hg, point to low temperatures (<250°C), a strong magmatic input, and acidic fluids. Classification of Nimbus as a VHMS deposit with epithermal characteristics, i.e. belonging to the hybrid bimodal felsic group of Piercey (2011), is consistent with its position near the margin of the Kalgoorlie Terrane. Hybrid bimodal–felsic VHMS deposits typically form in slightly less juvenile crust compared with classic Noranda-type Cu–Zn deposits, i.e. those within the Gindalbie association of Barley et al. (2008), and are often associated with subsurface phase separation and a strong magmatic input into the hydrothermal system (Mercier-Langevin et al., 2011).

Post-conference excursion — granite–greenstone geology between Kalgoorlie and Leonora

This excursion (Figs 20 and 21) examines the geology between Kalgoorlie and Leonora in the context of the distribution of mineral deposits through the region. Departing from Kalgoorlie, the excursion will visit structural and lithological localities along the western side of the Kalgoorlie Terrane and explore the relationship between the Kalgoorlie Terrane of the Eastern Goldfields Superterrane and the adjacent, older successions of the Youanmi Terrane. The second day is spent visiting gold deposits and geological localities in the Leonora district. Returning to Kalgoorlie on the third day, the excursion visits felsic volcanic rocks of the Gindalbie calc-alkaline association and various stratigraphic components of the Kalgoorlie Terrane.

All locality descriptions by S Wyche, NL Patison and MJ Pawley unless otherwise indicated.

Locality 1: Western Mining Corporation SM7 nickel laterite pit (MGA 307372E 6652923N)

Modified from Hill et al. (2001)

The supracrustal rocks that extend from Siberia to Menzies, and farther north through to Kurrajong, are broadly correlative with rocks of the Kalgoorlie–Kambalda region. There is one striking feature of the komatiitic rocks — a laterally extensive unit of coarse-grained olivine adcumulate. This is the most extensive body of olivine adcumulate known in the Yilgarn Craton. It forms part of the Walter Williams Formation, which can be traced continuously from southwest of Siberia to the shores of Lake Ballard northwest of Menzies, and to the Kurrajong Anticline in the Mount Ida greenstone belt (Fig. 22).

The Walter Williams Formation is a layered body, traceable over an area of about 35 × 130 km, consisting of a lower zone of olivine cumulates and an upper zone of gabbroic rocks (Gole and Hill, 1990; Hill et al., 1995). The proportion of olivine cumulates to gabbro varies along strike as does the igneous porosity within the lower olivine-cumulate zone.

The formation is interpreted as part of a very large komatiite flow field. The southern part formed as a vast sheet lobe, resulting in the development of an extensive thick pile of olivine cumulates. In the north, the flow underwent ponding, fractionation in situ, and repeated influxes of new batches of lava (Gole and Hill, 1989, 1990).

Stratigraphic profiles through the Walter Williams Formation (Fig. 23) show the gross layering and lateral lithological variations. South of Ghost Rocks (see Locality 17), the lower ultramafic zone of the Walter Williams Formation is dominated by a thick olivine-adcumulate layer, which grades laterally to olivine mesocumulates and orthocumulates to the north between Ghost Rocks and Lake Ballard, and at Kurrajong. North from Yunndaga, the upper zone of the Walter Williams Formation is a layered gabbro, which thickens from approximately 30–40 m at Yunndaga to 100 m at Ghost Rocks and 180 m at Kurrajong.

Estimates of the true thickness of the unit are greatly hampered by the lack of dip information, and the relative thicknesses shown in Figure 23 are conjectural. At Vetters Hill (Locality 19), the estimated thickness is about 200 m, just south of Menzies it is only 50 m, and at Ghost Rocks it is again 100–200 m. The unit certainly appears to thin from an area about 10 km south of Menzies northward to Lake Ballard, although this may in part be due to deformation, as some of the rocks in this area are highly strained.

Several exposures of the Walter Williams Formation will be visited in the course of this excursion.

Exposures in the Western Mining Corporation SM7 nickel laterite pit provide a spectacular illustration of the unique style of weathering of very olivine-rich rocks in the Tertiary laterite profile. Adcumulates have been converted to a 'silica cap' containing more than 90% chalcedonic silica, but perfectly preserving the original adcumulate texture and, commonly, the textures associated with serpentinization of olivine. Pseudomorphs of adcumulate with fine-bladed antigorite along grain boundaries are present on the northern side of the openpit. This is the best locality for collecting samples of silica cap. The openpit was mined for silica flux (with a bonus of up to 2% Ni) for the WMC nickel smelter. The nickel laterite mining operations elsewhere in the Yilgarn Craton (as at the nearby Cawse deposit) mine the nickeliferous clays from the profile overlying the silica cap layer — these have been eroded in this locality.

Locality 2: Ularring Monzogranite (MGA 263474E 6686771N)

The Ularring Monzogranite (Wyche, 2004) is an ovoid pluton within the southern part of the Mount Ida greenstone belt that cuts across structures in the Ida Fault zone (Figs 20 and 21). The Ida Fault is the boundary between the Youanmi Terrane to the west, and the Eastern Goldfields Superterrane to the east (Fig. 3; Cassidy et al., 2006). The fault is prominent on aeromagnetic images (Figs 2 and 21), and it is interpreted, based on seismic data, to be an east-dipping listric structure that can be traced to a depth of 25–30 km, where it offsets the boundary between the upper and lower crust, but not the crust-mantle boundary (Drummond et al., 2000; Goleby et al., 2004).

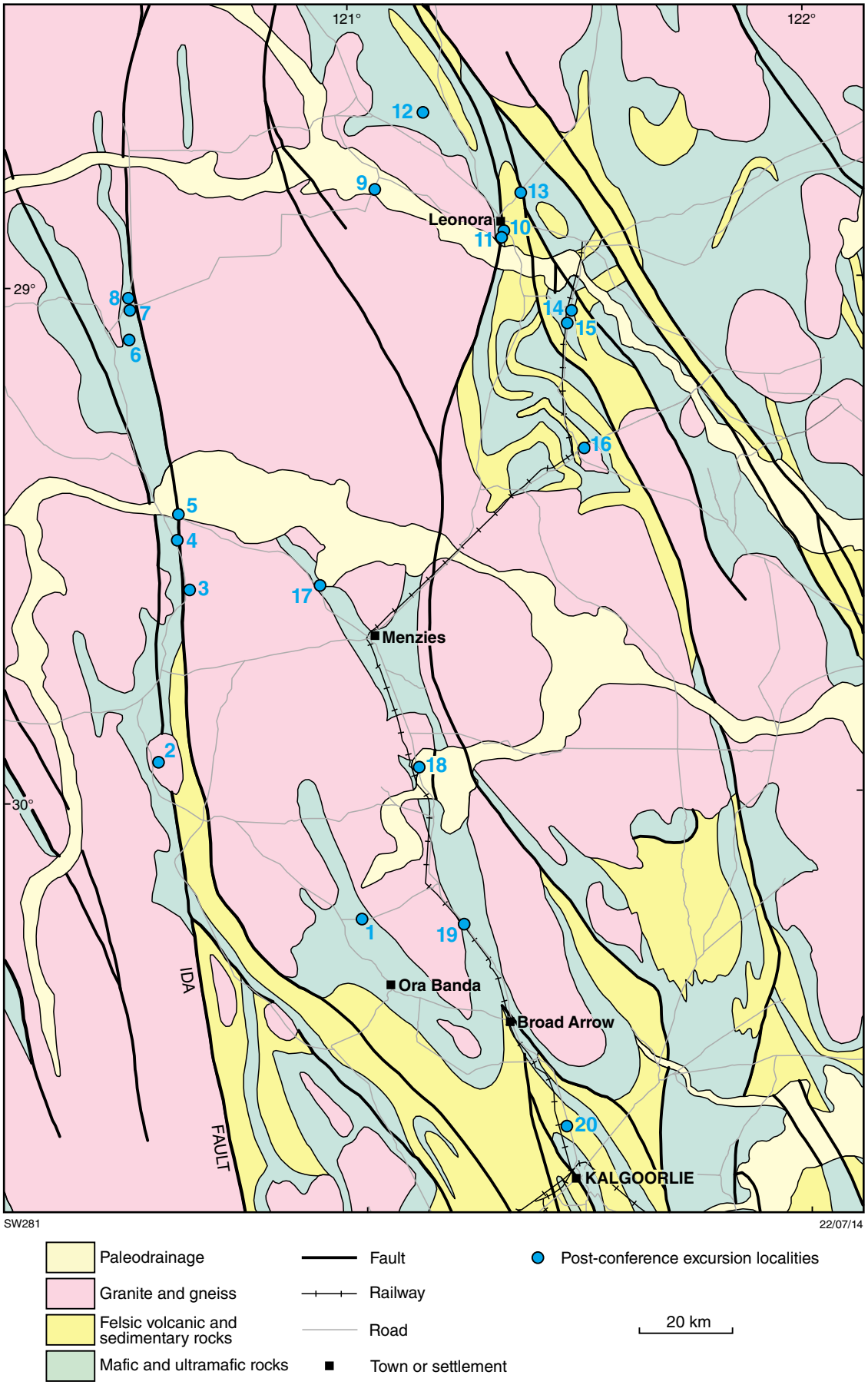

Figure 20. Post-conference excursion localities

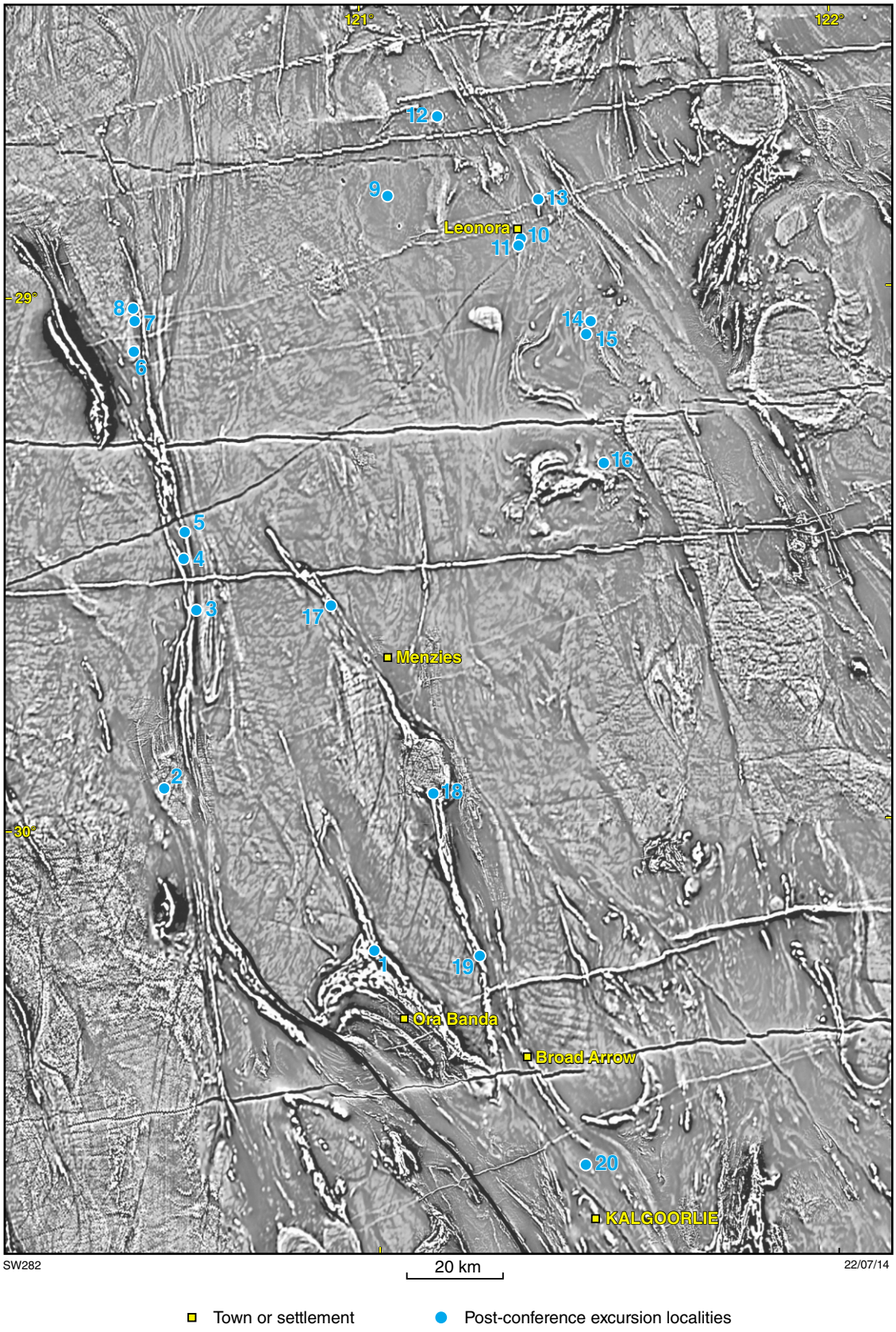

Figure 21. Post-conference excursion localities shown on a TMI 1VD aeromagnetic image

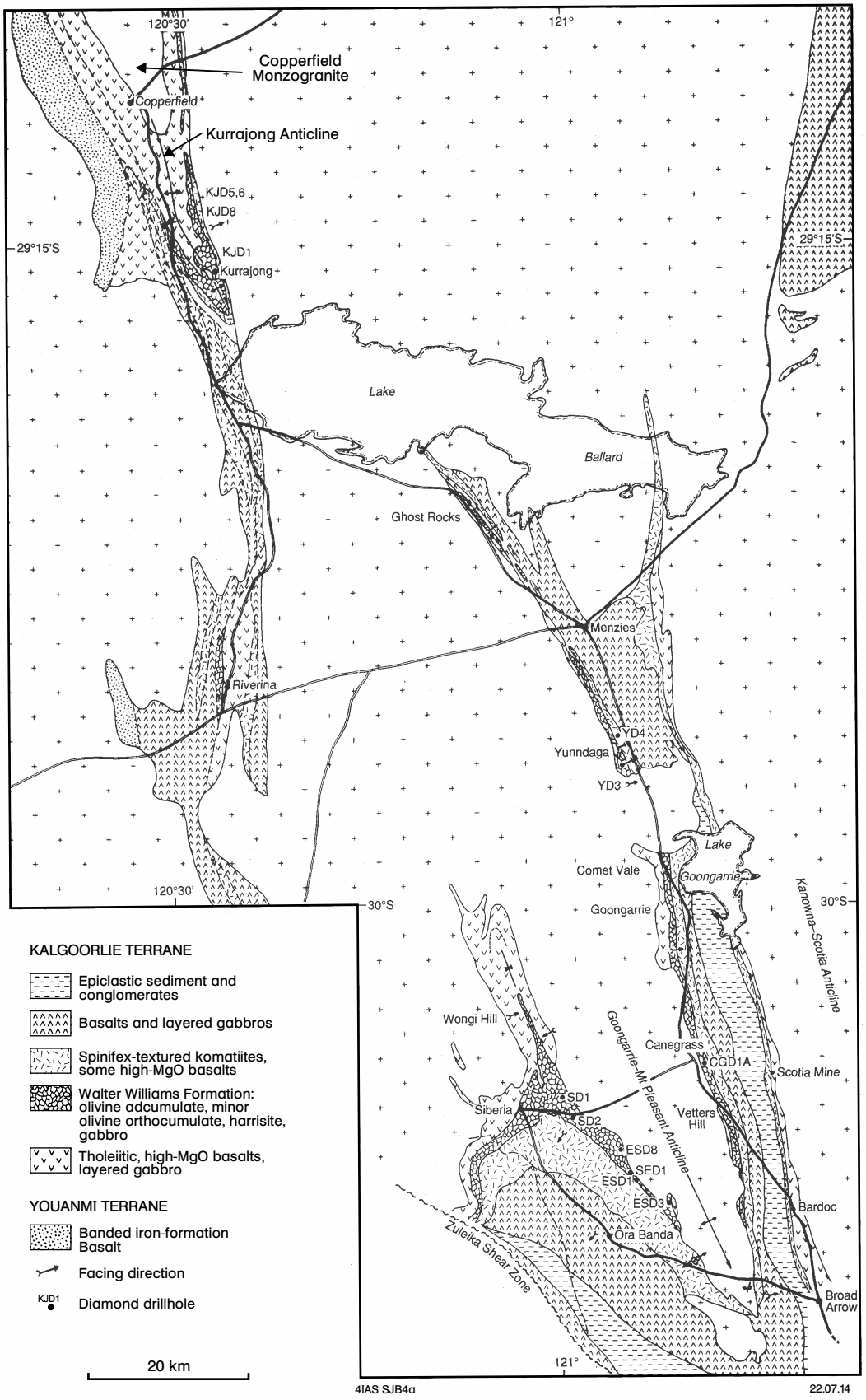

Figure 22. Geological map of the Walter Williams Formation showing the distribution of the olivine adcumulate unit. Data from CSIRO mapping, incorporating data from GSWA mapping by Swager et al. (1995), and mapping by J Hallberg, N Harrison, and N Herriman (modified from Hill et al., 2001)

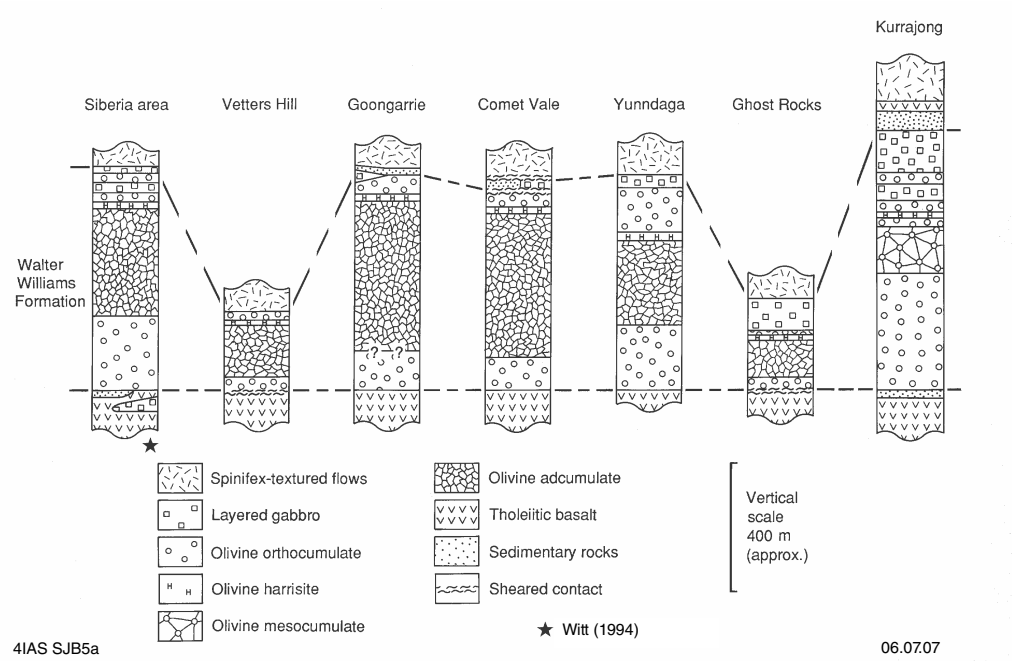

Figure 23. Stratigraphic profiles through the Walter Williams Formation. See Figure 7 for locations (modified from Hill et al., 2001)

The Ularring Monzogranite is a fine- to coarse-grained, weakly seriate, biotite monzogranite that contains minor opaque oxides, muscovite, and rare apatite. Secondary minerals include epidote, chlorite, and rare fluorite. Although weakly recrystallized, the Ularring Monzogranite is mainly undeformed, cut only by several north-northeasterly trending faults with displacements up to 500 m and locally filled by quartz. These structures represent the last clear tectonic activity in the region prior to the emplacement of Proterozoic mafic and ultramafic dykes. The SHRIMP U–Pb zircon age of 2632 ± 4 Ma (Nelson, 2000) of the Ularring Monzogranite supports the 2640 ± 8 Ma (Nelson, 1996a) age of the last movement on the Ida Fault given by the age of the Clark Well Monzogranite to the north.

Locality 3: Gneiss and granite at 18 Mile Well (MGA 270176E 6723993N)

This locality is representative of gneiss and foliated granite that extends for more than 100 km along the eastern side of the Mount Ida greenstone belt. The Ida Fault, which separates the Kalgoorlie Terrane of the Eastern Goldfields Superterrane from the Youanmi Terrane, runs through and along the Mount Ida greenstone belt (Cassidy et al., 2006).

The gneiss and foliated granite on the eastern side of the Ida Fault grade into gneissic granite with decreasing strain to the east, away from the granite–greenstone contact and major fault zones. The best exposures of granitic gneiss and gneissic granite outcrop within about 5 km of the granite–greenstone contact, particularly in the northern part of the greenstone belt. The eastern and southern extents of these deformed rocks are evident on aeromagnetic images (Fig. 21), which also suggest that they have undergone complex polyphase folding.

The granitic gneiss (Williams et al., 1993; Wyche, 2004) is a fine- to coarse-grained, quartz–feldspar–biotite rock characterized by compositional banding defined by variations in grainsize and relative abundance of biotite. The gneiss is mainly granodioritic or monzogranitic in composition, and rocks are typically fine grained due to cataclastic grainsize reduction of the protolith. The rocks typically contain various proportions of quartz, K-feldspar, plagioclase, and biotite. Accessory minerals may include opaque oxides, zircon, apatite, garnet, and titanite. Secondary minerals may include sericite, muscovite, epidote, titanite, and chlorite. The gneiss contains concordant slivers of amphibolite and mafic schist up to 2 m thick. Banding is on a scale of millimetres to tens of centimetres, and there is a common shallow-plunging mineral lineation. Some bands contain feldspar porphyroclasts up to 5 cm across, but pressure shadows around these grains do not give clear shear sense. Some of the numerous quartz and pegmatite veins that cut the gneiss at various angles are tightly folded. The lack of any clear shear sense suggests a very strong compressional component to the last stages of deformation. SHRIMP U–Pb zircon geochronology on similar gneiss and intrusive granites to the north of this locality suggest a protolith age for the gneiss of c. 2809 Ma and a major metamorphic event at c. 2670 Ma (Dunphy et al., 2003).

This metamorphism may correspond to the last major movement on the Ida Fault.

Fresh outcrop that gives a three-dimensional view of the rock can be seen at a blast site about 160 m east of the road (MGA 270176E 6723993N).

Locality 4: The Mount Ida greenstone belt near Henderson Well (MGA 267432E 6734649N)

The flats to the east of the road comprise poorly outcropping metamorphosed mafic igneous rocks with minor metasedimentary rocks. The northerly trending ridge to the east is composed of sheared mafic volcanic rocks.

Locality 4a: Metasedimentary rocks

About 50 m to the northeast of the road (MGA 267489E 6734669N) is a small outcrop of sedimentary rocks. These include laminated shales and mudstones with local fine-grained, well-sorted sandstone beds that are up to 1 cm thick. A solid-state foliation, parallel to bedding, has produced a well-developed parting in the rocks. The fine-grained rocks suggest deposition in a quiet environment and their context suggests they were interflow sediments within the primarily volcanic succession.

To the east of the sedimentary rocks is fine- to medium-grained, weakly deformed dolerite, which is either, a high-level intrusion within the mafic volcanic succession or part of a thick, ponded basalt flow.

Locality 4b: Mafic schist

About 300 m farther to the northeast (MGA 267728E 6734791), there is a thick sequence of variably deformed, komatiitic basalts with subordinate tholeiitic basalt. The komatiitic basalts are commonly variolitic with abundant spherical to oblate leucocratic varioles that are up to 10 mm across. The oblate varioles occur in the more deformed rocks and represent the flattening of the originally spherical features.

There is also a strain gradient in this area, which is controlled by variations in the competency of the different rock types. Strain increases to the east of the variolitic basalt where there is a strongly deformed package of tremolite ± chlorite schists which represent deformed and metamorphosed komatiite, peridotite and komatiitic basalt.

Locality 5: Pillow basalts at Snake Hill (Lake Ballard MGA 267771E 6740248N)

The 'Inside Australia' installation by British sculptor Antony Gormley was commissioned for the 2003 Perth International Arts Festival. The figures are based on body scans of the residents of Menzies. He is well known for his 'Angel of the North' sculpture near Newcastle in the UK <www.antonygormley.com>.

Pillow-lava structures in a weakly to strongly deformed, steeply east-dipping unit of komatiitic basalt on Snake Hill indicate east younging. This outcrop lies within a broad zone of deformation associated with the Ida Fault. Because of the intense deformation in this area due to movement on the Ida Fault, it is not possible to place this unit into a stratigraphic context but it belongs to the Kalgoorlie Terrane stratigraphic succession. The best outcrops of pillow structures are found on the eastern side of the hill, about two-thirds of the way up (MGA 267771E 6740248N). They can be reached by a footpath that begins at the base of the hill on the south side.

Locality 6: Copperfield Monzogranite (MGA 257100E 6777895N)

Modified from Rattenbury (1993)

The Copperfield Monzogranite outcrops in the core of the Kurrajong Anticline (Fig. 22) within the Mount Ida greenstone belt. The granite slightly transgresses the greenstone belt stratigraphy, which suggests an intrusive relationship. The contact, however, is strongly deformed. The granite has a very well-developed, pervasive stretching lineation, particularly around the pluton margins. The granite also has a weakly developed foliation which is subparallel to the boundary with the mafic–ultramafic volcanic rocks around the Kurrajong Anticline. The contact between the mafic metavolcanic rocks and the lineated Copperfield Monzogranite is strongly sheared but the fabric intensity diminishes southwards and eastwards into the mafic–ultramafic metavolcanic rocks indicating that penetrative ductile deformation is localized in the lower part of the stratigraphy. The metavolcanic rocks are pervasively lineated east of the Copperfield Monzogranite, and have been crenulated by the axial planar cleavage of an upright fold.

The granite lineation is formed by relatively large, unstrained quartz grains up to 2 mm long, separated by 1–3 mm plagioclase grains and 0.3 – 0.8 mm microcline. The plagioclase is typically unstrained with muscovite inclusions. The microcline occurs as subgrains with small mismatches in twin boundary orientations across grain boundaries. Dark green-brown biotite is the predominant mafic mineral present, with minor magnetite and apatite. Dynamic recrystallization of microcline is indicative of high temperatures during significant strain. The weak foliation within the granite and the foliation within the greenstone belt suggest that the deformation predated the upright folding, despite the occurrence of the stretching lineation subparallel to the Kurrajong Anticline fold axis. Several attempts to date this granite have been unsuccessful owing to a lack of zircons suitable for SHRIMP analysis.

Locality 7: Copperfield (MGA 257295E 6784295N)

The region has been a significant gold producer with historic production from numerous deposits in greenstones at the margins of the Copperfield Monzogranite. Gold was discovered here in 1895 and there were towns at Mount Ida to the east and at Copperfield. The Timoni gold deposit to the south has been worked intermittently since the discovery of gold in the area.

The westernmost limit of the Ida Fault zone lies to the west of the workings around Copperfield. Historical gold production data suggest a significant decrease in the amount of gold hosted by greenstones west of the Ida Fault in this area.

Locality 8: Forest Belle Gabbro (MGA 256975E 6786901N)

The Forest Belle Gabbro (Wyche, 2004) is a distinctive, coarse to very coarse grained metagabbro with very coarse ophitic texture. Tabular aggregates of plagioclase crystals, up to 5 cm across, are enclosed by very coarse oikocrysts of clinopyroxene, which have been pseudomorphed by pale to dark green, strongly pleochroic amphibole. Individual plagioclase grains are up to 5 mm long. The size of the oikocrysts is difficult to determine, but crystallographic continuity across several plagioclase grains indicated by reflections on cleavage planes suggests that they may exceed 5 cm across in places. Plagioclase typically makes up at least 50% of the rock, but may be more than 70%. The rock contains scattered, interstitial grains of opaque oxide up to 1 mm, and fine-grained epidote is a common minor secondary mineral constituent. The Forest Belle Gabbro is typically massive, but is strongly foliated near the contact with the Copperfield Monzogranite where it is cut by auriferous quartz veins.

Locality 9: Raeside paleodrainage (MGA 310128E 6810415N)

The Raeside paleodrainage is a major system. An account of the paleodrainage sytems of the Yilgarn Craton from Anand and Paine (2002) is given in the notes for Locality 10 in the Pre-conference excursion guide (this volume). Lake Raeside, which occupies the Raeside paleodrainage, filled after Cyclone Bobby in 1996. The flowing water cut the Goldfields Highway 10 km south of Leonora for about six weeks.

Locality 10: Mount Leonora (MGA 337979E 6801512N)

The view west from Mount Leonora looks across the Sons of Gwalia openpit to the Raeside batholith (Fig. 24). The Mount George lineament, which lies close to a line of chert ridges that can be seen to the north, is a discontinuity that may represent a sheared unconformity between the older, c. 2800 Ma succession (Baggott, 2006) to the west that hosts mineralization at Sons of Gwalia and a younger succession to the east (see Locality 13) that may be related to either the Gindalbie or Kurnalpi associations of Barley et al. (2008).

The following description of the rocks at Mount Leonora has been modified from Czarnota et al. (2008).

At Mount Leonora, kyanite–andalusite aluminous schist has a strongly foliated matrix assemblage consisting of quartz aggregate ribbons – graphite – skeletal andalusite – skeletal kyanite(–muscovite). Andalusite occurs as synkinematic poikiloblastic and as skeletal masses containing inclusion trails aligned with the foliation (Fig. 25a). The early andalusite poikiloblasts are boudinaged and flattened leading to being enveloped by the foliation as a result of ongoing progressive deformation (Fig. 25b). Late-stage ?sillimanite forms within the foliation. In sample Y242, post-kinematic kyanite laths grow across the foliation at high angles (Fig. 25d). Some kyanite grains are kinked during late-stage flattening across the foliation (Fig. 25c). Retrogressive muscovite forms on kyanite margins. Skeletal andalusite grows out from kyanite margins, growing preferentially along foliation planes (Fig. 25d). Sequence of mineral growth is from quartz–graphite–muscovite1 matrix foliation parageneses to rare sillimanite growth followed by kyanite growth and finally late-stage muscovite2 and andalusite2 growth. These relations indicate an anticlockwise turn around the alumino-silicate triple junction (Fig. 26). The main foliation also contains later stage sillimanite growth and is overprinted by post-kinematic kyanite laths, indicating burial with heating through the peak of metamorphism. Kyanite laths are partially enveloped by late-stage andalusite beards, indicating post-peak decompression with cooling back into the andalusite field. For a comprehensive overview of metamorphic conditions in the Eastern Goldfields Superterane, see Goscombe et al. (2009).

Locality 11: Sons of Gwalia mine — gold in extension during formation of the late basins (MGA 337665E 6800124N)

Modified after Czarnota et al. (2008)

The Sons of Gwalia mine is an excellent example of an extensional shear zone developed in greenstones of the Kalgoorlie Terrane that are exposed as a narrow (less than 10 km) sliver adjacent to a major granite batholith (Raeside). The granite margin, like the adjacent greenstones, is sheared with extensional kinematics (Williams et al., 1989). The shear zone 'faces' the dominant contractional vector that has been traditionally assigned to D_2 (Swager, 1997). In this example, the dominant ductile fabric is an extensional schistosity to mylonite in places, which dips moderately to gently to the east. It is not a contractional S_2 fabric, illustrating the contention here that foliation intensity and orientation makes an unreliable marker for correlating structural events.

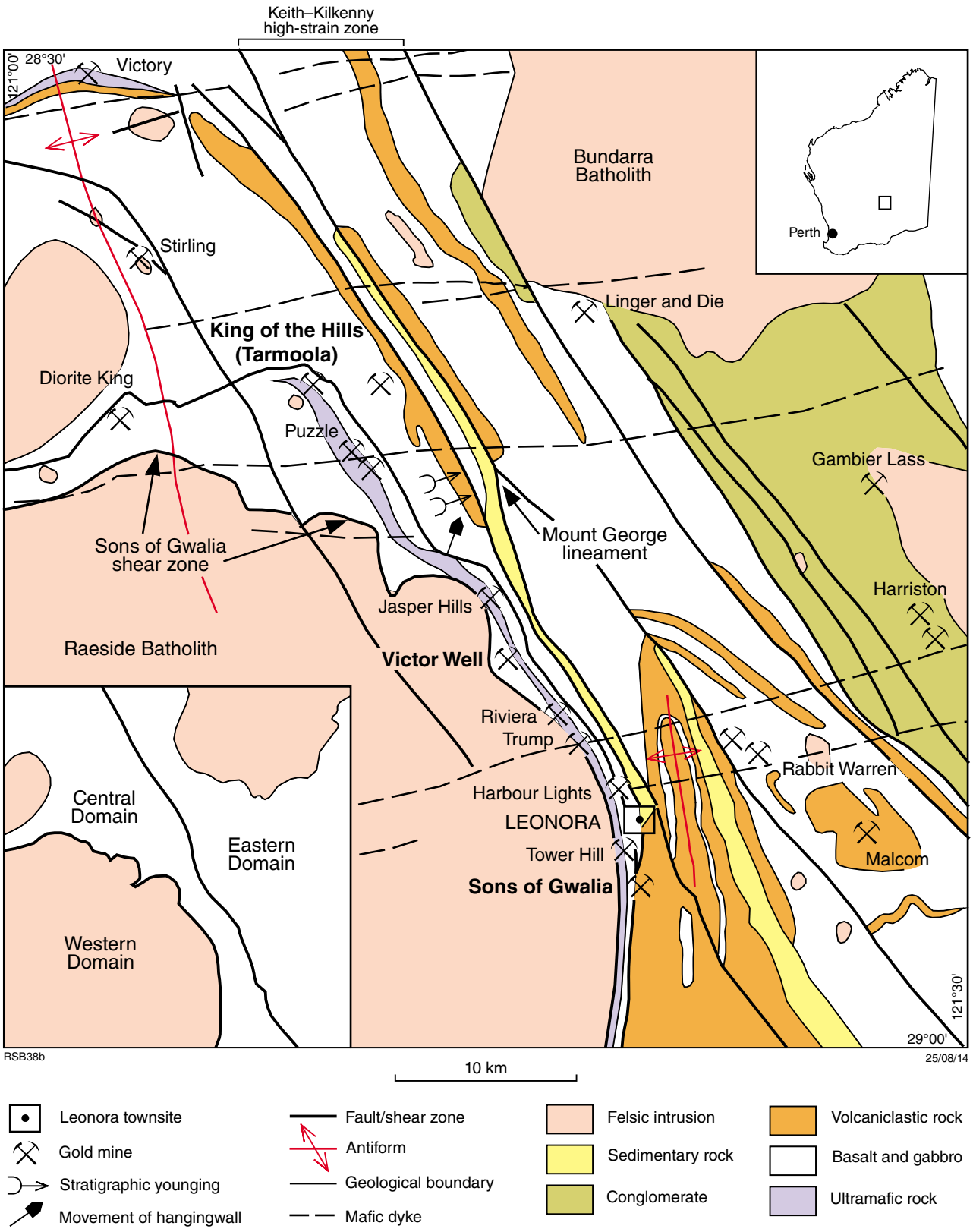

Figure 24. Simplified geological map of the Leonora district. Note the large granite batholith (Raeside) in the southwest of the map and the enveloping shear zones (extensional) that mantle the granite–greenstone contact (modified from Duuring et al., 2001; Czarnota et al., 2008)

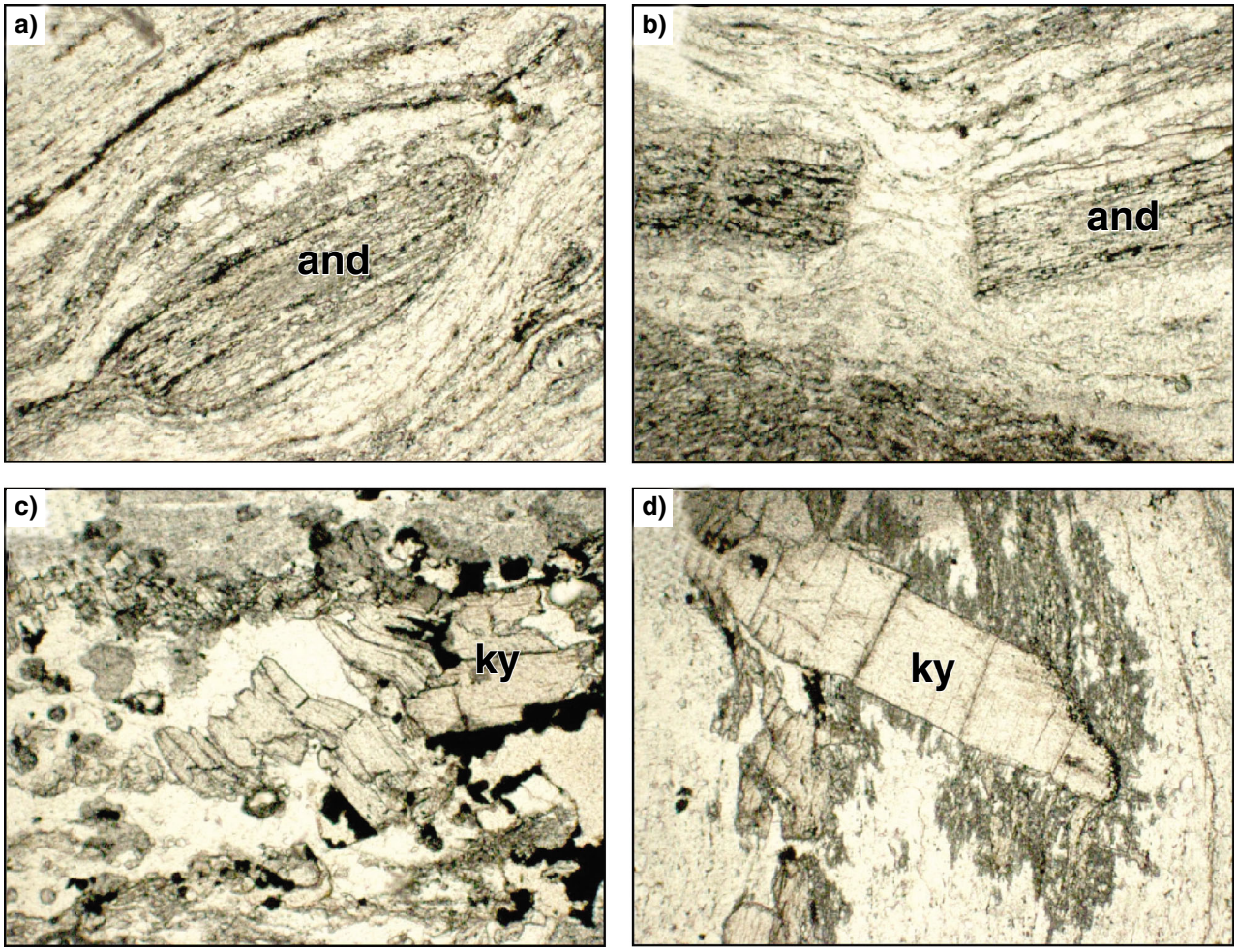

Figure 25. Mount Leonora: sample Y242: a) early enveloped andalusite (×2.5 ppl); b) boudinaged andalusite (×2.5 ppl); c) kinked kyanite (×6.3 ppl); d) early skeletal andalusite over-printed by kyanite, or alternatively late skeletal andalusite growth on post-kinematic kyanite (×6.3 ppl) (after Czarnota et al., 2008)

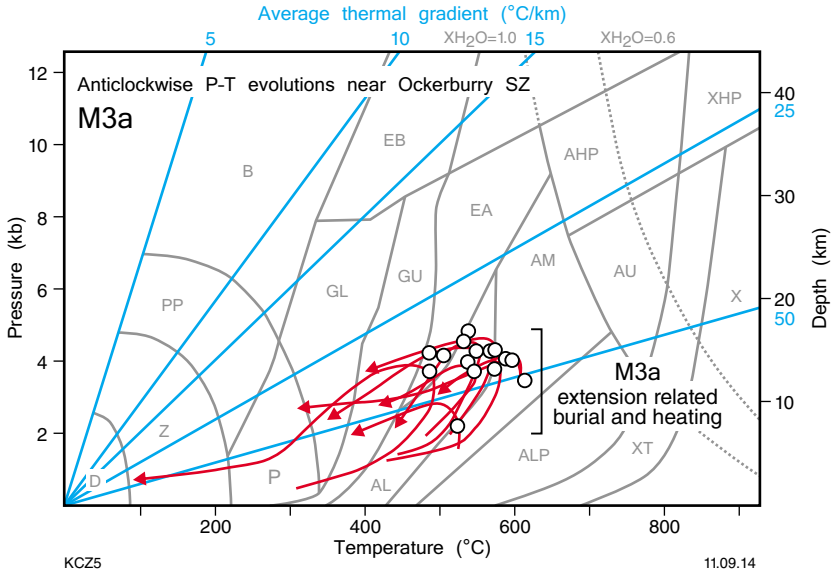

Figure 26. Peak pressure–temperature (P–T) loci and P–T evolutions from samples with anticlockwise P–T evolutions in the vicinity of the Ockerburry Shear Zone (Figure after Czarnota et al., 2008)

Sons of Gwalia is the third largest gold deposit in the Eastern Goldfields Superterrane. It is the southernmost deposit in the Leonora camp (Fig. 24), and is located 3 km south of the township along the Sons of Gwalia shear zone (SGSZ). Parallel shear zones host the other major gold deposits in the camp, namely Tower Hill and Harbour Lights (Figs 24 and 27a). The deposit is hosted in a sequence of tholeiitic pillow basalts and minor interflow sedimentary rocks (Fig. 28a), which are intruded by dolerite sills. The greenstones of the Leonora camp are thought to be older than 2750 Ma, based on a Re–Os age on molybdenite at Tower Hill (Witt, 2001). The Raeside batholith is a high-Ca granite-dominated batholith with intrusions ranging in age from 2760 ± 4 to 2669 ± 7 Ma (Cassidy, 2006). The youngest of these intrusions display the extensional kinematics observed at the Gwalia deposit and hence date the extension and associated Au mineralization to less than 2670 Ma.

Williams et al. (1989) identified the main tectonic mode in the camp as extensional, with high strains being accommodated along east-dipping shear zones that juxtaposed amphibolite- and greenschist-facies rocks. Using P–T estimates of rocks in a deep diamond drillhole through the Gwalia shear zone, Williams and Currie (1993) estimated around 3 kb of pressure and greater than 200°C temperature differences (extensional excision) had occurred across this shear zone. Work by Blewett and Czarnota (2007) also confirmed that the dominant tectonic mode was extensional ductile shearing with downthrows towards the east for the entire camp district.

The Gwalia orebody (three vertically stacked en echelon lenses) lies within the pervasive S3 foliation in a chlorite–sericite schist with numerous quartz–carbonate veinlets (Coates, 1993) and plunges within the SGSZ down to the southeast, parallel to the stretching lineation (Fig. 27a). The extreme linear-aspect ratio of the orebodies and the parallelism of the stretching lineation indicate that extension was the principal control on the formation of this gold deposit.

Locality 11a: View north of the Sons of Gwalia openpit

Views to the north show the main fabric elements consisting of the stratigraphy, lodes, and pervasive foliation, all of which dip around 35° to the east (Fig. 29a,b). The western lode is exposed just west of the portal and the main lode is characterized as a distinct bleached and brown layer east of the portal, halfway towards the eastern edge of the pit.

The dip of the pervasive fabric is consistent with the dip of reflectors imaged on the east–west NY1 seismic line across the Sons of Gwalia deposit (Fig. 29d). The strong reflectors define a 5 km-wide zone parallel to the Raeside granite batholith margin. Through extrapolation of the kinematics from the Sons of Gwalia line of deposits we infer this zone to be a 5 km-wide extensional shear zone. This interpretation is consistent with the geometry outline in the seismic data. In the hangingwall to this shear zone, the youngest part of the Yilgarn Craton stratigraphy (late basin) is preserved, consistent with extensional tectonics (Fig. 29c). A similar relationship occurs with respect to the Pig Well late basin, although the granite batholith controlling the localization of the shear zone does not outcrop but is imaged at 3 km depth. The reflectors related to the SGSZ roll into a detachment above a granite dome displaying an open concave geometry consistent with development in an extensional tectonic mode (Fig. 29d).

Locality 11b: Extensional kinematics of the Sons of Gwalia shear zone

The SGSZ is expressed as a pervasive foliation (D_3) within the pit (Fig. 28a–f). The pervasive fabric overprints an earlier set of quartz veins and foliation that appear locally to be early reverse shear veins (Fig. 28b,f). These veins may represent evidence for an earlier phase of contraction before the dominant extensional fabric-forming event (cf. King of the Hills mine). While most asymmetric folds indicate extensional tectonics, some folded veins have conflicting senses of vergence, indicating that the axial-plane foliation contains a strong flattening component of strain. These folded veins are likely to be the result of the particular angle between one conjugate vein set and the later extensional shearing (Fig. 28c). However, some quartz veins appear to have been formed during the extensional fabric-forming event. These veins are less deformed and cut the foliation, but have asymmetric folds with axial planes parallel to the main foliation, consistent with down-to-the-east normal kinematics (Fig. 30b).

Across the pit, the L_3 boudins and fold axes rotate towards the stretching lineation, suggesting a tendency towards sheath-like folding related to normal down-to-the-southeast shearing along high-strain zones (Fig. 27a). While the spread of fold-axis orientations may be a function of the original vein orientation, the spread of boudin neck lineations suggests strong transposition into the ‘a’ or shear direction (Fig. 27a).

Consistent S–C and C’ planes at a range of scales and most asymmetric folds indicate extensional tectonics. A large-scale extensional C’ plane is evident in the northwest corner of the pit, west of the portal entry (Fig. 30a). In rare outcrops the main shearing fabric (S_3) also hosts a crenulation in the microlithons between the phyllosilicate domains, implying a likely earlier phase of deformation (Fig. 28b).

Sets of white carbonate veins, many conjugate with northwest and southeast dips, are locally cut by related brittle sinistral-reverse faults that dip steeply to the northwest (Fig. 30c). These structures are assigned to D_{4b} and the resolved shortening direction ($\sigma 1$) associated with this event is approximately east–west (east-southeast – west-northwest) compression. An example of this set of veins is evident at the northern end of the western wall. The last event observed in the pit are east-northeasterly striking sinistral faults associated with carbonate veining. These are brittle faults associated with D_5 approximate northeast–southwest compression (Figs 30c and 31).

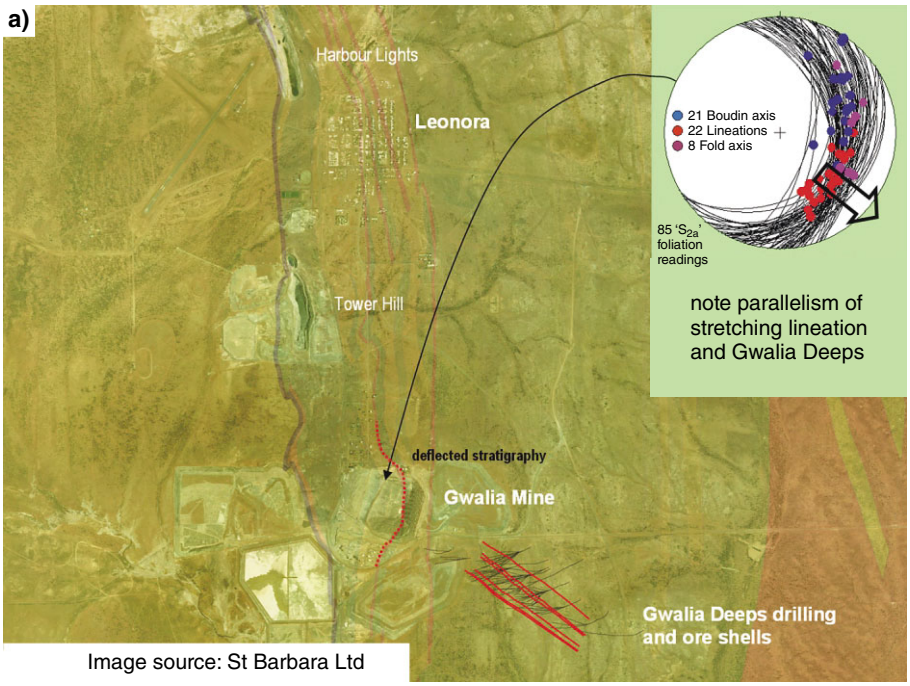

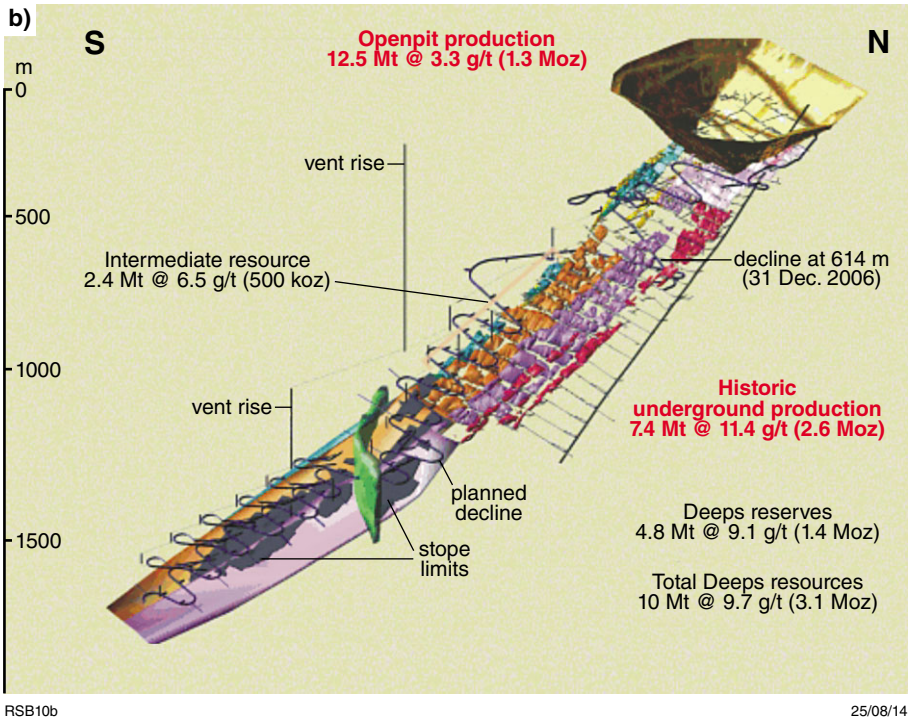

Figure 27. **a) Orthophotograph of the Leonora area showing the location of Gwalia Mine and Gwalia deeps to the southeast of the openpit and parallel to the stretching lineation (courtesy St Barbara Ltd); b) geometry of the Gwalia openpit and associated Gwalia deeps. Note the extremely attenuated aspect ratio of the ore zone, despite the host lithologies and shear zones extending north and south of the mine (courtesy St Barbara Ltd) (after Czarnota et al., 2008)**

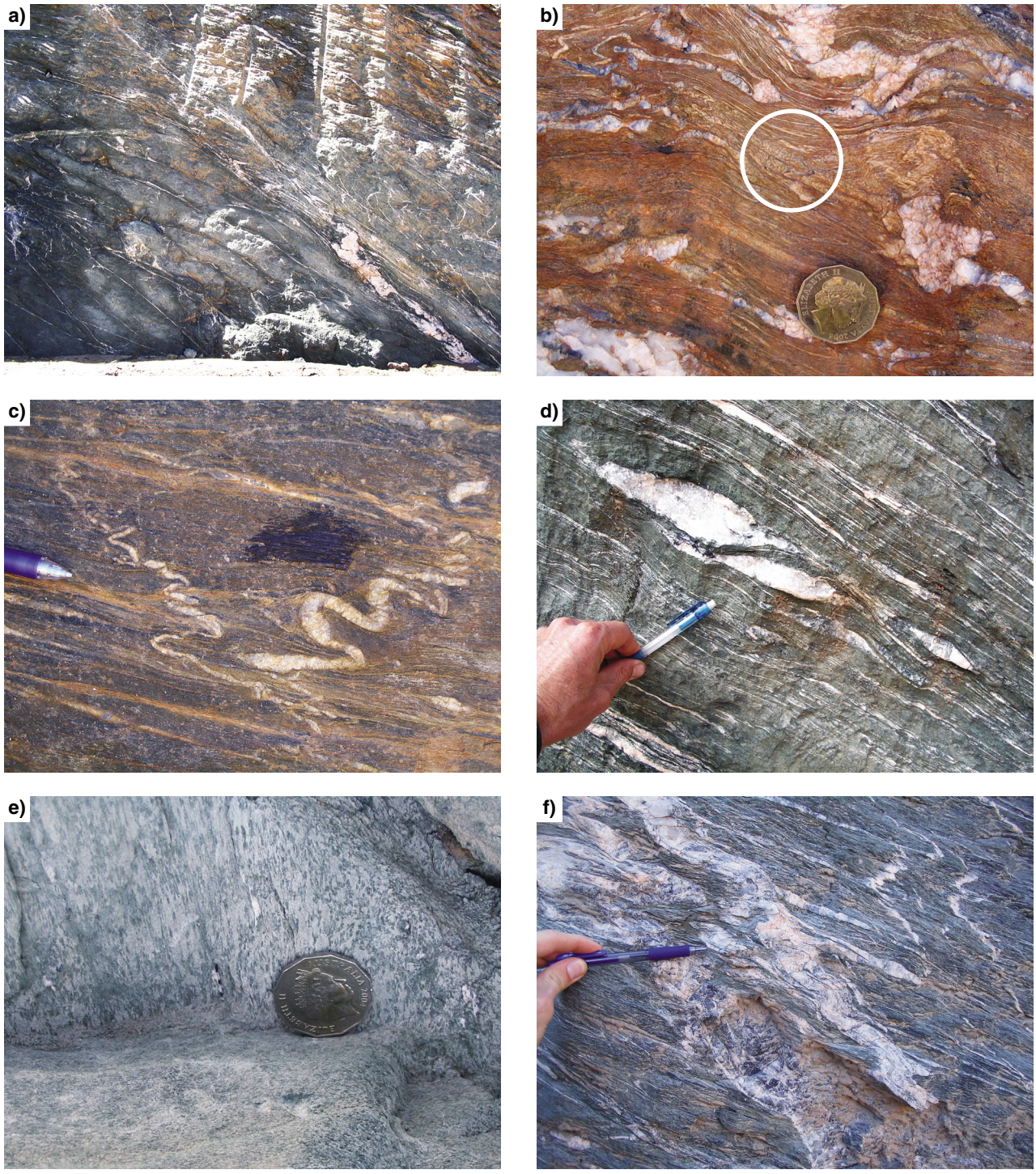

Figure 28. Compilation of photographs from Gwalia openpit: a) relict pillow lavas showing the basalt stratigraphy is upward facing to the east (view north); b) complex crenulations of early foliation (?$S_{1/2}$ shown in the circle) overprinted by the main S_3 extensional fabric (view north onto wall); c) conjugate veins flattened by a steeply inclined σ1 (developed during extension) and developing gently dipping axial planes to F_3 folds (view north onto wall); d) S–C–C' extensional fabric elements all showing down-to-the-east and southeast extension (view north onto wall); e) amphibole defining a down-dip stretching lineation (view west); and f) D_3 extensional overprint on earlier veins that may be originally developed during D_2 contraction (e.g. King of the Hills; view north onto wall) (after Czarnota et al., 2008)

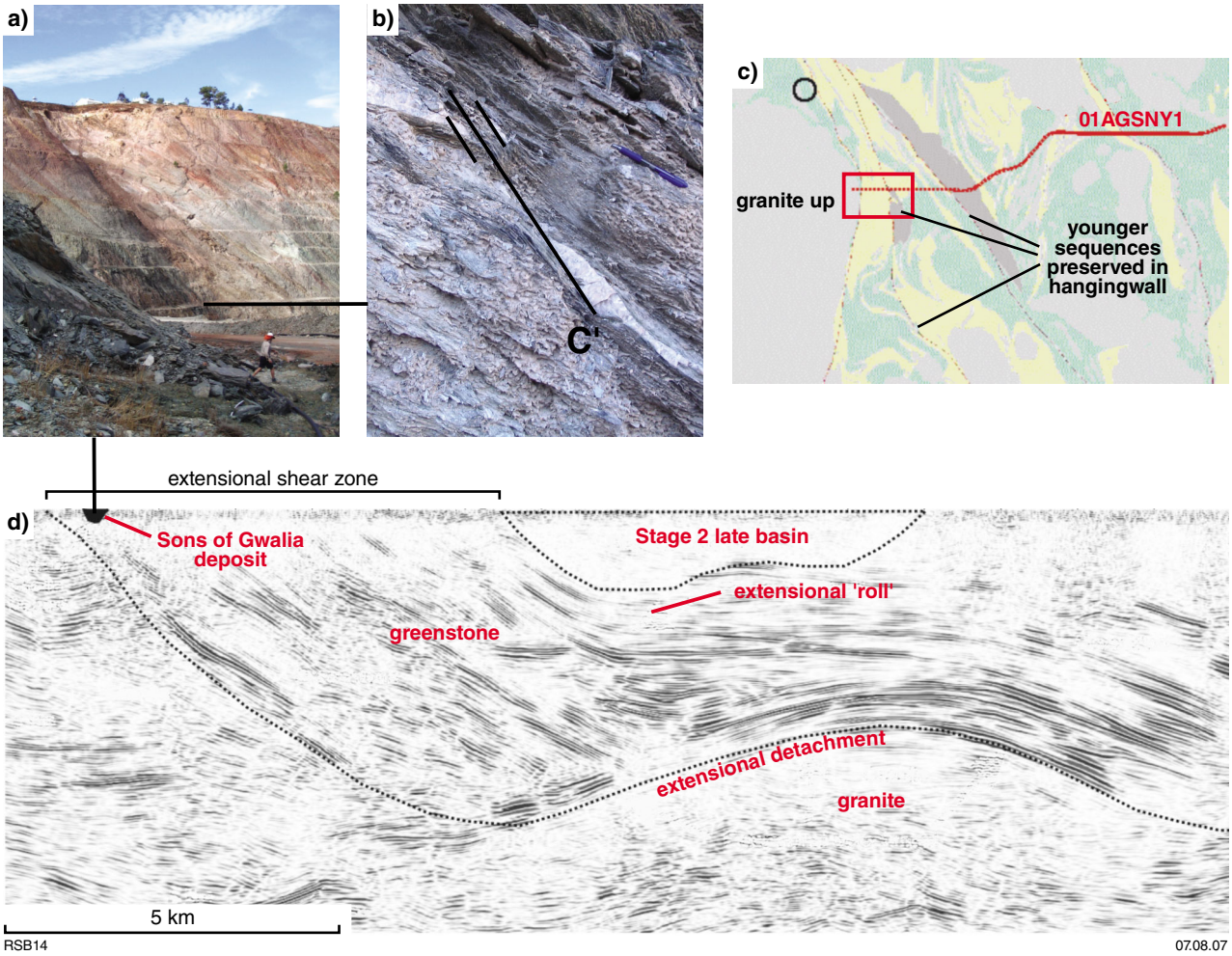

Figure 29. Compilation of extension recorded on a range of scales in the Leonora area: a) note parallelism of the layering (foliation) in the pit (view north) with the seismic events imaged in the section (d); b) extensional C' plane at the mesoscale; c) map of the seismic line crossing major faults with the youngest successions (late basins) in the hangingwall; d) east–west seismic line through the Gwalia pit vicinity to around 6 km depth shows extensional S–C and C' planes in the events at this scale. These intense bands of reflectivity (shearing) are up to 5 km wide and roll onto a granite dome at depth. This rolling of the fabric onto a detachment is consistent with extension (after Czarnota et al., 2008)

Figure 30. (facing) Compilation of photographs from Gwalia openpit: a) steep C' extensional shear planes developed over a limited vertical height (see arrow). Their depth extent may be related to the rheology contrast and thickness of layers being extended and boudinaged (view north); b) quartz veins overprint the main S_3 extension foliation and are dragged and offset by ongoing progressive D_3 extension (view north); c) S_3 foliation cut by later D_4 veins which are cut by a D_{4b} sinistral reverse fault. View west-southwest of a moderately inclined surface (after Czarnota et al., 2008)

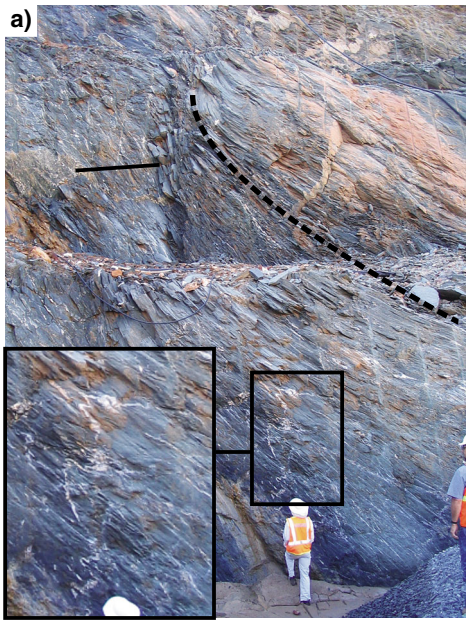

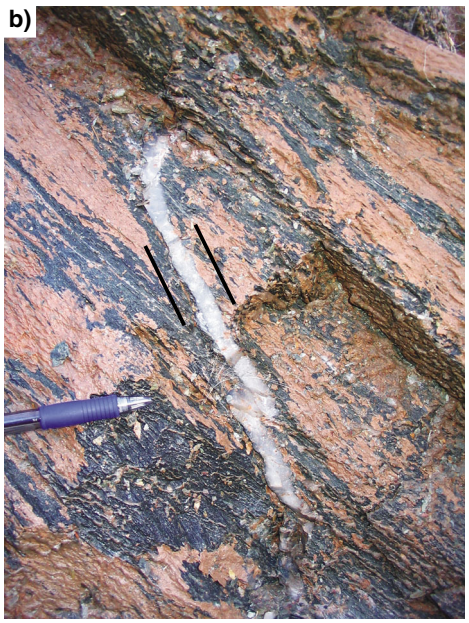

RSB12 07.08.07

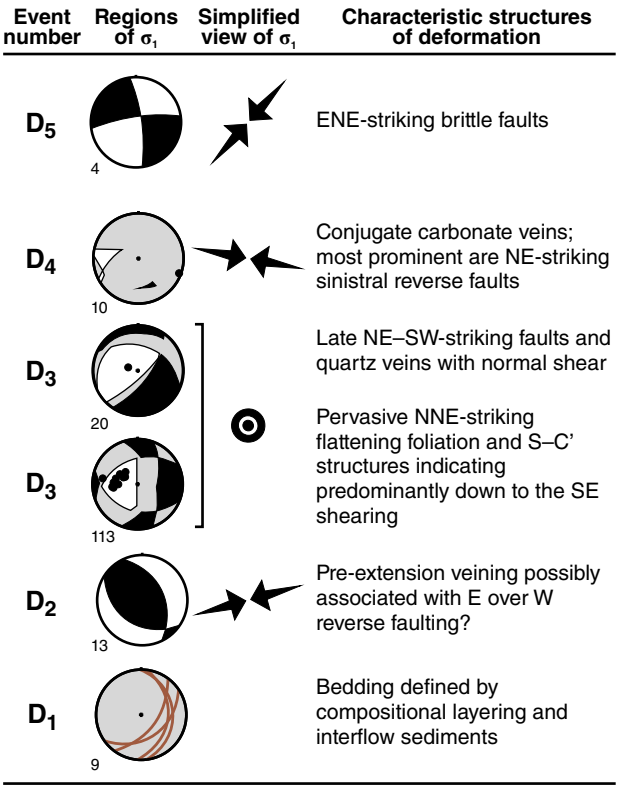

Figure 31. Stereographic compilation of structural elements in the Gwalia openpit. Note the dominant fabric elements developed during D_3 extension (after Czarnota et al., 2008)

Locality 12: King of the Hills (Tarmoola)* — contractional gold with an extensional overprint (MGA 320753E 6827328N)

Modified after Czarnota et al. (2008)

The Tarmoola openpit gold mine is an example of the role of competency contrasts (granite–greenstone) in localizing structures and hence permeability, fluid flow, and ultimately mineralization. The purpose of visiting Tarmoola is to illustrate the relationship between contractional gold and later overprinting by extensional shearing, inferred to be related to doming and the development of the late basins. A more extreme version of this extension is found in Gwalia (Locality 11).

Tarmoola (King of the Hills) lies approximately 30 km north of Leonora, on the northern end of the Raeside batholith (Fig. 24). The deposit is cored by a trondhjemite with diorite dykes dated at 2667 ± 8 Ma (LP Black, unpublished Geoscience Australia data). Recent studies (Blewett and Czarnota, 2007) have identified five phases of deformation, and as with other deposits in the region, the King of the Hills (Tarmoola) deposit has a significant component of extensional deformation (Skwarnecki, 1988; Vearncombe, 1992).

The greenstone stratigraphy is upward facing, based on numerous pillow lavas. The first fabric is developed in the greenschist-facies mafic and ultramafic rocks that are intruded by the trondhjemite. The fabric is patchy in distribution and preserved as a steeply dipping, east–west striking, penetrative foliation. The kinematics on this fabric are uncertain. It is a hard event to correlate across the Tarmoola openpit and the significance of this fabric with respect to regional deformation events is unclear. It is interpreted as part of the long-lived D_1 extensional event (Fig. 32).

The second event involved the development of an extensional S–C' shear fabric that is especially well developed in the talc schists. Sigma 1 was subvertical during D_1, with extension off to the northeast and southwest (Fig. 32).

Gold is hosted in spectacular D_2 quartz–carbonate (–fuchsite) veins related to dextral strike-slip shearing along the northeast-striking east edge of the Tarmoola trondhjemite. The dominant dextral shear planes are expressed as continuous sheeted quartz veins along the southeast wall of the south pit. Associated with these dominant shear veins are synthetic (dominant set) and antithetic en echelon quartz–carbonate(–fuchsite) veins (Fig. 33a–d). Brecciation occurs at many of the intersections of the synthetic and antithetic shear-vein sets, with fuchsite-altered wallrock incorporated into a blow out of quartz–carbonate veins (Fig. 33c).

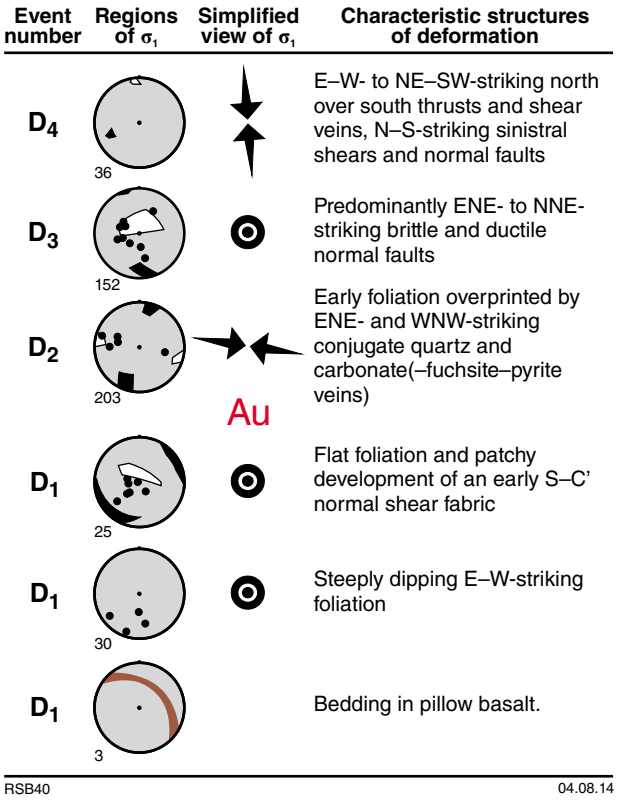

Figure 32. Stereographic compilation of structural elements into discrete events at the King of the Hills (Tarmoola) deposit. King of the Hills (Tarmoola) is an example of D_2 gold. Note how more than 200 structural readings resolve a very small S_1 sector to be just south of east–west and an orthogonal S_3 that is subhorizontal. It is likely that this subhorizontal S_3 reflects the overall transpression associated with D_2 contraction (as recorded in the granites), or the geometry of the trondhjemite contact with the greenstones (after Czarnota et al., 2008)

The above veins cut an associated north- to north-northeasterly striking S_2 foliation associated with the dominant shear veins. Mohr circle analysis by Duuring et al. (2001) showed that the presence of this pre-existing foliation would preferentially localize shear failure along the eastern edge of the trondhjemite. The D_2 contraction is well constrained, with σ1 oriented just south of east and σ3 oriented horizontally orthogonal to this with some local heterogeneity in the vicinity of the saddle pit (Fig. 34).

Some gold veins were deformed by a second extensional event, most notable in the saddle pit. This D_3 extensional event involved mostly down-to-the-north transport, with σ1 again vertical (Fig. 33d). The final event was the development of D_{4b} north-over-south thrusts (Fig. 33e–f) and shear veins, together with more steeply dipping sinistral faults and approximately north-trending normal faults.

* The King of the Hills gold mine is an underground extension of the Tarmoola openpit. The descriptions for for Locality 12 refer to observations in the Tarmoola openpit

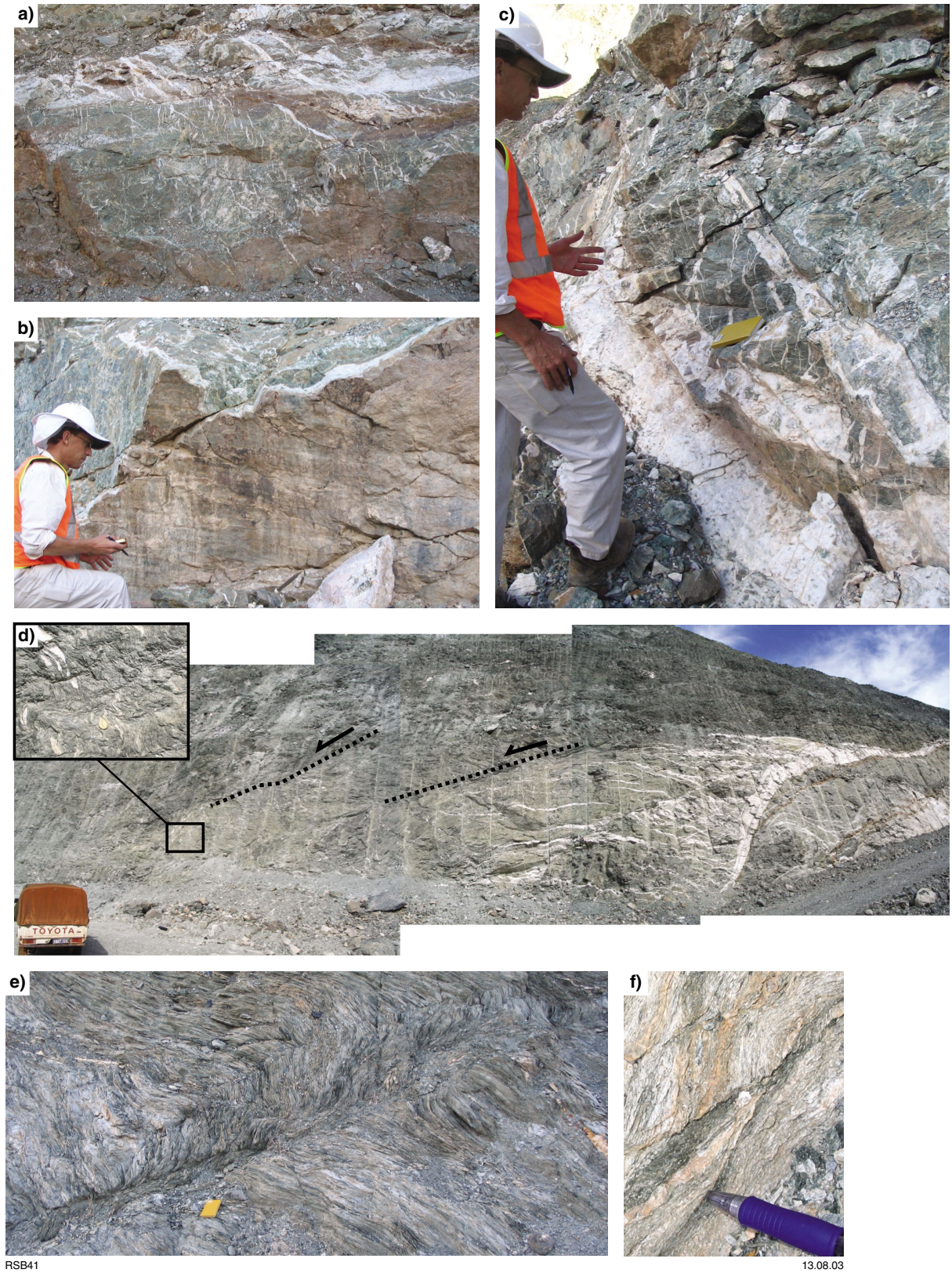

Figure 33. Compilation of photographs from Tarmoola openpit (King of the Hills): a) en echelon sinistral and dextral shear-vein arrays splaying from the main dextral fault (view southeast); b) dextral strike-slip fault strikes northeast–southwest and mirrors the margin of the trondhjemite (view southeast); c) detail of vein arrays and brecciation and fuchsite alteration associated with D_2 dextral shearing (view northeast); d) compilation of D_2 dextral strike-slip fault and spectacular wing-crack veins overprinted by normal (extensional) shearing during D_3. Inset shows detail of S_3 extensional crenulations (view southeast); e) top to the northeast D_5 thrusting overprints S_3 extensional crenulations in ultramafic schist (view northwest); f) detail of D_5 thrusts (view northwest) (after Czarnota et al., 2008)

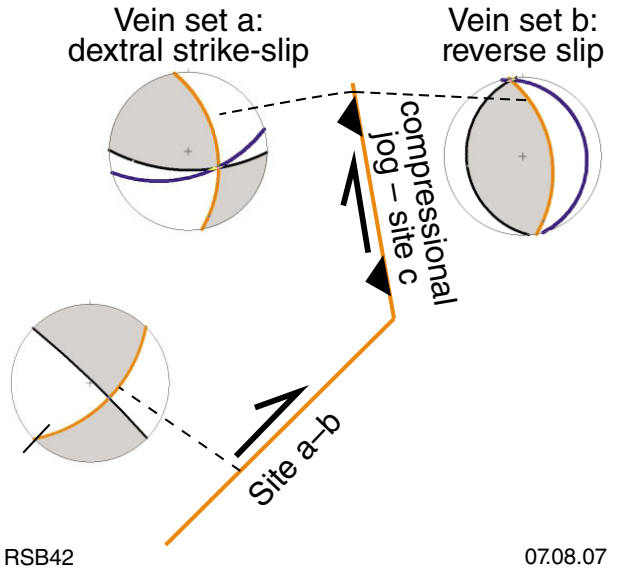

Figure 34. Schematic diagram illustrating how the geometry of faults (caused by a heterogeneous body like a granitoid) influences the structures observed at each location. Note how the structures change from reverse faults and veins to strike-slip under the same regional east–west contractional stress regime (after Czarnota et al., 2008)

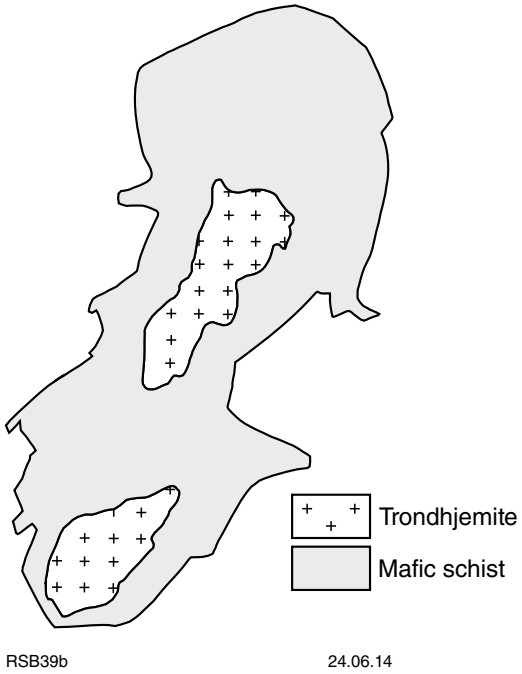

Figure 35. Distribution of trondhjemite in the Tarmoola openpit (modified from Duuring et al., 2001; Czarnota et al., 2008)

Locality 12a: Mineralized greenstone with steep contact with trondhjemite

This locality is at the southeastern part of the south pit and shows the steep contact with the main trondhjemite body and mafic schists (Fig. 35). The trondhjemite is largely unfoliated, and irregular apophyses of granite project outwards into the greenstone country rock. Sets of en echelon D_2 quartz–carbonate (gold-bearing) veins cut both the granite and greenstone. The dominant vein sets are dextral. The smaller synthetic and antithetic shear-vein sets display sinistral and dextral kinematics. An analysis of all the vein sets across the deposit resolves a maximum compression direction of approximately east–west. At the trondhjemite contact with the greenstones, notice the east-northeasterly striking brittle sinistral-normal quartz shear veins in the trondhjemite. These veins are consistent with formation during dextral movement along the main dextral sheeted veins under approximately east–west compression (Fig. 32).

All quartz vein sets overprint an earlier foliation (S_2) in the greenstone. Walk the section up the ramp and note the large steeply east-dipping wall of quartz with extension veins (sinistral and dextral en echelon sets) striking at acute angles to this main vein (Fig. 33c). Notice the horizontal lineation on the main quartz vein, consistent with dextral strike-slip shearing along this vein (Fig. 33b). The large veins that appear in the walls above are further examples of this vein set and the view is onto their dip direction so that they appear subhorizontal in this section provided by the openpit.

Warren Potma from the computational geoscience group at CSIRO funded by St Barbara Ltd conducted deformation driven fluid flow modelling of the Tarmoola deposit (Potma et al., 2007). Using detailed mine data around Tarmoola the geometry of the trondhjemite intrusion was determined and used as an input into the numerical modelling. Modelling of variable paleostress directions indicated that the results from models under east–west contraction resulted in the best fit between regions of known mineralization (Fig. 36a,d) and regions of greatest dilation and fluid flux in the model (Fig. 36b,c,e). These results agree with the paleostress direction determined for this event in this study (Fig. 31), illustrating that the numerical model is consistent with field observations. Based on the veracity of the modelling results in regions of known mineralization, Warren was able to predict a downdip extension of mineralization at the Tarmoola deposit (Fig. 36b,c) and three new mineralization targets around the Tarmoola trondhjemite (Fig. 36f).

Locality 12b: Extensional overprint of contractional gold

A spectacular east-dipping dextral D_2 vein with associated wing-crack veins is exposed in the west wall of the small saddle pit at the edge of the trondhjemite (Fig. 33d). This large vein is interpreted to be of the same set as the most prominent veins at Locality 12a (but in this case strikes north-northeast). There are three minor vein sets associated with this vein, indicating a dextral and reverse-slip component of shear along the main vein.

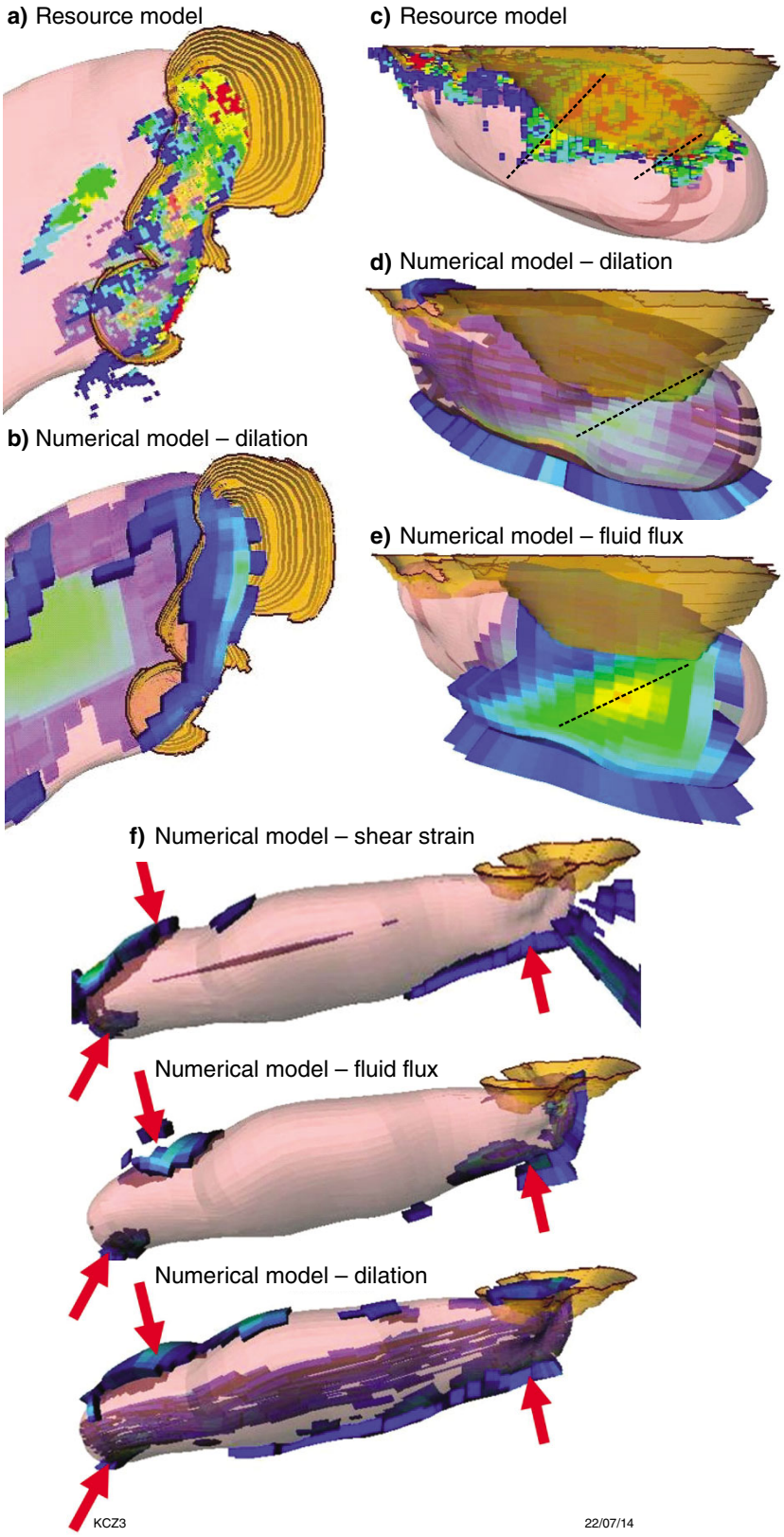

Figure 36. Results of deformation-driven fluid flow modelling under east–west contraction around the Tarmoola trondhjemite by Warren Potma from the computational geoscience group at CSIRO funded by St Barbara Ltd: a–c) are cross-section views looking west; d–e) are plan images with north at the top of the page; f) displays cross-section views looking north. Each figure shows the outline of the Tarmoola trondhjemite in pink and the Tarmoola openpit in orange; warm colours in the resource and numerical models indicate highs. Notice the replication of the plunging high-grade ore shoots from the resource model (a) in the numerical model (b–c) and the localization of dilation in the openpit (e) which corresponds to known mineralization in the resource model (d), (f) shows the location of three new gold targets (red arrows) in regions away from the mine (after Czarnota et al., 2008)

Using the P–T dihedra, the stress direction resolves as northeast–southwest compression (Fig. 31). This local variation in the stress field is due to a strike change of the greenstone–trondhjemite contact and the establishment of a restraining jog along the trondhjemite contact (Fig. 34). This feature is analogous to the north-northwest – south-southeast compression observed along some structures related to the regional sinistral strike-slip event. That is, the resolved stress field at a location may be influenced more by the fault orientation than the regional stress direction.

To the north (down the ramp), the wing-crack veins are overprinted by increasingly intense extensional shear zones and vertically flattened folds and crenulations (D_3). In the highest strain domains, the original vein geometry is largely obliterated by the extensional shearing (Fig. 33d inset). Analogies with the high strains at Gwalia are thus drawn. The extension is to the north and is interpreted to be related to doming from the Raeside batholith and development of the late basins.

Locality 12c: Late thrust overprinting extension

On the decline leaving the pit, a series of D_3 extensional shears are developed in talc–chlorite schists. These extensional shears are overprinted by D_{4b} thrusts with top to the northwest shear (Fig. 33e,f).

Locality 13: Felsic volcanic rocks near Leonora (MGA 341627E 6809720N

This well-exposed section of felsic volcanic rocks, although strongly weathered, shows excellent preservation of primary textures. Here weathering is much more advanced than, for example, the Melita Formation at Locality 14. This may be because rocks in Leonora have alteration-related compositions that are more prone to weathering or because these rocks have undergone a weathering event that did not affect rocks farther south. Similar degrees of weathering are seen in the Yerilla area (Kurnalpi Terrane) to the southeast of Melita.

Coarse autoclastic deposits with clasts up to several centimetres in size are common in the eastern part of the outcrop area. Grainsize typically decreases towards the west, where fine-grained sericitic schists with felsic protoliths are most common. Many of the rocks are quartz-phyric. At Locality 13, there are good examples of hyaloclastic breccia in which individual fragments can be very large (tens of centimetres). The rocks have characteristic jigsaw-fit texture with clasts surrounded by small amounts of hyaloclastite (Fig. 37), and are interpreted as subaqueous lava flows.

Primary bedding is seen locally in the finer-grained rocks. Tectonic fabric development and sericitic alteration also increases towards the west, approaching the Mount George lineament. Quartz–(?)tourmaline veining increases to the west, and many vein arrays have sinistral geometries.

The mafic rocks within this succession range from dolerite to gabbro. They are relatively less weathered and deformed compared to the felsic rocks.

No good geochemical or geochronological data are available for this succession. It is currently interpreted as an extension of Melita-type rocks. However, it is possible that these rocks are equivalent to Kurnalpi-type volcanic rocks like those at Welcome Well to the east (Barley et al., 2008).

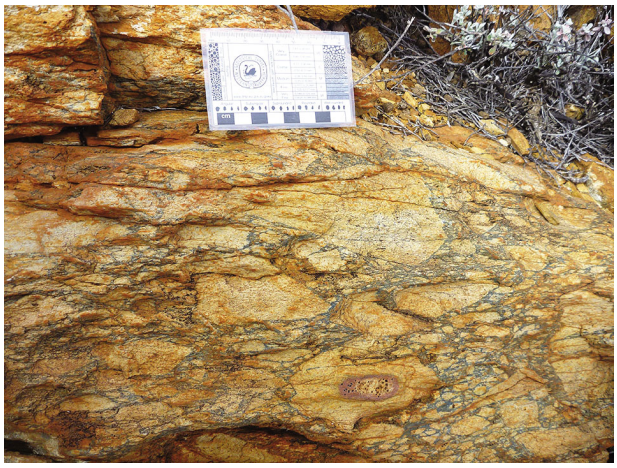

SW284 24/06/14

Figure 37. Deformed hyaloclastite breccia at Locality 13

Locality 14: Melita Formation (MGA 352558E 6784296N)

Hallberg (1985), Witt (1994), Brown et al. (2002) and Barley et al. (2008) have described two volcanic centres in the Melita area: the Jeedamya and Melita volcanic complexes. Mapping in this area is currently under revision and it is likely that the Jeedamya and Melita volcanic complexes will be assigned to the Melita Formation. These rocks represent Gindalbie association of high-HFSE bimodal calc-alkaline, intermediate–silicic volcanic rocks of Barley et al. (2008). Of the two, the Jeedamya centre is less well exposed, consisting of dacite and rhyolite pyroclastic rocks and related epiclastic rocks, felsic porphyry, and minor mafic extrusive and intrusive rocks. A SHRIMP U–Pb zircon age of c. 2683 Ma from the Melita volcanic complex (Brown et al., 2002) is within error of the age of the c. 2681 Ma Jeedamya volcanic complex to the south (Nelson, 1996b). Brown et al. (2002) considered the Melita volcanic complex to be a bimodal succession with coeval effusive submarine volcanism and voluminous (effusive, shallow intrusive and explosive) rhyolite volcanism in a shallow subaqueous setting.

On the eastern side of the fence south of the old Melita railway siding (MGA 352630E 6784570N), there is an east-dipping succession of fine to coarse fragmental rocks

of the Melita Formation. Here, Brown et al. (2002) have described a section which contains

> 'poorly sorted quartz-bearing volcaniclastic sandstones and fine breccias' which 'are generally massive to normally graded or diffusely bedded on a scale of cm–dm, with rarely preserved cross-bedding. Clasts are predominantly angular to subrounded fragments of porphyritic rhyolite, within a variably crystal-rich vitric (now recrystallized) matrix. Graded mm–cm-thick beds of fine-grained vitric to variably crystal-rich sandstone probably represent water-settled airfall tephra. Accretionary lapilli have been observed in some of these units.
>
> Thick (>10 m) units of massive to bedded volcaniclastic sandstone and breccia commonly grade upwards from breccias through massive crystal-rich sandstone, into planar-bedded sandstones. The breccias are matrix supported to locally clast supported and dominated by subrounded to angular clasts of porphyritic, commonly flow-banded rhyolite, and rare deformed pumice.'

They are locally intruded by dolerite.

At Locality 14, the outcrop is dominated by clast-supported, fragmental rhyolitic rocks with elongate, tightly packed, angular to sub-rounded clasts up to 10 cm. Just to the west, the rock is more feldspathic with common millimetre-scale euhedral to anhedral feldspar crystals.

Farther west (MGA 352538E 6784293N), there are some boulders with larger (commonly more than 30 cm), angular, close-packed fragments of feldspathic rhyolite with local jigsaw fit in a groundmass of the same material. The clasts are locally layered with some quartz phenocrysts. Also present are finer fragmental rocks, with subcentimetre-scale, angular fragments.

The hill to the north contains layered felsic volcanic rocks with alternating fine- and coarse-grained beds.

Locality 15: Basalt of the Melita Formation (MGA 351638E 6781581N)

According to Brown et al. (2002), basalt and basaltic andesite lavas are interbedded with all other units of the Melita volcanic complex. Basalts can be massive and pillowed and are locally interbedded with hyaloclastites. At this locality, massive basalt contains clasts of sediment and felsic breccia with local interbeds of thin-bedded sedimentary rock and breccia.

Locality 16: Dairy Monzogranite (MGA 355335E 6754710N)

Modified from Brown et al. (2001)

The Kookynie district contains a number of granitic intrusions that form a complex association with several distinct ages of emplacement (Hallberg, 1985). The northern part of the Mendleyarri batholith (Williams et al., 1976) is a complex composite pluton, including quartz-rich biotite–muscovite syenogranite and monzogranite. The western part of the batholith consists of foliated, lineated, massive to sheared biotite–hornblende, biotite, and biotite–muscovite monzogranite. The monzogranite contains anhedral quartz, plagioclase, and K-feldspar, and scattered biotite or muscovite with minor chloritized hornblende (Hallberg, 1985). In the Niagara district, the monzogranite has been subjected to deformation, resulting in shear zones and quartz veining hosting much of the gold mineralization in the district. The monzogranite is intruded by a variety of dykes and numerous veins of pegmatite, aplite, and muscovite granite (Hallberg, 1985). Syenogranite porphyry dykes cut all rocks in the Niagara area, and are probably related to the Dead Horse syenogranite to the south of the area.

The eastern part of the batholith consists of coarse-grained biotite–muscovite monzogranite and syenogranite. The granite is characterized by subhedral quartz grains up to 1.6 cm in diameter, anhedral plagioclase, K-feldspar, and minor muscovite with or without biotite, with some sericite, carbonate, and epidote alteration (Hallberg, 1985). A sparsely feldspar-phyric, medium-grained biotite monzogranite with minor hornblende granodiorite invades marginal granite and porphyry between Mount Niagara and east of Kookynie. This intrusion consists primarily of biotite monzogranite with blocky plagioclase (which may show oscillatory zonation), anhedral quartz and K-feldspar, biotite, and minor titanite, with or without green hornblende, and probably represents a later phase of the Mendleyarri batholith (Hallberg, 1985). Alteration is mainly epidote and chlorite, with minor carbonate and moderate sericite developed in places.

The Dairy Monzogranite is very felsic (more than 74% SiO_2), contains low Al_2O_3 and, for a given silica content, significantly higher concentrations of TiO_2, total FeO, MgO, Y, Zr, Nb, and to lesser extents LREE. Large ion lithophile element contents, especially Rb and Pb, are generally moderate to low, reflected in K_2O/TiO_2, Ce/Pb, and Zr/Rb ratios. These features are indicative of granites belonging to the high-HFSE group of Champion and Sheraton (1997).

Locality 17: Kalgoorlie Terrane stratigraphy at Ghost Rocks (MGA 298330E 6724968N)

At Ghost Rocks, a short southwest to northeast traverse, along and beside the track across the southwestern limb of a syncline (Fig. 38), crosses a mafic–ultramafic succession that is correlated with the Kalgoorlie Terrane stratigraphy at Kalgoorlie (see Pre-conference excursion Locality 1, this volume):

1. From the main road, there are small outcrops of basaltic schist (Missouri Basalt of Swager et al., 1995). Along the track, this passes into metagabbro and cumulate-textured metapyroxenite.

2. A narrow layer of olivine cumulate (MGA 298330E 6724968N) which is serpentinized and silicified (at a prominent mesa to the northwest). This is the Walter Williams Formation of Gole and Hill (1990) and Hill et al. (1995). A strongly cleaved grey shale/slate unit within the ultramafic unit (MGA 298532E 6724977N) was probably an interflow sediment.

3. Across a small gulley there is common outcrop and float of coarsely spinifex-textured komatiite (MGA 298399E 6724948N). Although foliated in places, the platy olivine-spinifex texture is well preserved. This is the Siberia Komatiite of Swager et al. (1995). Two shallow pits in the komatiite on top of the rise (MGA 298469E 6724949N; 298456E 6724937N) have exposed small patches of copper mineralization.

4. Metagabbro above the komatiite (MGA 298503E 6724944N).

5. Above the contact with the overlying metabasalt (MGA 298609E 6724962N), strongly cleaved metabasalt becomes more massive and locally very coarsely feldspar-phyric (MGA 298670E 6724962N).

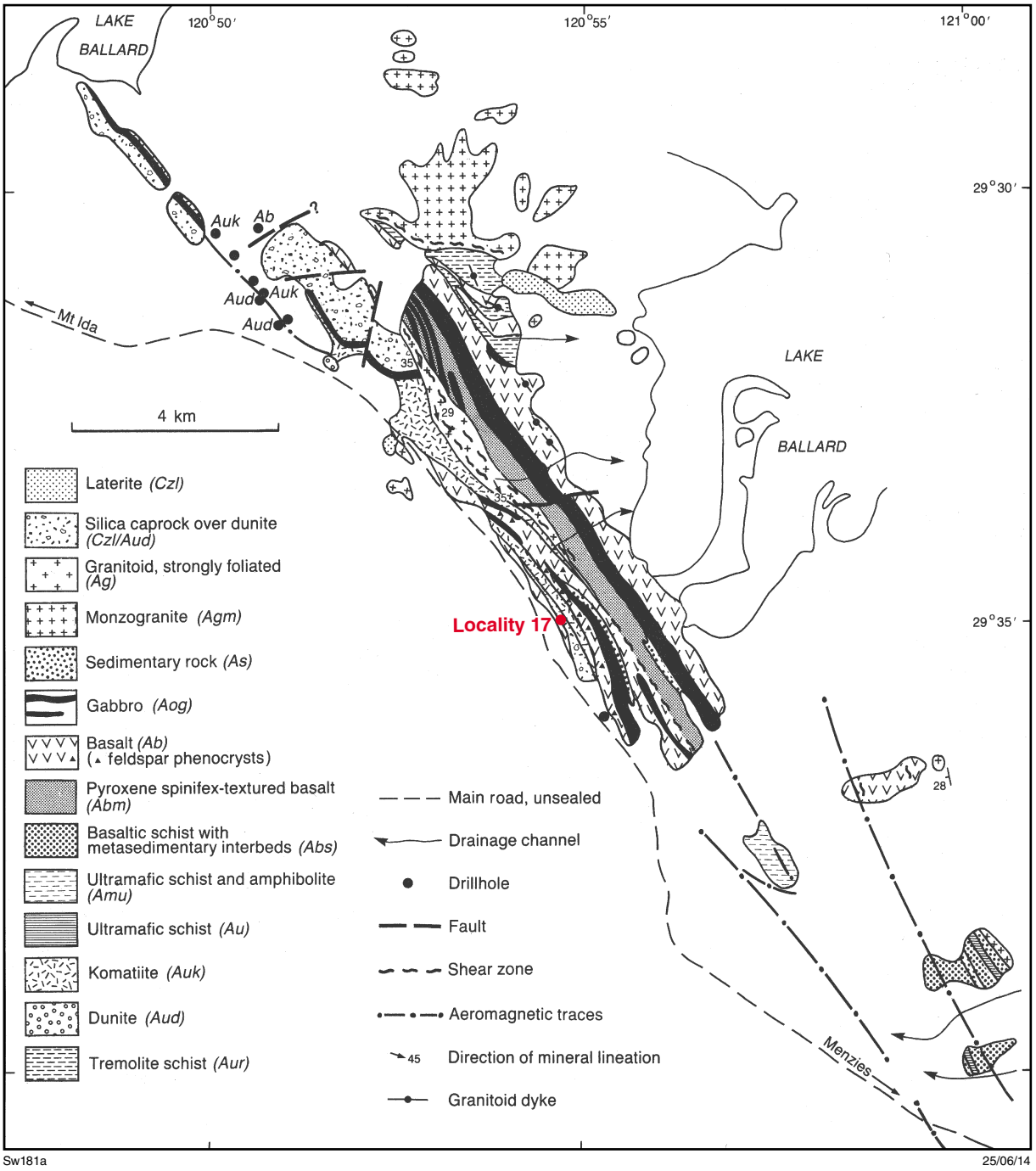

Figure 38. Interpreted geology of the Ghost Rocks area (modified from Swager, 1994)

Locality 18: Comet Vale ultramafic rocks (MGA 319710E 6685732N)

Modified from Hill et al. (2001)

Note: Participants are requested not to use hammers or remove sample material from this outcrop.

At this locality, the upper sections of the Walter Williams Formation and the overlying spinifex-textured flow sequence (Siberia Komatiite) are seen. At the beginning of the traverse (Fig. 39) on the old WMC grid baseline, and on the flat area immediately to the east, the adcumulate is covered by ferruginous laterite cap and adcumulate textures are preserved only in a few places. Down the eastern slope of the hill, lower down the laterite profile, adcumulate textures are well displayed in siliceous laterite. The olivine harrisite and its abrupt contact with the adcumulate can be seen just before the steep drop on the eastern side of the hill (MGA 319950E 6685657N). The harrisites have been etched by weathering and their three-dimensional shapes are well shown.

Down the slope, fine-grained orthocumulate with several 30 cm-thick pyroxenite layers outcrop (MGA 319960E 6685690N). On the flat ground farther east, only patchy low outcrop of orthocumulate is present. The rocks here are highly sheared and numerous pegmatites are present. Two major shear zones intersect in this area. Across the shear zones to the northeast are unstrained spinifex-textured flows that form part of the Siberia Komatiite volcanics. These are part of a rotated block, striking southeasterly, bounded to the south by a shear zone and to the north by intrusive granite.

Locality 19: Vetters Hill ultramafic rocks (MGA 329397E 6651857N)

Modified from Hill et al. (2001)

A complete section through the Walter Williams Formation is seen in the siliceous laterite that caps the Vetters Hill. The ultramafic unit is unusually thin at this locality, having an apparent thickness of about 150 m compared to 600–900 m elsewhere in its southern outcrop area. The facing is easterly and we shall walk down stratigraphy (at least initially). From the road to just past the fence are serpentinites with fine-grained orthocumulate and uncommon spinifex textures. Rubble covers the lower part of the hill, although there are a few low outcrops of orthocumulate. About three-quarters of the way up the hill (MGA 329397E 6651857N) there are olivine harrisites in thin rubbly outcrop. Above these and extending to the back slope is adcumulate-textured siliceous laterite. Laterite with orthocumulate textures is present just above the contact with strongly foliated metabasalt (MGA 329257E 6651927N). There is a marked contrast in the preservation of igneous textures for the ultramafic and mafic rocks over this contact. From the top of the hill, the dump at the Sand King openpit mine, near the western extent of the Walter Williams Formation, is visible. Well-developed, dark-brown silica cap over olivine adcumulates is developed around the northern end of the hill.

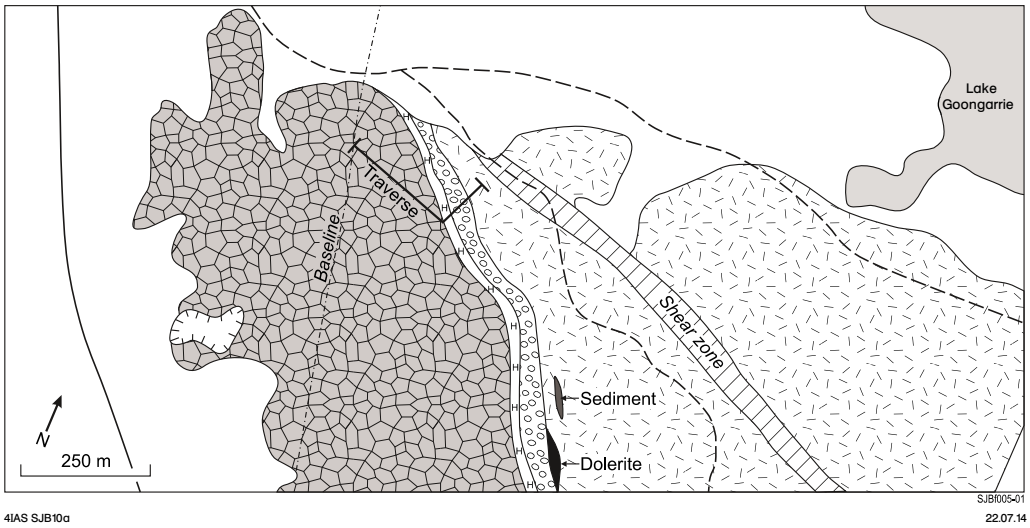

Figure 39. Geological map of the Comet Vale area showing Locality 25. See Figure 14 for legend (modified from Hill et al., 2001)

Locality 20: Black Flag Group sedimentary rocks at Gidji (MGA 351574E 6608250N)

Modified from Morris et al. (1993)

At Gidji, poorly exposed rhyolite in the breakaway is succeeded to the north by a poorly sorted open and closed framework breccia dominated by volcanic fragments. Immediately to the north, matrix-supported pebbly sandstone is succeeded by medium grained sandstone and shale interbeds. Low-angle cross-bedding indicates the sequence youngs northwards, with the rhyolite at the base.

Farther north, chaotically arranged blocks of thinly bedded felsic volcaniclastic sandstone form a clast supported breccia with little matrix. Individual blocks show graded bedding, cross-bedding and slump structures. Petrographically, the sandstones comprise 1–4 mm thick lamellae, which are individually size graded. The coarser lamellae consist of clasts of angular quartz, perthitic feldspar, plagioclase, subordinate muscovite, and rare subangular to rounded granoblastic and cryptocrystalline quartz and feldspar rock fragments. All phases are less than 1 mm in diameter and there is abundant secondary calcite and minor opaque material. The angularity of clasts and dominance of crystals indicates reworking of a crystal rich tuff.

Several explanations have been offered for this unit, including dewatering of a loosely consolidated sedimentary sequence, collapse of a volcanic cinder cone, and slumping of variably consolidated sediments (partial liquefaction) initiated by earthquake shock.

References

Ahmat, AL 1990, Locality 26, Alunite locality, olistostromes and stromatolites, *in* Kalgoorlie granite–greenstone terrain excursion localities; Third International Archaean Symposium Excursion Guidebook *edited by* SE Ho, JE Glover, JS Myers and JR Muhling: The University of Western Australia, Perth, Geology Department and University Extension, Publication no. 21, p. 281– 282.

Allibone, AH, Windh, J, Etheride, MA, Burton, D, Anderson, G, Edwards, PW, Miller, A, Graves, C, Fanning, CM and Wysoczanski, R 1998, Timing relationships and structural controls on the location of Au–Cu mineralisation at the Boddington gold mine: Economic Geology, v. 93, p. 245–270.

Anand, RR and Paine, MD 2002, Regolith geology of the Yilgarn Craton, Western Australia: implications for exploration: Australian Journal of Earth Sciences, v. 49, p. 3–162.

Arndt, NT and Jenner, GA 1986, Crustally contaminated komatiites and basalts from Kambalda, Western Australia: Chemical Geology, v. 56, p. 229–255.

Baggott, MSA 2006, Refined model for the magmatic, tectonometamorphic, and hydrothermal evolution of the Leonora District, Eastern Goldfields Province, Yilgarn Craton, Western Australia: The University of Western Australia, Perth (unpublished).

Barley, ME, Brown, SJA, Krapež, B and Kositcin, N 2008, Physical volcanology and geochemistry of a Late Archaean volcanic arc: Kurnalpi and Gindalbie Terranes, Eastern Goldfields Superterrane, Western Australia: Precambrian Research, v. 161, p. 53–76.

Barnes, SJ 2004, Introduction to nickel sulphide orebodies and komatiites of the Black Swan area, Yilgarn Craton, Western Australia: Mineralium Deposita, v. 39, p. 679–683.

Barnes, SJ (editor) 2006, Nickel deposits of the Yilgarn Craton: geology, geochemistry, and geophysics applied to exploration: Society of Economic Geologists, Special Publication 13, 210p.

Barnes, SJ, Lesher, CM and Sproule, RA 2007, Geochemistry of komatiites in the Eastern Goldfields Superterrane, Western Australia and the Abitibi Greenstone Belt, Canada, and implications for the distribution of associated Ni–Cu–PGE deposits: Applied Earth Science (Transactions of the Institute of Mining and Metallurgy Series B), v. 116, p. 167–187.

Barnes, SJ and Van Kranendonk, MJ 2014, Archean andesites in the east Yilgarn craton, Australia: Products of plume-crust interaction?: Lithosphere, v. 6, no. 2, p. 80–92.

Barnes, S, Van Kranendonk, M and Sonntag, I 2012, Geochemistry and tectonic setting of basalts from the Eastern Goldfields Superterrane, Yilgarn Craton: Australian Journal of Earth Sciences, v. 59, no. 5, p. 707–735 .

Bavinton, OA 1981, The nature of sulfidic metasediments at Kambalda and their broad relationships with associated ultramafic rocks and nickel ores: Economic Geology, v. 76, no. 6, p. 1606–1628.

Begg, GC, Hronsky, JMA, Arndt, NT, Griffin, WL, O'Reilly, S and Hayward, N 2010, Lithospheric, cratonic, and geodynamic setting of Ni–Cu–PGE sulfide deposits: Economic Geology, v. 105, p. 1057–1070.

Beresford, S, Stone, WE, Cas, R, Lahaye, Y and Jane, M 2005, Volcanological controls on the localization of the komatiite-hosted Ni–Cu–(PGE) Coronet Deposit, Kambalda, Western Australia: Economic Geology, v. 100, p. 1457–1467.

Bekker, A, Barley, ME, Fiorentini, M, Rouxel OJ, Rumble D and Beresford, SW 2009, Atmospheric sulfur in Archaean komatiite-hosted nickel deposits: Science, v. 326, p. 1086–1089.

Blewett, RS, and Czarnota, K 2007, Tectonostratigraphic architecture and uplift history of the Eastern Yilgarn Craton, Module 3 — Terrane Structure, Project Y1-P763: Geoscience Australia, Record 2007/15, 114p.

Blewett, RS, Czarnota, K and Henson, PA 2010a, Structural-event framework for the eastern Yilgarn Craton, Western Australia, and its implications for orogenic gold: Precambrian Research, v. 183, p. 203–209.

Blewett, RS, Henson, PA, Roy, IG, Champion, DC and Cassidy, KF 2010b, Scale-integrated architecture of a world-class gold mineral system: The Archaean eastern Yilgarn Craton, Western Australia: Precambrian Research, v. 183, p. 230–250.

Brauns, KA 1991, Palaeovolcanological and environmental setting of the Archaean Black Flag Beds, Kambalda, Western Australia: Monash University, Melbourne, BSc. (Hons) thesis (unpublished).

Brown, SJA, Barley, ME, Krapež, B and Cas, RAF 2002, The Late Archaean Melita Complex, Western Australia: shallow submarine bimodal volcanism in a rifted arc environment: Journal of Volcanology and Geothermal Research, v. 115, p. 303–327.

Brown, SJA, Krapež, B, Beresford, SW, Cassidy, KF, Champion, DC, Barley, ME and Cas, RAF 2001, Archaean volcanic and sedimentary environments of the Eastern Goldfields Province, Western Australia — a field guide: Geological Survey of Western Australia, Record 2001/13, 66p.

Campbell, IH and Hill, RI 1988, A two-stage model for the formation of the granite–greenstone terrains of the Kalgoorlie–Norseman area, Western Australia: Earth and Planetary Science Letters, v. 90, p. 11–25.

Cassidy, KF 2006, Geological evolution of the Eastern Yilgarn Craton (EYC), and terrane, domain and fault nomenclature, *in* 3D Geological Models of the Eastern Yilgarn Craton – Y2 Final Report pmd*CRC *edited by* RS Blewett and AP Hitchman: Geoscience Australia, Record 2006/04, p. 1–19 [DVD-ROM].

Cassidy, KF, Champion, DC, Krapež, B, Barley, ME, Brown, SJA, Blewett, RS, Groenewald, PB and Tyler, IM 2006, A revised geological framework for the Yilgarn Craton, Western Australia: Geological Survey of Western Australia, Record 2006/8, 8p.

Cassidy, KF, Champion, DC, McNaughton, N, Fletcher, IR, Whitaker, AJ, Bastrakova, IV and Budd, A 2002, The characterisation and metallogenic significance of Archaean granitoids of the Yilgarn Craton, Western Australia: Minerals and Energy Research Institute of Western Australia (MERIWA), Project no. M281/AMIRA Project no. 482 (unpublished report no. 222).

Champion, DC and Cassidy, KF 2007, An overview of the Yilgarn and its crustal evolution, *in* Proceedings of Geoconferences (WA) *edited by* FP Bierlein and CM Knox-Robinson: Geoscience Australia; Kalgoorlie '07, Kalgoorlie, Western Australia, 25–27 September 2007, Record 2007/14, p. 8–13.

Champion, DC and Sheraton, JW 1997, Geochemistry and Nd isotope systematics of Archaean granites of the Eastern Goldfields, Yilgarn Craton, Australia: implications for crustal growth processes: Precambrian Research, v. 83, p. 109–132.

Coates, SP 1993, Geology and grade control at the Sons of Gwalia Mine Leonora, Western Australia, *in* Proceedings of the International Mining Geology Conference *edited by* I Robertson, W Shaw, C Arnold, and L Kevin: Australian Institute of Mining and Metallurgy 5/93, Publication Series, p. 125–132.

Compston, W, Williams, IS, Campbell, IH and Gresham, JJ 1986, Zircon xenocrysts from the Kambalda volcanics: age constraints and direct evidence for older continental crust below the Kambalda–Norseman greenstones: Earth and Planetary Science Letters, v. 76, p. 299–311.

Cox, S and Ruming, K 2004, The St Ives mesothermal gold system, Western Australia – a case of golden aftershocks?: Journal of Structural Geology, v. 26, p. 1109–1125.

Connors, KA, Stolz, EMG and Hanneson, JE 2002, Early fault architecture at St Ives: implications for Au and Ni mineralisation, *in* Applied Structural Geology for Mineral Exploration and Mining *edited by* S Vearncombe: Australian Institute of Geoscientists, Bulletin, v. 36, p. 29–31.

Crawford, AJ 2012, Petrographic report – 17 rocks from the Nimbus Project, Western Australia: Unpublished report for MacPhersons Resources Ltd.

Czarnota, K, Blewett, RS and Goscombe, B 2008, Structural and metamorphic controls on gold through time and space in the Central Eastern Goldfields Superterrane — a field guide: Geological Survey of Western Australia, Record 2008/9, 66p.

Czarnota, K, Champion, DC, Goscombe, B, Blewett, RS, Cassidy, KF, Henson, PA and Groenewald, PB 2010, Geodynamics of the eastern Yilgarn Craton: Precambrian Research, v. 183, p. 175–202.

Dentith, M, Evans, S, Thiel, S, Gallardo, L, Joly, A and Romano, SS 2012, A magnetotelluric traverse across the southern Yilgarn Craton: Geological Survey of Western Australia, Record 2012/6.

Drummond, BJ, Goleby, BR and Swager, CP 2000, Crustal signature of Late Archean tectonic episodes in the Yilgarn craton, Western Australia: evidence from deep seismic sounding: Tectonophysics, v. 329, p. 193–221.

Dunphy, JM, Fletcher, IR, Cassidy, KF and Champion, DC 2003, Compilation of SHRIMP U–Pb geochronological data, Yilgarn Craton, Western Australia, 2001–2002: Geoscience Australia, Geoscience Australia Record 2003/15, 139p.

Duuring, P, Hagemann, SG, and Love, RJ, 2001, A thrust ramp model for gold mineralization at the Archaean trondhjemite-hosted Tarmoola Deposit; the importance of heterogeneous stress distributions around granitoid contacts: Economic Geology, v. 96, p. 1379–1396.

Fiorentini, ML 2010, Chapter 4 — The Kambalda Nickel Camp, *in* Controls on giant minerals systems in the Yilgarn Craton – a field guide *compiled by* TC McCuaig, J Miller, and S Beresford: Geological Survey of Western Australia, Record 2010/26, p. 81–110.

Fiorentini, ML, Barley, ME, Pickard, A, Beresford, SW, Rosengren, N, Cas, R and Duuring, P 2005, Age constraints of the structural and stratigraphic architecture of the Agnew–Wiluna greenstone belt: implications for the age of komatiite–felsic association and interaction in the Eastern Goldfields Province, Western Australia: Minerals and Energy Research Institute of Western Australia (MERIWA) Report No. 255, 39p.

Fiorentini ML, Rosengren N, Beresford SW, Grguric B and Barley ME 2007, Controls on the emplacement and genesis of the MKD5 and Sarah's Find Ni–Cu–PGE deposits, Mount Keith, Agnew–Wiluna Greenstone Belt, Western Australia: Mineralium Deposita, v. 126, p. 847–877.

Glicken, H 1991, Sedimentary architecture of large volcanic-debris avalanches, *in* Sedimentation in Volcanic Settings *edited by* RV Fisher and GA Smith: SEPM Special Publication, 45, p. 99–106.

Gole, MJ, and Hill, RET 1989, The Walter Williams Formation: the result of a regionally extensive single komatiite eruptive event, Yilgarn Block, Western Australia: Geological Society of Finland, Bulletin, v. 61, p. 24.

Gole, MJ and Hill, RET 1990, The refinement of extrusive models for the genesis of nickel deposits: implications from case studies at Honeymoon Well and the Walter Williams Formation: Minerals and Energy Research Institute of Western Australia, Report 68, 93p.

Goleby, BR, Blewett, RS, Korsch, RJ, Champion, DC, Cassidy, KF, Jones, LEA, Groenewald, PB and Henson, PA 2004, Deep seismic reflection profiling in the Archaean northeastern Yilgarn Craton, Western Australia: implications for crustal architecture and mineral potential: Tectonophysics, v. 388, p. 119–133.

Goscombe, B, Blewett, RS, Czarnota, K, Groenewald, PB and Maas, R 2009, Metamorphic Evolution and Integrated Terrane Analysis of the Eastern Yilgarn Craton: Rationale, Methods, Outcomes and Interpretation: Geoscience Australia, Record 2009/23, 270p.

Gresham, JJ and Loftus-Hills, GD 1981, The geology of the Kambalda nickel field, Western Australia: Economic Geology, v. 76, p. 1372–1416.

Grey, K 1981, Small conical stromatolites from the Archaean near Kanowna, Western Australia, *in* Annual report for the year 1980: Geological Survey of Western Australia, p. 90–94.

Griffin, TJ, Hunter, WM, Keats, W and Quick, DR 1983, Description of excursion localities, *in* Abstracts and excursion guide *edited by* PC Muhling: Eastern Goldfields geological field conference 1983, Kalgoorlie, WA (unpublished).

Groves, DI and Gee, RD 1980, Regional geology and mineral deposits of the Kalgoorlie–Norseman region: Geological Society of Australia (WA Division); 2nd International Archaean Symposium, Perth, 1980, Excursion Guide, 112p.

Hadlow, H, Williams D, Pertel D and Geerdts, P 2011, Project review and due diligence report, MacPhersons Reward Gold Ltd, Nimbus Ag–Zn Project, Kalgoorlie, Western Australia: Report for MacPhersons Resources Ltd (unpublished).

Hall, G 2007, Exploration success in the Yilgarn Craton insights from the Placer Dome experience the need for integrated research, *in* Proceedings of Geoconferences (WA) *edited by* FP Bierlein and CM Knox-Robinson: Geoscience Australia; Kalgoorlie '07 Conference, 25–27 September 2007: Record 2007/14, p. 199–202.

Hallberg, JA 1972, Spilitic lavas at Mt Hunt, Western Australia: Journal of the Royal Society of Western Australia, v. 55, p. 45–56.

Hallberg, JA 1985, Geology and mineral deposits of the Leonora–Laverton area, northeastern Yilgarn Block, Western Australia: Geological Survey of Western Australia, Record 1983/8, 140p.

Hallberg, JA 1987, Postcratonization mafic and ultramafic dykes of the Yilgarn Block: Australian Journal of Earth Sciences, v. 34, p. 135–149.

Hand, J 1998, The sedimentological and stratigraphic evolution of the Archaean Black Flag Beds, Kalgoorlie, Western Australia: implications for regional stratigraphy and basin setting within the Kalgoorlie Terrane: Monash University, Melbourne, PhD thesis (unpublished), 251p.

Henderson, I, Goodz, M and Vearncombe, J 2012, Nimbus: Fault-hosted Ag–Zn–Pb–Au mineralization near Kalgoorlie, Western Australia: Structural Geology and Resources 2012 – Extended Abstracts, Australian Institute of Geoscientists Bulletin 56, p. 89–92.

Hill, RET, Barnes, SJ and Dowling, SE 2001, Komatiites of the Norseman–Wiluna greenstone belt, Western Australia — a field guide: Geological Survey of Western Australia, Record 2001/10, 71p.

Hill, RET, Barnes, SJ, Gole, MJ and Dowling, SJ 1995, The volcanology of komatiites as deduced from field relationships in the Norseman–Wiluna greenstone belt, Western Australia: Lithos, v. 34, p. 159–188.

Hunter,WM 1990a, Locality 18, Kurrawang Formation, *in* Kalgoorlie granite–greenstone terrain excursion localities; 3rd International Archaean Symposium Excursion Guidebook *edited by* SE Ho, JE Glover, JS Myers and JR Muhling: The University of Western Australia, Perth, Geology Department and University Extension, Publication no. 21, p. 264–266.

Hunter,WM 1990b, Locality 14, Mungari, *in* Kalgoorlie granite–greenstone terrain excursion localities; 3rd International Archaean Symposium Excursion Guidebook *edited by* SE Ho, JE Glover, JS Myers and JR Muhling: The University of Western Australia, Perth, Geology Department and University Extension, Publication no. 21, p. 257– 260.

Huston, DL, Champion, DC and Cassidy, KF 2005, Tectonic controls on the endowment of Archean cratons in VHMS deposits: evidence from Pb and Nd isotopes, *in* Proceedings of the Eighth Biennial SGA Meeting *edited by* J Mao and FP Bierlein, Beijing, China, 18–21 August 2005: Springer, p. 15–18.

Ivanic, TJ, Wingate, MTD, Kirkland, CL, Van Kranendonk, MJ and Wyche, S 2010, Age and significance of voluminous mafic–ultramafic magmatic events in the Murchison Domain, Yilgarn Craton: Australian Journal of Earth Sciences, v. 57, p. 597–614.

Keats, W 1987, Regional geology of the Kalgoorlie–Boulder gold-mining district: Geological Survey of Western Australia, Report 21, 44p.

Kinny, PD, Williams, IS, Froude, DO, Ireland, TR and Compston, W 1988, Early Archaean zircon ages from orthogneisses and anorthosites at Mount Narryer, Western Australia: Precambrian Research, v. 38, p. 325–341.

Kositcin, N, Brown, SJA, Barley, ME, Krapež, B, Cassidy, KF and Champion, DC 2008, SHRIMP U–Pb zircon age constraints on the Late Archaean tectonostratigraphic architecture of the Eastern Goldfields Superterrane, Yilgarn Craton, Western Australia: Precambrian Research, v. 161, p. 5–33.

Krapež, B and Barley, ME 2008, Late Archaean synorogenic basins of the Eastern Goldfields Superterrane, Yilgarn Craton, Western Australia. Part III. Signatures of tectonic escape in an arc–continent collision zone: Precambrian Research, v. 161, p. 183–199.

Krapež, B, Barley, ME and Brown, SJA 2008, Late Archaean synorogenic basins of the Eastern Goldfields Superterrane, Yilgarn Craton, Western Australia. Part I. Kalgoorlie and Gindalbie Terranes: Precambrian Research, v. 161, p. 135–153.

Krapež, B, Brown, SJA, Hand, J, Barley, ME and Cas, RAF 2000, Age constraints of recycled crustal and supracrustal sources of Archaean metasedimentary sequences, Eastern Goldfields Province, Western Australia: evidence from SHRIMP zircon dating: Tectonophysics, v. 332, p. 89–133.

Krapež, B and Hand, JL 2008, Late Archaean deep-marine volcaniclastic sedimentation in an arc-related basin: the Kalgoorlie Sequence of the Eastern Goldfields Superterrane, Yilgarn Craton, Western Australia: Precambrian Research, v. 161, p. 89–113.

Lesher, CM 1983, Localization and genesis of komatiite-associated Fe–Ni–Cu sulphide mineralization at Kambalda, Western Australia: University of Western Australia, Perth, PhD thesis (unpublished), 199p.

Lesher, CM and Campbell, IH 1993, Geochemical and fluid dynamic modeling of compositional variations in Archean komatiite-hosted nickel sulfide ores in Western Australia: Economic Geology, v. 88, p. 804–816.

Lesher, CM and Keays, RR 2002, Komatiite-associated Ni–Cu–PGE deposits: geology, mineralogy, geochemistry, and genesis, *in* The Geology, Geochemistry, Mineralogy, and Mineral Beneficiation of Platinum-Group Elements *edited by* LJ Cabri: Canadian Institute of Mining, Metallurgy and Petroleum, Special Volume 54, p. 579–618.

Marston, RJ, 1984, Nickel mineralization in Western Australia: Geological Survey of Western Australia, Mineral Resources Bulletin 14, 271p.

MacPhersons Resources Ltd, 2014, MacPhersons Resources Ltd, Perth, viewed 18 August 2014, <http://www.mrpresources.com.au/nimbus.php>.

McCuaig, TC, Beresford, S and Hronsky, J 2010, Translating the mineral systems approach into an effective exploration targeting system: Ore Geology Reviews, v. 38, p. 128–138.

Mercier-Langevin P, Hannington, MD, Dubé, B and Bécu, V 2011, The gold content of volcanogenic massive sulfide deposits: Mineralium Deposita, v. 46 no. 5–6, p. 509–539.

Miller, J, Blewett, R, Tunjic, J and Connors, K 2010, The role of early formed structures on the development of the world class St Ives Goldfield, Yilgarn, WA: Precambrian Research, v. 183, p. 292–315.

Mole, DR, Fiorentini, ML, Thebaud, N, McCuaig, TC, Cassidy, KF, Barnes, SJ, Belousova, EA, Mudrovska, I and Doublier, MP 2010, Lithospheric controls on the localization of komatiite-hosted nickel-sulfide deposits: evolving early Earth, *in* Fifth International Archean Symposium Abstracts *edited by* IM Tyler and CM Knox-Robinson: Geological Survey of Western Australia, Record 2010/8, p. 101.

Morris, PA 1998, Archaean felsic volcanism in parts of the Eastern Goldfields region, Western Australia: Geological Survey of Western Australia, Report 55, 80p.

Morris, PA, Barnes, SJ and Hill, RET 1993, Eruptive environment and geochemistry of Archaean ultramafic, mafic and felsic volcanic rocks of the eastern Yilgarn Craton, IAVCEI Canberra 1993 excursion guide: Australian Geological Survey Organisation, Record 1993/62, 40p.

Nelson, DR 1995, 100758: felsic volcanic breccia, Perkolilli; Geochronology Record 28: Geological Survey of Western Australia, 4p.

Nelson, DR 1996a, 112117: biotite monzogranite, Clark Well; Geochronology Record 498: Geological Survey of Western Australia, 4p.

Nelson, DR 1996b, 110225: porphyritic metadacite, Carpet Snake Soak; Geochronology Record 519: Geological Survey of Western Australia, 4p.

Nelson, DR 2000, 142994: biotite monzogranite, Ularring Rock; Geochronology Record 292: Geological Survey of Western Australia, 4p.

Nemchin, AA and Pidgeon, RT 1998, Precise conventional and SHRIMP baddeleyite U–Pb for the Binneringie Dyke, near Narrogin, Western Australia: Australian Journal of Earth Sciences, v. 45, p. 673–675.

Neumayr, P, Walshe, J, Hagemann, S, Petersen, K, Roache, A, Frikken, P, Horn, L and Halley, S 2008, Oxidized and reduced mineral assemblages in greenstone belt rocks of the St. Ives gold camp, Western Australia: vectors to high-grade ore bodies in Archaean gold deposits?: Mineralium Deposita, v. 43, p. 363–371.

Nguyen, TP 1997, Structural controls on gold mineralisation at the Revenge Mine and its tectonic setting in the Lake Lefroy area, Kambalda, Western Australia: University of Western Australia, Perth, PhD thesis (unpublished), 205p.

Nguyen, PT, Cox, SF, Harris, LB and Powell, CM 1998, Fault-valve behaviour in optimally oriented shear zones: An example at the Revenge gold mine, Kambalda, Western Australia: Journal of Structural Geology, v. 20, p. 1625–1640.

Pawley, MJ, Wingate, MTD, Kirkland, C, Wyche, S, Hall, CE, Romano, SS and Doublier, MP 2012, Adding pieces to the puzzle: episodic crustal growth and a new terrane in the northeast Yilgarn Craton, Western Australia: Australian Journal of Earth Sciences, v. 59, no. 5, p. 603–623,

Piercey, SJ 2011, The setting, style, and role of magmatism in the formation of volcanogenic massive sulfide deposits: Mineralium Deposita, v. 46, p. 449–471.

Potma, WA, Schaubs, PM, Robinson, JA, Sheldon, HA, Roberts, PA, Zhang, Y, Zhao, C, Ord, A and Hobbs, BE 2007, Regional geology of the Archaean nuclei of the Western Shield, *in* Procceeedings of Geoconferences (WA) Inc. *edited by* FP Bierlein and CM Knox-Robinson: Geoscience Australia; Kalgoorlie '07 Conference, 25–27 September 2007, Record 2007/14, p. 214–217.

Rasmussen, B, Fletcher, IR, Muhling, JR and Wilde, SA 2010, In situ U–Th–Pb geochronology of monazite and xenotime from the Jack Hills belt: Implications for the age of deposition and metamorphism of Hadean zircons: Precambrian Research, v. 180, p. 26–46.

Rattenbury, MS 1993, Stop 5, Copperfield granite, *in* Kalgoorlie 93 — an international conference on crustal evolution, metallogeny, and exploration of the Eastern Goldfields, excursion guidebook *edited by* PR Williams and JA Haldane: Australian Geological Survey Organisation, Record 1993/54, p. 73–83.

Reading, AM, Kennett, BLN and Goleby, B 2007, New constraints on the seismic structure of West Australia: evidence for terrane stabilization prior to assembly of an ancient continent: Geology, v. 35, p. 379–382.

Rosengren, NM, Cas, RAF, Beresford, SW and Palich, BM 2005, Reconstruction of an extensive Archaean dacitic submarine volcanic complex associated with the komatiite-hosted Mt Keith nickel deposit, Agnew-Wiluna Greenstone Belt, Yilgarn Craton, Western Australia: Precambrian Research, v. 161, p. 34–52.

Ruming, KJ 2006, Controls on lode gold mineralisation in the Victory Thrust Complex, St Ives Goldfield, Western Australia: The University of Newcastle, Newcastle, New South Wales, PhD thesis (unpublished).

Said, N and Kerrich, R 2009, Geochemistry of coexisting depleted and enriched Paringa Basalts, in the 2.7 Ga Kalgoorlie Terrane, Yilgarn Craton, Western Australia: evidence for a heterogeneous mantle plume event: Precambrian Research, v. 174, p. 287–309.

Skwarnecki, MS 1988, Alteration and deformation in a shear zone hosting gold mineralisation at Harbour Lights, Leonora, WA, *in* Archaean gold mineralisation in a normal-motion shear zone at Harbour Lights, Leonora, Western Australia *edited by* SE Ho and DI Groves: University of Western Australia, Geology Department and University Extension, Abstracts 12, p. 111–129.

Smithies, RH and Champion, DC 1999, Late Archaean felsic alkaline igneous rocks in the Eastern Goldfields, Yilgarn Craton, Western Australia: a result of lower crustal delamination?: Journal of the Geological Society, London, v. 156, p. 561–576.

Squire, RJ, Allen, CM, Cas, RAF, Campbell, IH, Blewett, RS and Nemchin, AA 2010, Two cycles of voluminous pyroclastic volcanism and sedimentation related to episodic granite emplacement during the late Archean: Eastern Yilgarn Craton, Western Australia: Precambrian Research, v. 183, p. 251–274.

Squire, RJ, Cas, RAF, Clout, JMF and Behets, R 1998, Volcanology of the Lunnon Basalt and its relevance to nickel sulfide-bearing trough structures at Kambalda, Western Australia: Australian Journal of Earth Sciences, v. 45, p. 695–715.

Stone, WE and Archibald, NJ 2004, Structural controls on nickel sulfide ore shoots in Archean komatiite, Kambalda, WA: the volcanic trough controversy revisited: Journal of Structural Geology, v. 26, p. 1173–1194.

Stone, WE, Beresford, SW and Archibald, NJ 2005, Structural setting and shape analysis of nickel sulphide shoots at the Kambalda Dome, Western Australia: implications for deformation and remobilization: Economic Geology, v. 100, p. 1441–1455.

Swager, CP 1989, Structure of the Kalgoorlie greenstones — regional deformational history and implications for the structural setting of gold deposits within the Golden Mile: Geological Survey of Western Australia, Report 25, p. 59–84.

Swager, CP 1990, Locality 12, Hannan Lake and Mount Hunt, *in* Kalgoorlie granite–greenstone terrain excursion localities; 3rd International Archaean Symposium Excursion Guidebook *edited by* SE Ho, JE Glover, JS Myers and JR Muhling: The University of Western Australia, Perth, Geology Department and University Extension, Publication no. 21, p. 252–253.

Swager, CP 1994, Geology of the Menzies 1:100 000 sheet (and adjacent Ghost Rocks area): Geological Survey of Western Australia, 1:100 000 Geological Series Explanatory Notes, 31p.

Swager, CP 1997, Tectono-stratigraphy of late Archaean greenstone terranes in the southern Eastern Goldfields, Western Australia: Precambrian Research, v. 83, p. 11–42.

Swager, CP, Goleby, BR, Drummond, BJ, Rattenbury, MS and Williams, PR 1997, Crustal structure of granite–greenstone terranes in the Eastern Goldfields, Yilgarn Craton, as revealed by seismic profiling: Precambrian Research, v. 83, p. 43–56.

Swager, CP, Griffin, TJ, Witt, WK, Wyche, S, Ahmat, AL, Hunter, WM and McGoldrick, PJ 1995, Geology of the Archaean Kalgoorlie Terrane — an explanatory note (reprint of Record 1990/12): Geological Survey of Western Australia, Report 48, 26p.

Taylor, T 1984, The palaeoenvironmental and tectonic setting of Archaean volcanogenic rocks in the Kanowna District near Kalgoorlie, Western Australia: University of Western Australia, Perth, MSc. thesis (unpublished).

Travis, GA, Woodall, R and Bartram, GD 1971, The geology of the Kalgoorlie Goldfield, in Symposium on Archaean Rocks edited by JE Glover: Geological Society of Australia, Special Publication no. 3, p. 175–190.

Trofimovs, J, Cas, RAF and Davis, BK 2004a, An Archaean submarine volcanic debris avalanche deposit, Yilgarn Craton, western Australia, with komatiite, basalt and dacite megablocks: the product of dome collapse: Journal of Volcanology and Geothermal Research, v. 138, p. 111–126.

Trofimovs, J, Davis, BK and Cas, RAF 2004b, Contemporaneous ultramafic and felsic intrusive and extrusive magmatism in the Archaean Boorara Domain, Eastern Goldfields Superterrane, Western Australia, and its implications: Precambrian Research, v. 131, p. 283–304.

Trofimovs, J, Davis, BK, Cas, RAF, Barley, ME and Tripp, GI 2006, Reconstructing the event stratigraphy from the complex structural — stratigraphic architecture of an Archaean volcanic–intrusive–sedimentary succession: the Boorara Domain, Eastern Goldfields Superterrane, Western Australia: Australian Journal of Earth Sciences, v. 53, p. 303–327.

Van Kranendonk, MJ, Ivanic, TJ, Wingate, MTD, Kirkland, CL and Wyche, S 2013, Long-lived, autochthonous development of the Archean Murchison Domain, and implications for Yilgarn Craton tectonics: Precambrian Research, v. 229, p. 49–92.

Vearncombe, JR 1992, Archaean gold mineralization in a normal motion shear zone at Harbour Lights, Leonora, Western Australia: Mineralium Deposita, v. 27, p. 182–191.

Vielreicher, NM, Groves, DI, Snee, LW, Fletcher, IR and McNaughton, NJ 2010, Broad synchroneity of three gold mineralization styles in the Kalgoorlie gold field: SHRIMP, U–Pb, and $^{40}Ar/^{39}Ar$ geochronological evidence: Economic Geology, v. 105, p. 187–227.

Walshe, JL, Neumayr, P, Cleverley, J, Petersen, K, Andrew, A, Whitford, D, Carr, GR, Kendrick, M, Young, C and Halley, S 2009, Question 3: Multiple fluid reservoirs in Eastern Yilgarn gold systems, *in* Concepts to Targets: a scale-integrated mineral systems study of the Eastern Yilgarn Craton: pmd*CRC, Project Y4, Final Report, Part III, p. 113–152.

Wang, Q, Schiøtte, L and Campbell, IH 1998, Geochronology of supracrustal rocks from the Golden Grove area, Murchison Province, Yilgarn Craton, Western Australia: Australian Journal of Earth Sciences, v. 45, p. 571–577.

Watchorn, RB 1998, Kambalda – St Ives gold deposits, in Geology of Australian and Papua New Guinea Ore Deposits edited by DA Berkman and DH Mackenzie: The Australasian Institute of Mining and Metallurgy, Melbourne, Victoria, p. 243–254.

Weinberg, RF, Hodkiewicz, PH and Groves, DI 2004, What controls gold distribution in Archean terranes?: Geology, v. 32, p. 545–548.

Western Australia Department of Mines and Petroleum, 2014, Resources data files, viewed July 2014 <http://www.dmp.wa.gov.au/1521.aspx>.

Wilde, SA, Valley, JW, Peck, WH and Graham, CM 2001, Evidence from detrital zircons for the existence of continental crust and oceans on the Earth 4.4 Gyr ago: Nature, v. 409, p. 175–178.

Williams, DAC and Hallberg, JA 1973, Archaean layered intrusions of the Eastern Goldfields region, Western Australia: Contributions to Mineralogy and Petrology, v. 38, p. 45–70.

Williams, IR, Gower, CF and Thom, R (compilers) 1976, Edjudina, Western Australia: Geological Survey of Western Australia, 1:250 000 Geological Series Explanatory Notes, 29p.

Williams, PR and Currie, KL 1993, Character and regional implications of the sheared Archaean granite–greenstone contact near Leonora, Western Australia: Precambrian Research, 62, p. 343–365.

Williams, PR, Nisbet, BW and Etheridge MA 1989, Shear zones, gold mineralization and structural history in the Leonora district, Eastern Goldfields Province, Western Australia: Australian Journal of Earth Sciences, v. 36, p. 383–403.

Williams, PR, Rattenbury, MS and Witt, WK (compilers) 1993, A field guide to the felsic igneous rocks of the northeast Eastern Goldfields Province, Western Australia: core complexes, batholiths, plutons and supracrustals, *in* Kalgoorlie 93 — an international conference on crustal evolution, metallogeny and exploration in the Eastern Goldfields, Excursion Guide *compiled by* PR Williams and JA Haldane: Australian Geological Survey Organisation, Record 1993/53, p. 23–74.

Witt, WK 1994, Geology of the Melita 1:100 000 sheet: Geological Survey of Western Australia, 1:100 000 Geological Series Explanatory Notes, 63p.

Witt, WK 2001, Tower Hill gold deposit, Western Australia; an atypical, multiply deformed Archaean gold–quartz vein deposit: Australian Journal of Earth Sciences, v. 48, p. 81–99.

Woodall, R 1965, Structure of the Kalgoorlie goldfield, *in* Geology of Australian Ore Deposits (2nd edition) *edited by* J. McAndrew: Commonwealth Mining and Metallurgical Congress, 8th, Australia and New Zealand, 1965, Publications, v. 1, p. 71–79.

Wyche, S 2004, Menzies, Western Australia (2nd edition): Geological Survey of Western Australia, 1:250 000 Geological Series Explanatory Notes, 38p.

Wyche, S (compiler) 2007, Stratigraphy and structure of the Kalgoorlie Terrane at Hannan Lake and Mount Hunt — a field guide: Geological Survey of Western Australia, Record 2007/15, 11p.

Wyche, S, Kirkland, CL, Riganti, A, Pawley, MJ, Belousova, E and Wingate, MTD 2012, Isotopic constraints on stratigraphy in the central and eastern Yilgarn Craton, Western Australia: Australian Journal of Earth Sciences, v. 59.

Yeats, CJ, McNaughton, NJ and Groves, DI 1996, SHRIMP U–Pb geochronological constraints on Archean volcanic-hosted massive sulfide and lode gold mineralization at Mount Gibson, Yilgarn Craton, Western Australia: Economic Geology, v. 91, p. 1354–1371.

RECORD 2014/10

GEOLOGICAL SETTING OF MINERAL DEPOSITS IN THE EASTERN YILGARN CRATON — A FIELD GUIDE

Wyche

This Record is published in digital format (PDF) and is available as a free download from the DMP website at <www.dmp.wa.gov.au/GSWApublications>.

Further details of geological products produced by the Geological Survey of Western Australia can be obtained by contacting:

Information Centre
Department of Mines and Petroleum
100 Plain Street
EAST PERTH WESTERN AUSTRALIA 6004
Phone: (08) 9222 3459 Fax: (08) 9222 3444
www.dmp.wa.gov.au/GSWApublications